Revisiting the spindle assembly checkpoint and elucidating chromosome congression in *Arabidopsis thaliana*

Dissertation with the aim of achieving a doctoral degree at the

Faculty of Mathematics, Informatics and Natural Sciences

Department of Biology

University of Hamburg

Submitted by

Konstantinos Lampou

2023 in Hamburg, Germany

Supervisor: Prof. Dr. Arp Schnittger

First Examiner: Prof. Dr. Arp Schnittger
Second Examiner: Dr. Magdalena Weingartner

Date of oral defence: 7th of September 2023

Table of Contents

Abstract

The spindle assembly checkpoint (SAC) is an evolutionarily conserved checkpoint among eukaryotes that ensures segregation fidelity by preventing the onset of anaphase until all kinetochores are attached in a stable, bipolar configuration to spindle microtubules. The inner workings of the SAC are very well understood in metazoan and yeast model systems, but little is known in other model and non-model organisms.

Considering how powerful comparative biology can be in elucidating core biological principles, I set out to explore the meiotic SAC in *Arabidopsis thaliana*. I temporally dissected the association of SAC components with the kinetochore, revealing the stepwise assembly and disassembly of the kinetochore-bound SAC complex, which at least for one of these components is regulated by three conserved kinases. Active checkpoint signaling could not be maintained for over 6 hours under severe microtubule-destabilizing conditions and the nuclear envelope reformed upon silencing of the SAC, a feature that seems to be conserved across the plant lineage. I discovered that BUB3.3 is most probably not a *bona fide* SAC component, but rather involved in chromosome congression. BUB3.3 interacted with KINESIN-7O, a plant homolog of CENP-E, a protein known to promote chromosome congression, lateral to end-on conversion of kinetochore-microtubule attachments, and maintenance of end-on attachments. Single and double mutants of *BUB3.3* and *KIN7O* exhibited identical phenotypical defects, suggesting that the proteins work in the same pathway. I propose a revised model of the SAC, a novel mechanism for chromosome congression through a KIN7O-BUB3.3 module, and a potential role for chromosomes acting as spindle organizing centers *in planta*.

Finally, considering the propensity of plants for polyploidization and the challenges that polyploidization poses to the meiotic cell division machinery in particular, I wondered about a possible role of the SAC in tetraploid meiosis. A SAC-dependent metaphase delay was observed only in meiosis I, but neither in meiosis II nor mitosis. I hypothesize that it is caused by impaired chromosome bi-orientation due to multivalent formation and/or chromosome entanglement.

Zusammenfassung

Der Spindel-Kontrollpunkt (SK) ist ein evolutionär konservierter Kontrollpunkt bei Eukaryoten, der die Treue Chromosomentrennung gewährleistet, indem er den Beginn der Anaphase verhindert, bis alle Kinetochore in einer stabilen, bipolaren Konfiguration an Spindelmikrotubuli angeheftet sind. Der Mechanismus des SKs ist in Metazoen- und Hefemodellsystemen sehr gut verstanden, über andere Modellorganismen und Nichtmodellorganismen ist jedoch wenig bekannt.

In Anbetracht dessen, wie wirkungsvoll die Vergleichende Biologie bei der Aufklärung zentraler biologischer Prinzipien sein kann, machte ich mich daran, den meiotischen SK in *Arabidopsis thaliana* zu erforschen. Ich habe die Assoziation von SK-Komponenten mit dem Kinetochor zeitlich analysiert und dabei den schrittweisen Auf- und Abbau des Kinetochor-gebundenen SK-Komplexes enthüllt, der zumindest für eine dieser Komponenten durch drei konservierte Kinasen reguliert wird. Unter schweren Mikrotubuli-destabilisierenden Bedingungen konnte das aktive Kontrollpunkt-Signal nicht über 6 Stunden aufrechterhalten werden und die nukleare Hülle reformierte sich nach der Abschaltung des SK, ein Merkmal, das in der gesamten Pflanzenlinie erhalten geblieben zu sein scheint. Ich habe herausgefunden, dass BUB3.3 höchstwahrscheinlich keine echte SK-Komponente ist, sondern eher an der Ausrichtung der Chromosomen in der Metaphasenplatte beteiligt ist. BUB3.3 interagierte mit KINESIN-7O, einem pflanzlichen Homolog von CENP-E, einem Protein, von dem bekannt ist, dass es die Ausrichtung der Chromosomen in der Äquatorialebene fördert, die laterale Kinetochor-Mikrotubuli Anhaftungen zu frontalen umwandelt und die Aufrechterhaltung der letzteren fördert. Einzel- und Doppelmutanten von *BUB3.3* und *KIN7O* wiesen identische phänotypische Defekte auf, was darauf hindeutet, dass die beiden Proteine Teil desselben Mechanismus sind. Ich schlage ein überarbeitetes Modell des SK vor, einen neuen Mechanismus für die Ausrichtung der Chromosomen in der Metaphasenplatte durch ein KIN7O-BUB3.3 Komplex und eine mögliche Rolle von Chromosomen als Spindelorganisationszentren in Pflanzen vor.

Angesichts der Neigung von Pflanzen zur Polyploidisierung und der Herausforderungen, die diese insbesondere für die meiotische Zellteilungsmaschinerie mit sich bringt, fragte ich mich schließlich nach einer möglichen Rolle des SK bei der tetraploiden Meiose. Eine SK-abhängige Metaphasenverzögerung wurde nur bei Meiose I, aber weder bei Meiose II noch bei Mitose beobachtet. Ich vermute, dass sie durch eine beeinträchtigte bipolare Chromosomen-Orientierung aufgrund der Bildung von Multivalenten und/oder Chromosomenverschränkung verursacht wurde.

General Introduction

Mitosis and meiosis can be compared to an elegant chromosome choreography that culminates in the equal chromosome segregation in two identical daughter cells in mitosis or four cells with half the genomic content of the parent in meiosis. However, despite its undoubted beauty and elegance, cell division like any other (cell) biological process is susceptible to errors; all the more so, because of the highly complex series of events that take place during preparation to divide and during the chromosome separation itself. Errors should be avoided at all costs because chromosome missegregation can have detrimental consequences not only for the daughter cells, but for the entire organism and/or the organism's progeny, potentially endangering genome stability over generations. Thus, it is no surprise that eukaryotes have evolved an extensive network of proteins that regulate the stepwise progress of the cell-cycle and license irreversibly the transition from one phase to the next (Harashima et al., 2013).

I became particularly interested in one specific licensing mechanism, called the spindle assembly checkpoint (SAC), that ensures proper chromosome segregation by prohibiting the metaphase-to-anaphase transition until all chromosomes are attached in a stable, bipolar orientation to spindle microtubules (MTs) (Lara-Gonzalez et al., 2021; London & Biggins, 2014; McAinsh & Kops, 2023; Musacchio, 2015). Although I am going to provide detailed, mechanistic insight into the SAC in the subsequent sections, suffice it to say for now that the importance of the SAC is evident by its remarkable conservation across the eukaryotic kingdom, suggesting that the core SAC system was set in place already in the last eukaryotic common ancestor (Kops et al., 2020; Vleugel et al., 2012). Equally astonishing is the major diversification that the SAC has undergone in the different lineages with gene duplications, deletions and/or fusions, indicating that the SAC might be evolutionarily adapted to the needs of the respective lineage/species (Kops et al., 2020). Indeed, flowering plants are such an appealing case study of SAC evolution, considering that the SAC is redundant for their survival and development under non-stress conditions as well as the divergence in protein interactions and

recruitment hierarchies compared to other organisms (de Oliveira et al., 2012; Komaki & Schnittger, 2017; Kops et al., 2020; Su et al., 2021; H G Yu et al., 1999).

A brief history of SAC research

The role of plants in paving the way to some of the major SAC discoveries has been rather underappreciated so far. The first observations hinting at the existence of a mechanism inhibiting premature anaphase onset were done in blood lily endosperm cells (Bajer & Molè-Bajer, 1955). Bajer & Molè-Bajer (1955) observed that the metaphase-to-anaphase transition was halted until all chromosomes aligned at the metaphase plate which they interpreted as a "wait" signal, though the role of the spindle-kinetochore connections in this process was not understood at the time. The existence of the spindle as a subcellular structure was already known since the 1870s (McIntosh & Hays, 2016), though it would take almost a century to establish that the spindle consists of MTs. This was discovered in plant cells (Ledbetter & Porter, 1963) and the spindle was subsequently shown to be a dynamic structure in annelid oocytes (Inoué & Sato, 1967). It was also generally recognized that the spindle interacts with and exerts pulling and pushing forces on the chromosomes (Maiato et al., 2017; McIntosh & Hays, 2016), though the fact that "spindle filaments" physically interact with a specific structure on the chromosome, called the kinetochore, was discovered only in the mid 1960s (Brinkley & Stubblefield, 1966). Detailed analysis of chromosome behavior in spermatocytes of several ostracods led Dietz (1957) to propose that only bi-oriented homologous chromosome pairs, i.e., homologs pulled from opposing spindle poles, are stabilized at the metaphase plate by tension forces generated through the spindle, while mono-orientation and pole-proximal localization are inherently unstable configurations that need to be rectified (Fig. 1). Inspired by this, Nicklas & Koch (1969) unequivocally demonstrated that tension forces exerted artificially on syntelically attached chromosomes, i.e., both kinetochores are attached to MTs emanating from the same spindle pole (Fig. 1), stabilized these erroneous attachments. These experiments triggered a decade-long debate, that still persists to this day, on whether tension generated by the spindle or MT

occupancy of the kinetochore or maybe both synergistically are sensed by the SAC, a topic that I will discuss in detail in the subsequent section.

The next great breakthrough regarding the SAC came in 1991 with two parallel, independent genetic screens in budding yeast for mutants unable to arrest in metaphase despite the absence of a spindle (Hoyt et al., 1991; Li & Murray, 1991). These screens identified most core components of the SAC that are conserved across species, marking the beginning of the molecular era of discoveries in the SAC. Considering the hypothesis formulated by the influential review of Murray & Kirschner (1989) a couple years before, i.e., that cells arrest in mitosis until the spindle has been properly assembled and that an incorrectly assembled spindle generates the "wait" anaphase signal, the checkpoint was called the "spindle assembly checkpoint", a misnomer that still persists to this day. The concept of cell-cycle checkpoints was proposed around the same time (Hartwell & Weinert, 1989) and it would take a couple more years to discover that the unattached kinetochores are the origin of the "wait" signal, providing evidence for attachment rather than tension being monitored (Rieder et al., 1994, 1995). The debate of attachment versus tension had officially begun.

End-on attachment or tension – The core SAC sensing conundrum
It is self-evident that there can be no tension without attachment, be it correct (amphitelic/bi-oriented) or incorrect (syntelic or merotelic) (Fig. 1). Inversely, lack of tension weakens K-MT attachments with kinetochores becoming even unattached (G.-Y. Chen et al., 2021; J. M. King & Nicklas, 2000), while tension strengthens K-MT attachments (Akiyoshi et al., 2010; Cane et al., 2013; G.-Y. Chen et al., 2021; J. M. King & Nicklas, 2000). Since it is very difficult to experimentally disentangle the two inherently intertwined processes, there has been a long debate regarding the input signal of the SAC. To complicate things even further, there are two distinct types of tension, namely (i) interkinetochore tension, i.e., the two sister chromatids/homologous chromosomes are pulled apart, and (ii) intrakinetochore tension, i.e. the kinetochore itself is deformed by forces exerted on it (Maresca & Salmon, 2009; Uchida et al., 2009, 2021). Furthermore,

there are also two types of attachment, namely (i) end-on attachments, i.e., kinetochores are attached to the plus-end of spindle MTs, and (ii) lateral attachments, i.e., kinetochores interact with the MT lattice mediated by variable motor proteins, such as the plus-end directed kinesin-7/CENP-E (Kapoor et al., 2006) (Fig. 1).
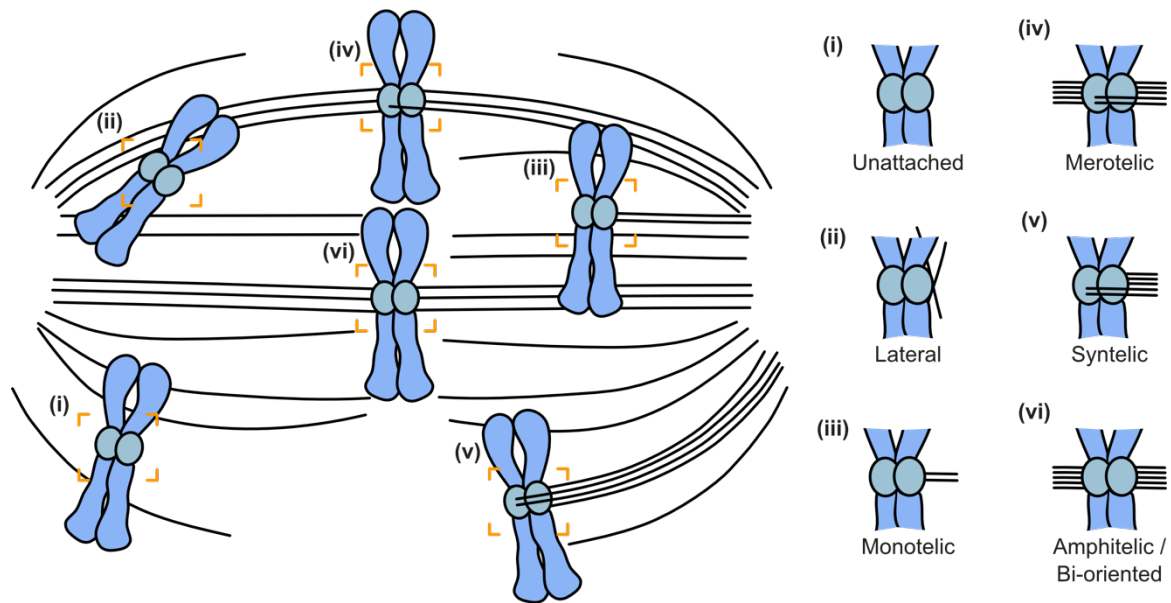
Figure 1 Schematic representation of all possible K-MT attachment configurations. An acentriolar, barrel-shaped plant mitotic spindle with multiple chromosomes was drawn based on figure 3 from Craske & Welburn (2020). The two oval structures in the center of each chromosome indicate the kinetochores of the two sister chromatids and the black lines represent MTs. **(i)** Unattached: Kinetochores are devoid of any K-MT connections. **(ii)** Lateral: Kinetochores interact with the lattice of adjacent kinetochore MTs or the lattice of randomly oriented MTs in the search and capture process during prometaphase. **(iii)** Monotelic: Only one kinetochore forms end-on K-MT attachments. **(iv)** Merotelic: One kinetochore forms K-MT attachments with MTs emanating from both spindle poles. **(v)** Syntelic: Both kinetochores form K-MT attachments with MTs emanating from a single spindle pole. **(vi)** Amphitelic / Bi-oriented: Kinetochores form K-MT attachments with MTs emanating from opposing spindle poles.

Several studies have tried to disentangle the contribution of end-on attachments in satisfying the SAC from tension-dependent mechanisms with variable degrees of success and the plethora of solid, yet at least partially contradictory, scientific results leave one baffled as to which is the major – if not the only – mechanism of SAC satisfaction. Although I wish to take no deliberate side in this debate, I will try to illustrate my view through a brief presentation of some convincing studies for both models which have been excellently reviewed in McAinsh & Kops (2023) (the

case for end-on attachment), as well as McVey et al. (2021) and Musacchio (2011) (the case for tension), and I will attempt a synthesis at the end bringing the two apparently opposing models together.

The case for end-on attachment

The arguments in favor of an attachment-dependent mechanism are numerous and very convincing. Our focus will be in human cells and not budding yeast, because in the latter a single MT binds per kinetochore (O'Toole et al., 1999; Weiss & Winey, 1996), a situation not found in human cells (McEwen & Dong, 2010) or presumably angiosperms (Jensen, 1982; Hong Guo Yu et al., 1997). I will succinctly illustrate a variety of treatments and genetic backgrounds that lower inter- and intrakinetochore tension, but generate end-on and not lateral K-MT attachments that eventually lead to SAC satisfaction (Drpic et al., 2015; Dudka et al., 2018; Etemad et al., 2015; Kuhn & Dumont, 2017, 2019; Magidson et al., 2016; O'Connell et al., 2008; Roscioli et al., 2020; Tauchman et al., 2015). (i) O'Connell et al. (2008) and Drpic et al. (2015) generated mitotic cells with unreplicated genomes, meaning that spindle MTs were pulling on unpaired kinetochores, i.e., no inter- but intrakinetochore tension could be generated (Drpic et al., 2015). They observed that the SAC was active in these cells and that it was eventually satisfied upon formation of end-on attachments. (ii) Tauchman et al. (2015) and Etemad et al. (2015) mutated a protein physically mediating K-MT attachments in a way that results in hyperstable K-MT attachments. Even when chromosomes were not aligned at the metaphase plate or could not be bi-oriented due to chemical induction of a monopolar spindle in the mutant cells, and without full intrakinetochore stretch, the SAC was still satisfied. (iii) The work of Kuhn & Dumont (2017) complemented these observations. They showed that end-on but not lateral attachments silenced the SAC and that tension generated through lateral K-MT attachments was not sufficient to inactivate the SAC. (iv) Furthermore, chemically or genetically lowering K-MT occupancy and thus, interkinetochore stretch, did not trigger the error correction machinery, and led to SAC satisfaction with submaximal K-MT occupancy (Dudka et al., 2018; Kuhn & Dumont, 2019). (v) Finally, Magidson et al. (2016) and Roscioli et al. (2020) confirmed that they could

not detect a central SAC component on tensionless, but only on unattached kinetochores. They also showed that unattached kinetochores are the cause for the metaphase arrest caused by taxol, a chemical that stabilizes MTs by preventing their depolymerization, and not the lack of inter- or intrakinetochore as previously thought. Indeed, K-MT attachments are weakened and, in some cases, completely dissociate due to the lack of tension, showcasing how intertwined the two processes are (G.-Y. Chen et al., 2021; King & Nicklas, 2000). Besides, Magidson et al. (2016) and Roscioli et al. (2020) could show that attachment to MTs with and without tension caused conformational rearrangements in two core components of the outer kinetochore as well as the shape of the outer kinetochore in general, hinting at distinct pathways from the SAC reacting to the status of attachment and tension. In conclusion, overwhelming amount of evidence suggests that the SAC senses K-MT end-on attachments and occupancy rather than inter- or intrakinetochore tension.

The case for tension

So, why even consider tension as a viable possibility, if all the latest research suggests otherwise? Scientific debate on the matter is very lively and follows in my view a very interesting trend. Tension was a very attractive hypothesis from the observations of Nicklas & Koch (1969) till the early 2010s as it provided a direct link between bi-orientation, the checkpoint and the error correction machinery. This was followed by a wave of studies presented in the paragraph above, which started from the mid 1990s with the seminal work of Rieder et al. (1995) and culminated in the 2010s. These studies suggested that the checkpoint machinery is satisfied only through end-on attachments independently of the tension status. However, as Musacchio (2011) has emphasized, the assumption that the mechanisms of error correction and spindle checkpoint are distinct is the root of the end-on attachment versus tension debate. Hence, Musacchio (2011) proposed an attractive synthesis, namely that the error correction and spindle checkpoint machinery constitute a single sensory apparatus.

It is the protein kinase Aurora B that muddies the waters between the error correction and spindle checkpoint machinery. On the one hand, Aurora B destabilizes incorrect attachments by phosphorylating key kinetochore components mediating K-MT attachments (DeLuca et al., 2011; Welburn et al., 2010; Yoo et al., 2018; Zaytsev et al., 2014). By creating unattached kinetochores, it triggers the SAC, which in turn inhibits the metaphase-to-anaphase transition until all chromosomes have formed stable, end-on attachments with spindle MTs. On the other hand, Aurora B, called Ipl1 in budding yeast, appears to monitor and respond to the tension status of kinetochores by differentially phosphorylating targets that regulate K-MT attachments (Biggins & Murray, 2001; Mukherjee et al., 2019; Welburn et al., 2010). The recent study by G.-Y. Chen et al. (2021) provides, for instance, evidence for distinct Aurora B-mediated tension-dependent error-correction pathways for syntelic (low interkinetochore tension) and merotelic (high intrakinetochore tension) attachments in human cells. Along these lines, Cane et al. (2013) show how the Aurora B-mediated error-correction can be overridden by molecularly increasing tension across syntelically attached chromosomes in fruit fly mitotic cells, hyperstabilizing these erroneous attachments not unlike what Nicklas & Koch (1969) reported more than half a century ago. The detailed models regarding tension sensing by Aurora B are intriguing, yet beyond the scope of this chapter and the interested reader is referred to the excellent review by McVey et al. (2021). A lot more prescient is the question posed by Musacchio (2011), which, in my opinion, also settles the debate of the dichotomy between the error correction and the spindle checkpoint mechanism. If Aurora B is directly implicated in the SAC, in addition to its undeniable function in error correction, then one should favor the idea that error correction and the SAC are a single, complex sensory apparatus with multiple branches that feedback on each other. Indeed, several studies show a direct role of Aurora B in regulating the SAC (Foley et al., 2011; Hauf et al., 2003; Liang et al., 2020; Roy et al., 2022; Santaguida et al., 2011; Saurin et al., 2011) and vice versa (Broad et al., 2020; Hadders et al., 2020; Jelluma et al., 2008; Van Der Waal et al., 2012). So, although the SAC senses K-MT end-on attachments and occupancy, tension directly feedbacks on these parameters, suggesting that

the answer lies potentially neither completely here nor completely there, but as is often the case, somewhere in the middle.

An attempt at a synthesis

As Musacchio (2011) has proposed, it is rather difficult to envision two distinct biochemical pathways, that (i) sense different, yet deeply interrelated mechanochemical aspects of K-MT attachments (end-on attachment and tension), (ii) their components cross-regulate each other and are involved in aspects of both pathways, and (iii) their components localize close to each other, since kinetochore-proximal pools of Aurora B have been discovered as well (Broad et al., 2020; Hadders et al., 2020; Liang et al., 2020). They rather suggest that the two pathways are part of a single sensory apparatus that performs the functions of error correction as well as spindle checkpoint signaling.

I would like to expand on this thought and without wanting to discount the essential contributions of many labs and their brilliant research, I would like to argue from the point of view of biological relevance on the dichotomy of end-on attachment versus tension. Besides the fact that the two pathways complement each other and are intertwined on multiple levels, the works supporting the prevalence of end-on attachment and the irrelevance of tension have reached this conclusion by inducing artificial situations that are very far from anything a cell would encounter in nature (e.g. monopolar spindles). Although this is undoubtedly a quintessential way to learn about the inner workings of biochemical pathways, it begs the question of whether these conclusions would hold true in a more nuanced situation like the one found in natural settings, i.e., an intermediate situation where both attachment and tension co-exist and fluctuate to different extents.

The fact that the SAC is triggered by unattached or insufficiently occupied kinetochores and similarly, silenced, when a threshold of end-on K-MT attachments is reached, is based on solid scientific evidence (reviewed in Lara-Gonzalez et al., 2021; London & Biggins, 2014; McAinsh & Kops, 2023; Musacchio, 2015). Additionally, recent works have highlighted that the response of the SAC is

not an "all-or-nothing" but rather proportional to the number of unattached or insufficiently occupied kinetochores (Collin et al., 2013; Dick & Gerlich, 2013; Etemad et al., 2019). It is no surprise, in my opinion, that generating persistent and/or hyperstabilized end-on K-MT attachments, while lowering tension, eventually leads to SAC satisfaction, because one can imagine that low tension under high MT occupancy of kinetochores might not necessarily activate the error correction pathway. Indeed, it has been observed that metaphase plate aligned kinetochores come under low tension during chromosome oscillations in unperturbed metazoan metaphase cells (Burroughs et al., 2015; Wan et al., 2012). Besides, there are multiple feedback controls regulating the SAC and the error correction machinery preventing aberrant (de-)activation (Lara-Gonzalez et al., 2021; McAinsh & Kops, 2023; McVey et al., 2021). So, although tension is clearly neither sufficient nor necessary to silence the SAC, the established tension-responsiveness of Aurora B as well as its regulation of and by SAC components, suggest that the two pathways converge and are probably not distinct.

The plant SAC – A gateway to polyploidization?

Our knowledge of all these fascinating and complicated mechanisms, that I briefly highlighted above, stems to a disproportionately large extent from metazoan and yeast model systems. The rise of comparative biology and the obvious advantages that the study of analogous mechanisms in evolutionarily distant organisms brings with it have reignited the interest in studying the cell division machinery in other eukaryotic clades (reviewed in Akiyoshi & Gull, 2013; Drinnenberg & Akiyoshi, 2017; Komaki & Schnittger, 2016; Kops et al., 2020). These studies have revealed that while the level of mechanistic understanding that we have achieved studying traditional metazoan (e.g. fruit flies, frogs, mammals and worms) and yeast model organisms is beyond any doubt stunning, it is rather incomplete as it heavily skews our point of view to only one part of the eukaryotic evolutionary tree, namely opisthokonts (Burki et al., 2020).

The plant lineage is particularly interesting for studying the SAC, since plants have maintained a canonical SAC response, but have undergone significant diversifi-

cation in protein sequence due to loss of important protein-protein interaction motifs, and consequently, rearrangement of protein-protein interaction hierarchies as well as functional diversification, potentially through gene duplication events (Komaki & Schnittger, 2017; Kops et al., 2020; Su et al., 2021; Tromer et al., 2016; Vleugel et al., 2012). Additionally, the SAC is dispensable for survival and growth under non-stress conditions in plants (Komaki & Schnittger, 2017; H G Yu et al., 1999), which is reminiscent of the situation in budding yeast (Hoyt et al., 1991; Li & Murray, 1991). However, the arguably most interesting feature of the plant SAC is the fact that it is a weak checkpoint (Komaki & Schnittger, 2017). More specifically, mitotic plant cells when treated with a high concentration of a drug that inhibits MT polymerization, i.e., with no or at least no detectable MTs, silenced the checkpoint after about 2 hours and reformed a nuclear envelope (Komaki & Schnittger, 2017). Comparable observations have been made in other flowering plants (Molè-Bajer, 1958; Nebel & Ruttle, 1938). Under similar conditions, the single-cell algae *Chlamydomonas reinhardtii* can cycle through multiple rounds of DNA replication without nuclear division (Tulin & Cross, 2014) and somatic cells of the bryophyte *Physcomitrella patens* can become polyploid as a consequence of failed cytokinesis (Kozgunova et al., 2019). Considering that the last common ancestor of Streptophytes (Arabidopsis) and Chlorophytes (Chlamydomonas) was ~ 729 to 1106 million years ago (Kumar et al., 2022) as well as their strikingly similar behavior under severe MT-destabilizing conditions, one can hypothesize either convergent evolution or – much more likely – that this feature existed already in their last common ancestor. Interestingly, the fungus *Aspergillus nidulans* also silenced the SAC and reformed a nuclear envelope upon prolonged mitotic arrest (De Souza et al., 2011), potentially a case of convergent evolution for sessile organisms that move through space by growth.

Conclusively, the plant SAC exhibits some unique features that are of particular interest for at least two major reasons. First, plant breeders have exploited the propensity of plants for polyploidization upon treatment with MT poisons for the longest time as a method for crop improvement (Younis et al., 2014). Secondly, whole-genome duplication events (Bomblies et al., 2016; Comai, 2005; Hollister,

2015; Panchy et al., 2016; Van De Peer et al., 2017) and hybridization followed by polyploidization (P. S. Soltis & Soltis, 2009) are far from rare events in the evolutionary trajectory of green plants. A weak SAC might have facilitated these events, thus shaping the green plant evolution in its own way.

Scope of the thesis

The main research aim of the thesis was to expand our currently limited mechanistic knowledge of the Arabidopsis SAC. I decided to use male meiocytes as the model system in this endeavor due to (i) the importance of proper chromosome segregation in meiosis for the viability of the progeny and transgenerational genomic stability, (ii) highly synchronous initiation of metaphase within a single anther allowing for the simultaneous observation of multiple cells in metaphase, (iii) the mono-orientation of sister chromatid kinetochores in metaphase I generating a brighter signal than single sister chromatid kinetochores, and (iv) lack of growth-dependent movement in anthers contrary to mitotic cells in the root meristem.

In Chapter 1, I set out to generate a cytological and functional framework of the Arabidopsis meiotic SAC. Adapting and optimizing the live-cell imaging platform developed by Prusicki et al. (2019) for imaging with higher spatiotemporal resolution than previously possible, I have temporally dissected the association of SAC components with the kinetochore. I provide evidence for three conserved kinases recruiting a core SAC protein to the kinetochore and show that the meiotic SAC cannot be maintained for over 6 hours, similar to the observations in mitotic cells of various plant species reported in other studies. Finally, I show that a null mutant in *BUB3.3*, previously thought to be a core SAC component in Arabidopsis, exhibits chromosome alignment defects, prolonged metaphase duration both in meiosis and mitosis as well as synthetic lethality when combined with other SAC mutants, which is contradictory with a role of BUB3.3 in the SAC. These observations hint at BUB3.3 being involved in establishing K-MT attachments and promoting the alignment of chromosomes at the metaphase plate.

In Chapter 2, I expand on the work performed in Chapter 1. Initially, I show that BUB3.3's closest homologs, i.e., BUB3.1 and BUB3.2, are not involved in the BUB3.3 pathway or a parallel pathway promoting chromosome congression to the metaphase plate. Instead, BUB3.3 physically interacts and works in the same pathway as KINESIN-7O (KIN7O). Single and double *BUB3.3* and *KIN7O* null mutants exhibit identical phenotypical defects, i.e., defective chromosome metaphase plate alignment and prolonged metaphase I duration, with no additivity observed. Together with the work in Chapter 1, I propose that BUB3.3 is not a *bona fide* SAC component and has evolved new functions in plants distinct from the SAC. My work points to a revised model of the plant SAC and uncovers a mechanism for chromosome congression mediated by the previously unknown KIN7O-BUB3.3 module. Finally, several lines of evidence point to a potential role of chromosomes acting as spindle organizing centers in plants.

In Chapter 3, considering the propensity of plants for polyploidization as well as the challenges polyploidization poses to the meiotic recombination and subsequently, chromosome division machinery, I explored the role of the SAC in tetraploid meiosis. I observed that tetraploid metaphase I was prolonged in a SAC-dependent manner compared to its diploid counterpart. This was, however, not the case in tetraploid meiosis II and mitosis, during which sister chromatids and not homologous chromosomes are segregated. Based on my results, I propose that incorrect kinetochore orientation in multivalents and/or entangled chromosomes are the most probable cause for the delay observed in metaphase I.

In summary, this work sets the stage for future studies by generating a detailed framework of the meiotic SAC in diploid and partially in tetraploid Arabidopsis, proposes a revised model of the Arabidopsis SAC, elucidates the function of the KIN7O-BUB3.3 module in chromosome metaphase plate alignment, and finally, proposes a potential role of chromosomes in organizing spindle architecture in plant cells.

Chapter 1

A cytological and functional framework of the meiotic spindle assembly checkpoint in *Arabidopsis thaliana*

Konstantinos Lampou[1], Shinichiro Komaki[2], Franziska Böwer[1], Maren Köhler[1], Arp Schnittger[1]

[1] Department of Developmental Biology, Institute for Plant Sciences and Microbiology, University of Hamburg, 22609 Hamburg, Germany

[2] Graduate School of Science and Technology, Nara Institute of Science and Technology, Nara, 630-0192 Japan

Contributions of authors

All experiments were performed exclusively by me, Konstantinos Lampou, unless stated explicitly in the list below. I am deeply indebted to Dr. Shinichiro Komaki, Franziska Böwer, and Maren Köhler for their significant contributions to this work.

Dr. Shinichiro Komaki has conducted the following experiments:

i. All reporters used in this study were generated and transformed by Dr. Komaki. They were published in Komaki & Schnittger (2017).

ii. He introgressed the BMF3 and TUA5 reporter in the *mad2* and *mps1* background via genetic crossing (Komaki & Schnittger, 2017).

iii. He introgressed the TUA5 reporter in the *mad2, mps1* and *bub3.3* background via genetic crossing.

iv. He generated the *BUB3.3::gBUB3.3* construct and transformed it in *bub3.3*.

Franziska Böwer confirmed my observations in several independent *bub3.3-2* transgenic lines with a chromosome marker and a tubulin reporter (data not included in the manuscript). We received the lines from the Bo Liu lab at UC Davis.

Maren Köhler has performed the semi-qRT expression analyses of Col-0, *bub3.3* and *bub3.3-2* seedlings.

Chapter organization

The chapter is written in the form of a manuscript, including the following sections: Abstract, Introduction, Results and Discussion, and finally, Materials and Methods. The main figures are designated as "Figure *X*", where *X* is the corresponding number starting at 1, and the supplementary figures are designated as "Figure EV*X*", where *X* is the corresponding number starting at 1, and "EV" stands for "expanded view". The supplementary figure(s) together with the main figure directly preceding it/them represent a thematical unit.

Abstract

The spindle assembly checkpoint (SAC) is a surveillance mechanism active during metaphase to prevent aneuploidy. The SAC is especially important during meiosis to maintain genome stability over generations and sustain fertility. However, despite its crucial role for reproduction and breeding, little is known about the plant meiotic SAC. Here, we present a cytological and functional framework of the SAC in male meiocytes of *Arabidopsis thaliana*. Using live-cell imaging, we have dissected the temporal association of SAC components with the kinetochore and have identified the three conserved kinases BMF1, MPS1, and AURORA as crucial regulators of the loading of BMF3 to kinetochores. Functionally characterizing core SAC components, we found that BUB3.3 has a predominant and previously not recognized function in chromosome congression. We suggest that BUB3.3 is involved in chromosome alignment. Furthermore, the meiotic SAC is only active for a limited time under severe microtubule-destabilizing conditions leading to the hypothesis that the relaxed nature of the meiotic SAC is a gateway to polyploidization and hence, might contribute to genome evolution in plants.

Introduction

Sexual reproduction requires the generation of gametes, which have only half of the chromosome number in comparison to their parental organism, so that after fertilization the full chromosome set is restored. The reduction of chromosome number relies on elaborated segregation events accomplished in meiosis.

The spindle assembly checkpoint (SAC) is a safe-guarding mechanism blocking the metaphase-to-anaphase transition in meiosis and mitosis until all kinetochores are correctly attached to spindle microtubules (MTs) emanating from opposing poles. Thus, the SAC ensures error-free chromosome segregation and consequently, defects in the SAC cause severe developmental maladies such as cancer and infertility. For this reason, the SAC has been well-explored in mammals. There, Mps1 is the conductor of SAC assembly. Mps1 is recruited to unattached kinetochores, where it phosphorylates several kinetochore components (Hiruma et al., 2015; Ji et al., 2015). These are recognized by Bub3 which further recruits Bub1 and BubR1 (Primorac et al., 2013; Vleugel et al., 2013, 2015). A Mad1-Mad2 heterotetramer binds then to Mps1-phosphorylated Bub1 (Ji et al., 2017; G. Zhang et al., 2017). Ultimately, the SAC produces a cytosolic inhibitor, the mitotic checkpoint complex (MCC), a tetrameric complex composed of BubR1, Bub3, Mad2, and Cdc20 (Sudakin et al., 2001). The MCC acts as a pseudosubstrate of the anaphase promoting complex/cyclosome (APC/C), a multi-subunit ubiquitin E3 ligase which licenses the metaphase-to-anaphase transition (Alfieri et al., 2016; Izawa & Pines, 2015; Lara-Gonzalez et al., 2011). Once all kinetochores are properly attached, the SAC is silenced.

Despite the overall similarities, there are kingdom- as well as species-specific features of the SAC. In our previous work, we studied the SAC in roots and functionally characterized the homologs of all SAC components in Arabidopsis revealing some conserved, but also several unique features of the plant mitotic SAC (Komaki & Schnittger, 2017). A characteristic feature of SAC proteins is their transient recruitment to and association with the unattached or incorrectly attached

kinetochore. Surprisingly, both BMF1, one of the three Arabidopsis Bub1/Mad3 family members, and MPS1 localize on the kinetochore throughout the cell-cycle. BMF1 was hypothesized to not be part of the SAC signaling cascade since the *bmf1* mutant is not hypersensitive to oryzalin, a drug that prevents MT polymerization (Komaki & Schnittger, 2017). MPS1, on the other hand, plays a key role in the plant SAC by recruiting MAD2 to the kinetochore. BubR1 functions seem to be shared between the two other Bub1/Mad3 family members, i.e., BMF2 and BMF3. BMF2 is probably part of the MCC as suggested by the presence of two KEN-boxes among other motifs essential for BubR1 function (Lara-Gonzalez et al., 2011; Malureanu et al., 2009), while BMF3 moves onto the kinetochore during prometaphase and is the platform upon which the MAD1-MAD2 complex assembles. Finally, there are three Bub3 homologs in Arabidopsis, of which only BUB3.3 appears to be involved in the SAC, while BUB3.1 and BUB3.2 localize to spindle MTs and are involved in phragmoplast formation (Komaki & Schnittger, 2017; H. Zhang et al., 2018). Reminiscent of yeast, the plant SAC is redundant for survival under non-stress conditions (Hoyt et al., 1991; Komaki & Schnittger, 2017; Li & Murray, 1991). On the other hand, under severe MT-destabilizing conditions, plant cells shut down the SAC after about 2 hours and rebuild a nuclear envelope, thus, generating a cell with a duplicated chromosome set.

Previous studies have indicated that there are differences between the meiotic and mitotic SAC (Gorbsky, 2015). Despite its importance for the viability of the progeny, little is currently known about the plant meiotic SAC. At the same time, meiocytes in Arabidopsis could be a powerful model system to study the SAC since meiotic divisions are highly synchronous in anthers, the male sexual organs (Prusicki et al., 2019). Moreover, due to the mono-orientation of kinetochores of the sister chromatids in meiosis I, it is presumably easier to detect and follow SAC components in comparison to the single sister chromatid kinetochores in mitosis.

Here, we have set out to generate a cell-biological and functional framework of the Arabidopsis SAC in meiosis. Using live-cell imaging of male meiocytes, we first explore dynamics of the SAC assembly and disassembly on kinetochores and

explore which kinases likely play a part in this. Interestingly, while our work shows that BMF1 is involved in the plant SAC, we also reveal that BUB3.3 does not seem to be a *bona fide* SAC component but rather promotes chromosome alignment to the metaphase plate.

Results and Discussion

Spatiotemporal localization and stepwise (dis-)assembly of SAC components in meiosis I

Using the functional genomic reporters developed previously (Komaki & Schnittger, 2017), we explored the localization of SAC components in space and time in meiosis I (Fig. 1) and meiosis II (Fig. EV1). TUA5 fused to TagRFP was used to identify meiotic stages based on MT organization patterns (Prusicki et al., 2019). Importantly, the TUA5 reporter also allowed us to visualize the spindle and monitor the timing of nuclear envelope breakdown (NEB) until anaphase onset (AO).

With the exception of the cytosolic localization of BMF2 and BUB3.3 (Fig. EV1A), all SAC reporters exhibited a dotted appearance indicative of their localization at kinetochores (Fig. 1A) similar to mitosis (Komaki & Schnittger, 2017). In contrast to human mitotic cells (Overlack et al., 2015; Stucke et al., 2002; Vleugel et al., 2015), but similar to mitosis in Arabidopsis, MPS1 and BMF1 localized on kinetochores already before NEB (Fig. 1A).

As a next step towards a cytological framework of the SAC, we sought to quantify when the other SAC proteins appeared on and disappeared from the kinetochore relative to the NEB in meiosis I. With a frame rate of 20 seconds, we determined that BMF3 appeared first on kinetochores after NEB, quickly followed by MAD1, and then, MAD2, which became visible on average after ~ 100 seconds after NEB (Fig. 1A, B). To better resolve the relative timing of BMF3 and MAD1, we then recorded movies with a frame rate of 5 seconds, revealing that BMF3 needed on average ~ 30 seconds and MAD1 ~ 50 seconds to appear on the kinetochore (Fig.

1B, C). To assess the validity of our assays, we determined the duration of metaphase I in our reporter lines. Indeed, we did not observe any significant difference in the duration of NEB to AO (t_{NEB-AO}) among all our reporter lines, indicating that these reporters do not interfere with the progression of metaphase I (Fig. 1E).
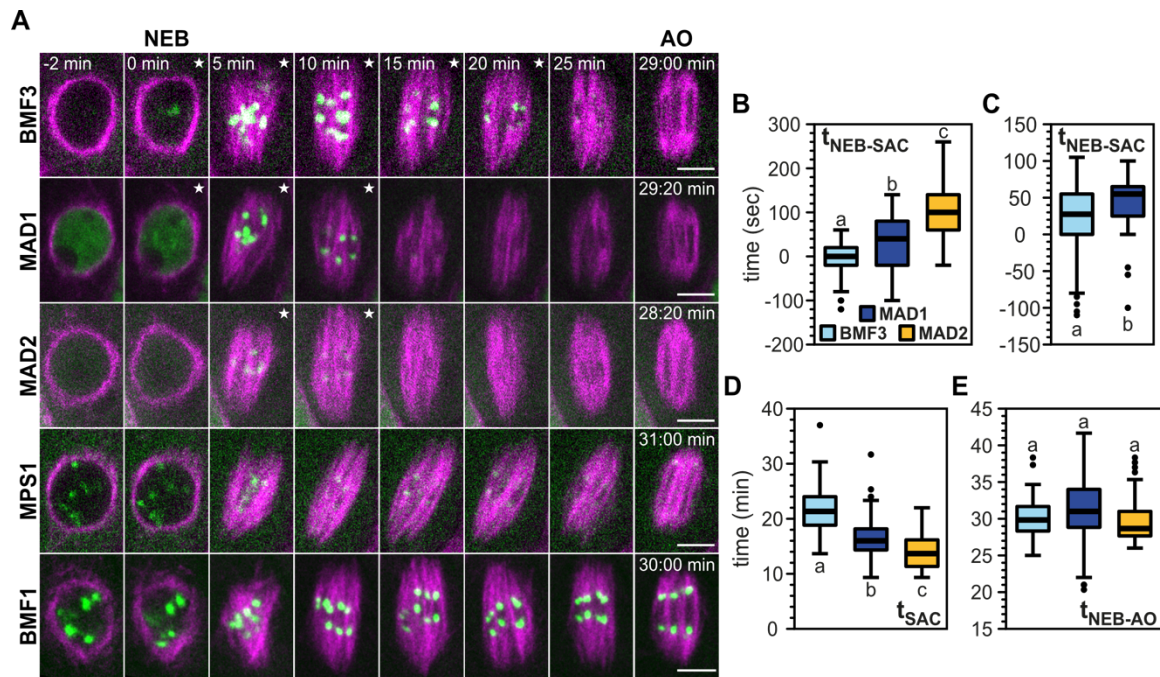
Figure 1 Spatiotemporal characterization of functional reporters of core SAC components in meiosis I. (A) Localization of core SAC proteins BMF3, MAD1, MAD2, MPS1, and BMF1 fused to GFP (green) together with TUA5 fused to TagRFP (magenta) decorating MTs in metaphase I. MPS1 and BMF1 localized at the kinetochore throughout metaphase and hence, they were excluded from further quantification in **(B)-(E)**. **(B, C)** Quantification of time needed for the kinetochore signal to appear relative to NEB. **(D)** Quantification of duration of the kinetochore signal for each reporter. To exemplify how we timed the kinetochore localization, the relevant frames are decorated with a white star (★) on the upper right corner. **(E)** Quantification of metaphase I duration defined as the time between NEB and AO for each reporter line. 2D movies were recorded with a frame rate of 20 **(A, B, D, E)** or 5 **(C)** seconds. For **(B, D, E)**, we used the same set of movies and quantified 44-84 cells from 8-9 different anthers for each reporter line. The values shown in **(C)** are from a different set of movies and we quantified 70-76 cells from 15-16 anthers for each reporter line. Different letters indicate significance (P < 0.01; pairwise comparison using Kruskal-Wallis test for independent samples with Bonferroni correction for multiple tests). Scale bars: 5 μm.

The disassembly of the kinetochore-bound SAC complex, determined by the disappearance of the dotty fluorescence signal, happened in the opposite order of the assembly, i.e., MAD2 disappeared first, i.e., ~ 14 minutes after NEB, followed by MAD1 after ~ 17 minutes, and finally, BMF3 after ~ 22 minutes (Fig. 1D). These

observations suggest a strict hierarchy in SAC association with and disassociation from kinetochores.
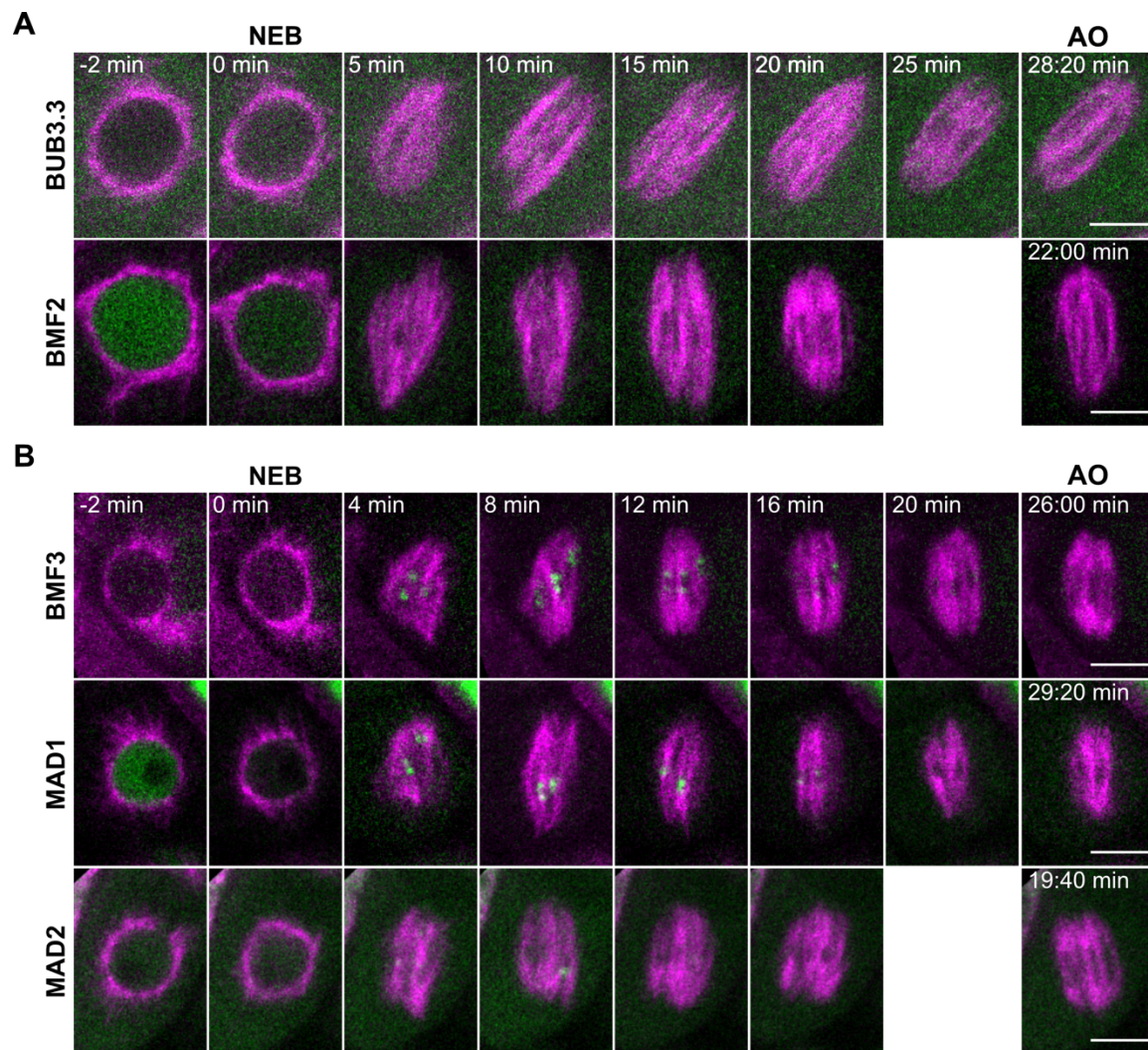
Figure EV1 Spatiotemporal localization of functional reporters of core SAC components in meiosis I and II. (A) Localization of BMF2 and BUB3.3 fused to GFP together with TUA5 labeled with TagRFP (magenta) in metaphase I. **(B)** Localization of BMF3, MAD1, and MAD2 fused to GFP (green) together with TUA5 labeled with TagRFP (magenta) in metaphase II. 2D movies were recorded with a frame rate of 20 seconds. Scale bars: 5 μm.

Next, we checked the localization of the BMF3, MAD1, and MAD2 reporters in meiosis II (Fig. EV1B). We did not observe any obvious difference between metaphase I and metaphase II. Hence, we will focus only on metaphase I from here onwards.

While the turnover dynamics of SAC proteins at the kinetochore have been studied extensively (Howell et al., 2004; Shah et al., 2004), to the best of our knowledge, there is no work in other model organisms showing the sequential association of SAC components with and disassociation from the kinetochore. Based on our observations, we conclude that the assembly and disassembly pattern reflect a general principle of SAC composition in Arabidopsis and likely other plant species.

BMF1, MPS1, and AURORA kinases positively affect the timely recruitment of BMF3 to the kinetochore

The stepwise (dis-)assembly of the SAC argued for a strict regulation of protein interactions at the level of the kinetochore, possibly through post-translational modifications. Phosphorylation is well known to control the interaction of SAC components and finetune the strength of the SAC in mammals, for instance by promoting the interaction of Bub3-Bub1 and Bub3-BubR1 dimers with Knl1 (preprint: Corno et al., 2022; Espert et al., 2014; Vleugel et al., 2013).

We have previously reported that the BMF3 kinetochore localization is not affected in *bmf1* and *mps1* mutants on a qualitative level (Komaki & Schnittger, 2017). Given the results above, we wondered, however, whether this would hold true on a quantitative level. For this, we genetically introgressed the BMF3 reporter into the *bmf1* and *mps1* backgrounds through crossing. When imaging these lines with identical settings, the BMF3 kinetochore signal in *bmf1* and *mps1* mutants appeared to be reduced compared to the wild type (WT) (Fig. 2A, EV2A). To quantify this effect, we measured the fluorescence intensity (FI) of BMF3 in the nucleus from NEB-AO. The BMF3 signal was normalized to the frame of the NEB and the maximum value for each cell was plotted (Fig. 2B). Our quantification uncovered a previously unnoticed effect of BMF1- and MPS1-dependent BMF3 recruitment to the kinetochore both regarding the protein amount (Fig. 2B) as well as the timing of recruitment ($t_{NEB-BMF3}$) (Fig. 2C).
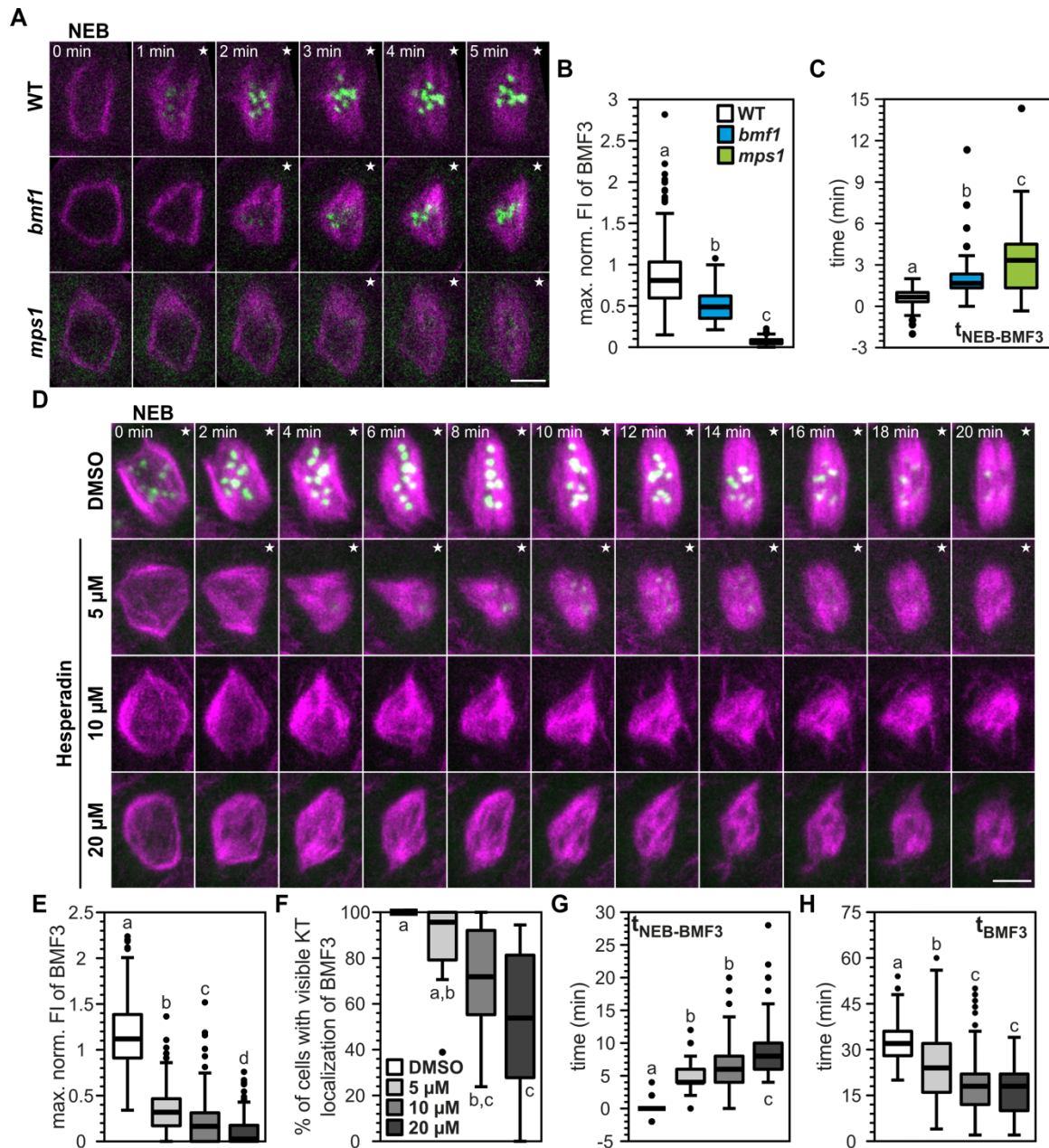
Figure 2 BMF1, MPS1, and AURORA kinases are involved in the kinetochore recruitment of BMF3 in metaphase I. (A) BMF3 recruitment in WT, *bmf1*, and *mps1* in metaphase I. BMF3 is fused to GFP (green) and TUA5 to TagRFP (magenta). **(B)** Quantification of maximum fluorescence intensity (FI) of BMF3 during metaphase I normalized to the frame of NEB: $(FI_{max}-FI_{NEB}) / FI_{NEB}$. **(C)** Quantification of time needed for the BMF3 kinetochore signal to appear relative to NEB. **(D)** Maximum projections of representative WT cells in metaphase I treated with 5, 10 or 20 μM hesperadin or the equivalent amount of DMSO. BMF3 is fused to GFP (green) and TUA5 to TagRFP (magenta). **(E)** Quantification of maximum FI of BMF3 during metaphase I normalized to the frame of NEB as in **(B)**. **(F)** Percentage of cells per anther with visible BMF3 on the kinetochore during metaphase I. **(G)** Quantification of time needed for the BMF3 kinetochore signal to appear relative to NEB. **(H)** Quantification of duration of the BMF3 kinetochore signal. The white star (★) on the upper right corner of the frames indicates BMF3 kinetochore localization. Movies were recorded with a frame rate of 20 seconds **(A-C)** or 2 minutes **(D-H)**. For **(A-C)**, we quantified 63-242 cells from 6-19 anthers per genotype. For **(E-H)**, we quantified 151-339 cells from 13-16 anthers per

40

treatment. Different letters indicate significance (P < 0.01; pairwise comparison using Kruskal-Wallis test for independent samples with Bonferroni correction for multiple tests). Scale bars: 5 μm.
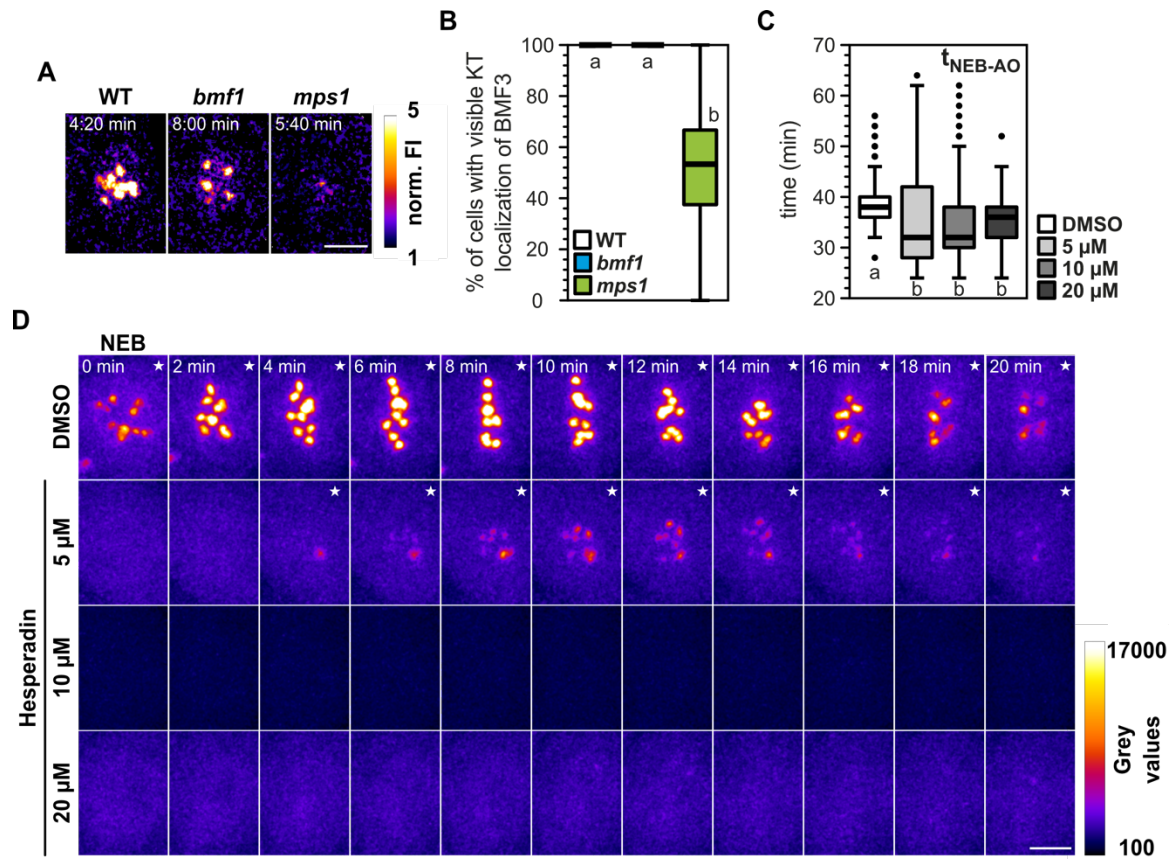
Figure EV2 BMF1, MPS1, and AURORA kinases are regulating the strength and timing of the BMF3 recruitment to the kinetochore in metaphase I. (A) Timepoints with maximum BMF3 FI from the same representative cells as in Fig. 2A. The FI was normalized to the timepoint of NEB. BMF3 is pseudocolored to visualize the decrease in normalized BMF3 signal strength in the *bmf1* and *mps1* backgrounds relative to the WT. **(B)** Percentage of cells per anther with visible BMF3 kinetochore signal during metaphase I. We quantified 75-225 cells from 6-19 different anthers per genotype. **(C)** Metaphase I duration of cells treated with 5, 10 or 20 μM hesperadin or the equivalent amount of DMSO. We quantified 263-339 cells from 13-16 different anthers per treatment. **(D)** Maximum projections of the BMF3 channel of the WT cells shown in Fig. 2D, which were treated with 5, 10 or 20 μM hesperadin or the equivalent amount of DMSO. BMF3 is pseudocolored to visualize the negative correlation between the BMF3 signal strength and hesperadin concentration. The white star (★) on the upper right corner of the frames indicates BMF3 kinetochore localization. Different letters indicate significance (P < 0.01; pairwise comparison using Kruskal-Wallis test for independent samples with Bonferroni correction for multiple tests). Scale bars: 5 μm.

Additionally, we scored visually whether the BMF3 kinetochore signal appeared after NEB. While 100 % of WT and *bmf1* cells displayed a BMF3 kinetochore signal, the percentage of cells having visually recognizable BMF3 kinetochore signal varied from 0 % to a 100 % in *mps1* anthers arguing for an especially prominent

role of MPS1 in recruiting BMF3 to the kinetochore (Fig. EV2B). It is unclear to us, what might cause the large variation between *mps1* cells with and without a recognizable BMF3 kinetochore signal within a single anther as well as between anthers.

There is strong evidence in mammalian cells that Aurora B (AurB) activates the SAC not only through destabilization of erroneous kinetochore-microtubule (K-MT) attachments but also through directly phosphorylating central regulators of the SAC (Roy et al., 2022; Santaguida et al., 2011; Saurin et al., 2011). There are two families of AUR kinases in plants: α-AUR kinases with AUR1 and AUR2 and β-AUR kinases with AUR3 (Demidov et al., 2009). AUR3 is the closest homolog of the mammalian Aurora B (AurB). AUR1 and AUR2 localize to the spindle while AUR3 localizes to the centromere during metaphase (Demidov et al., 2009; Komaki et al., 2020; Komaki & Schnittger, 2017). Hence, we hypothesized that the AUR kinase family might influence the plant SAC assembly and/or function in parallel to MPS1 and BMF1.

To test this hypothesis, we decided to use hesperadin, an AurB-specific inhibitor in mammals (Hauf et al., 2003), that has been shown to inhibit at least two of the three plant AURs, albeit AUR1 is inhibited at a much lower concentration than AUR3 (Demidov et al., 2009; Kurihara et al., 2006). We treated flowers with 5, 10 or 20 μM hesperadin or the equivalent amount of DMSO (Fig. 2D, EV2D). Similar to *bmf1* and *mps1*, increasing concentration of hesperadin resulted in ever decreasing maximum FI of BMF3 kinetochore signal (Fig. 2E) and fewer cells having a visible BMF3 kinetochore signal (Fig. 2F). Furthermore, the BMF3 kinetochore signal appeared at an increasingly later time after NEB (Fig. 2G) and persisted for shorter (t_{BMF3}) with higher concentrations of hesperadin (Fig. 2H). In addition, the spindle architecture became severely affected with an increasing concentration of hesperadin (Fig. 2D) while the metaphase I duration – albeit significantly ($P < 0.01$) shorter than in the DMSO control – remained unchanged with an increasing concentration of hesperadin (Fig. EV2C).

In conclusion, the major kinases BMF1, MPS1, and the AURORA family are orchestrating the timely and sufficient assembly of the SAC by regulating either directly or indirectly BMF3 localization. Given the AUR1/2/3 localization patterns, AUR3 is most probably responsible for recruiting BMF3 to the kinetochore. Considering that AurB and Mps1 both regulate each other (Jelluma et al., 2008; Santaguida et al., 2011; Saurin et al., 2011; Van Der Waal et al., 2012) and that AurB also regulates Bub1 in mammalian cells (Roy et al., 2022), it would be interesting to untangle in the future whether AUR3 is regulating MPS1 and BMF1 in plants and/or vice versa.

Putting the meiotic SAC to a test

As a next step, we decided to test whether the meiotic SAC is functional, considering that SAC mutants in Arabidopsis do not exhibit any severe developmental defects (Komaki & Schnittger, 2017). First, we compared the duration of the BMF3 kinetochore signal, which from here onwards we use as a proxy for an active SAC, and the metaphase I duration in the WT versus *mad2* (Fig. 3A, B). In support of an active meiotic SAC, the BMF3 kinetochore signal persisted for shorter in *mad2* (Fig. 3B) and correspondingly, the duration of metaphase I was ~ 30 % shorter than in the WT.

A prolonged SAC-dependent metaphase arrest can be caused in most animal and fungal cells by drugs that depress MT polymerization, such as oryzalin (Brito & Rieder, 2006; Rieder & Maiato, 2004). These drugs either weaken or abolish the formation of stable, end-on K-MT attachments, thus keeping the SAC in an active state. Supporting an active role of the SAC in meiosis, treatment with oryzalin led to a substantial increase in metaphase I duration in the WT but not in *mad2* mutants (Fig 3C, D).
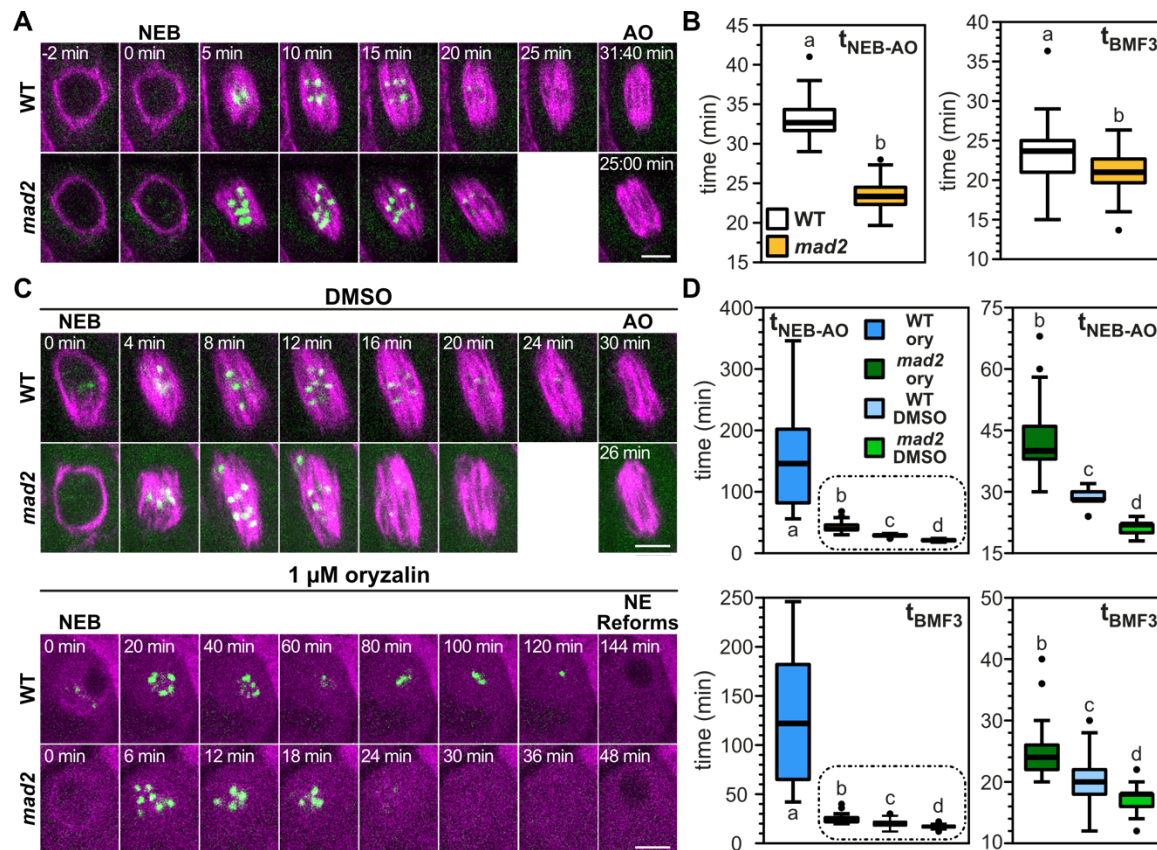
Figure 3 The meiotic SAC is functional, but permissive. (A) Representative WT and *mad2* cells. BMF3 is fused to GFP (green) and TUA5 to TagRFP (magenta). **(B)** Quantification of metaphase I (left) and of BMF3 kinetochore signal (right) duration in the WT and *mad2*. **(C)** Representative WT and *mad2* cells in metaphase I when treated with 1 *μ*M oryzalin or the equivalent amount of DMSO. Note that, in the oryzalin treatment, the SAC gets silenced and the NE reforms. **(D)** Quantification of metaphase I (up) and of BMF3 kinetochore signal (down) duration in the WT and *mad2*. The encircled box plots in the graphs on the left side, are shown larger on the right side. 2D movies were recorded with a frame rate of 20 seconds **(A, B)** or 2 minutes **(C, D)**. For **(B)**, we quantified 89-122 cells from 16-20 anthers per genotype. For **(D)**, we quantified 63-133 cells from 13-22 anthers per treatment and genotype. Different letters indicate significance (P < 0.01; pairwise comparison using Kruskal-Wallis test for independent samples with Bonferroni correction for multiple tests). Scale bars: 5 *μ*m.

Many animal and fungal cells that arrest in metaphase might either become apoptotic or exit mitosis without satisfying the SAC, a process termed "mitotic slippage" or "checkpoint adaptation" often causing aneuploidy (Rieder & Maiato, 2004). In contrast, mitotic slippage could not be detected in previous work analyzing Arabidopsis root cells (Komaki & Schnittger, 2017). Considering that there are noticeable differences between the mitotic and meiotic SAC activity in other species (Gorbsky, 2015), we monitored the SAC duration of oryzalin treated flowers and found that the metaphase I arrest in the WT was on average ~ 2.5

hours long and could never be sustained for longer than 6 hours (Fig. 3D). Correspondingly, the SAC was shut off within ~ 2 hours on average as indicated by the disappearance of the BMF3 kinetochore signal and eventually a NE reformed (Fig. 3C, D). This is reminiscent of the situation in Arabidopsis mitotic root cells, where an active SAC could be maintained for up to ~ 90 minutes (Komaki & Schnittger, 2017). Thus, SAC silencing followed by NE reformation appears to be a general principle of the Arabidopsis response to high concentration of MT-destabilizing drugs and possibly that of other plants (Molè-Bajer, 1958; Nebel & Ruttle, 1938). Surprisingly, all male meiocytes underwent a second NEB event marking the onset of meiosis II, indicating that NEB dynamics are independent of MTs (Fig. EV3A). In addition, we observed that interphase duration ($t_{Interphase}$) decreased from ~ 53-55 minutes in DMSO-treated cells to ~ 38-39 minutes in cells treated with oryzalin. Considering that this was the case both for the WT and *mad2*, this potentially indicates an important role of MTs in regulating directly or indirectly interphase duration.
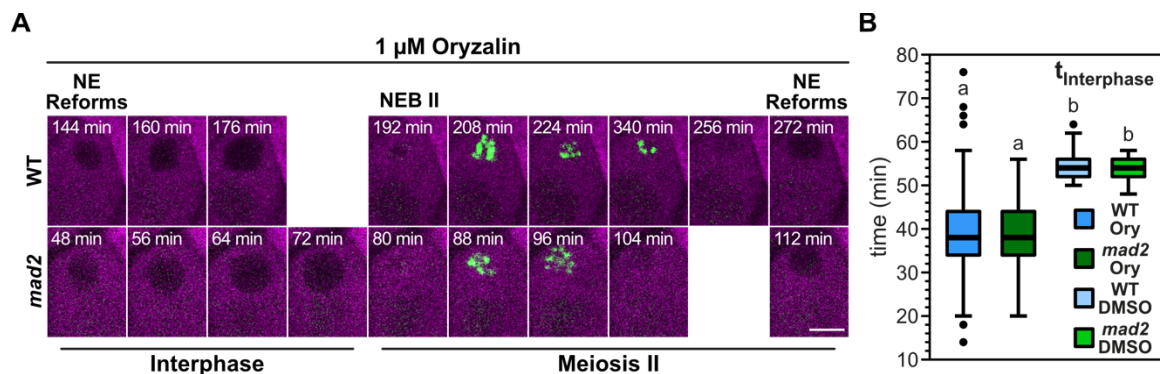
Figure EV3 Meiotic cells with depolymerized MTs proceed with meiosis II ending with a second NE reformation. (A) Interphase and metaphase II of the same representative WT and *mad2* cells as in Fig. 3C when treated with 1 μM oryzalin. BMF3 is fused to GFP (green) and TUA5 to TagRFP (magenta). Scale bar: 5 μm. **(B)** Quantification of interphase duration in the WT and *mad2*. 2D movies were recorded with a frame rate of 2 minutes. We quantified 69-119 cells from 13-22 anthers per treatment and genotype. Different letters indicate significance ($P < 0.01$; pairwise comparison using Kruskal-Wallis test for independent samples with Bonferroni correction for multiple tests).

It is noteworthy, that we observed meiocytes, which at the time they were placed on oryzalin, were in pachytene evident by the half-moon structure formed by MTs around the nucleus (Prusicki et al., 2019). We conclude that, once the commitment

to the meiotic program has been made, meiosis progresses even if essential components like MTs are not present. So, on the one hand, plant cells seem to be able to flexibly silence cell-cycle checkpoints such as the SAC or the pachytene checkpoint in order to progress with the meiotic program (De Jaeger-Braet et al., 2021; Chapter 1), but on the other hand, cannot escape from their commitment to the program itself.

In the single-cell algae *Chlamydomonas reinhardtii*, cells underwent several rounds of DNA replication without nuclear division under MT-destabilizing conditions (Tulin & Cross, 2014) and lagging chromosomes as well as cytokinesis failure in the bryophyte *Physcomitrium patens* led to somatic cell polyploidization (Kozgunova et al., 2019). Similarly, application of MT poisons, like colchicine, on mitotic cells of various angiosperms led to the re-formation of a NE without prior chromosome segregation (Molè-Bajer, 1958; Nebel & Ruttle, 1938), suggesting that NE reformation upon severe stress conditions is the rule rather than the exception in the plant lineage. Besides, colchicine and other drugs have long been exploited in plant breeding for generating polyploid offspring (Younis et al., 2014). Considering the prevalence, the challenges, but also the opportunities that whole-genome duplication events present (Bomblies et al., 2016; Comai, 2005; Hollister, 2015; Panchy et al., 2016; Te Beest et al., 2012; Van De Peer et al., 2017) as well as the evolutionary driving force of hybridization followed by polyploidization (P. S. Soltis & Soltis, 2009), we hypothesize that evolution in the plant lineage has been shaped by the weak nature of the SAC. A weak SAC could have facilitated major genomic changes to take place and hence, contributed to plant evolution.

Mutants in *BUB3.3* exhibit an unexpectedly long metaphase I and synthetic lethality in combination with mutants in other SAC components

Given a differential contribution of several SAC components in regulating metaphase duration in mammals (Meraldi et al., 2004) and yeast (Cairo et al., 2020; Vanoosthuyse et al., 2009; Yang et al., 2015), we next measured metaphase I duration in different SAC mutants. To this end, we divided the SAC mutants into two groups: (a) mutants of SAC genes that encode for kinetochore-bound proteins

(*mad1* and *mps1*) and (b) mutants of SAC genes that encode for proteins which are putatively components of the MCC (*bmf2* and *bub3.3*) (Komaki & Schnittger, 2017). Additionally, we looked at *mad2* which belongs to both groups.
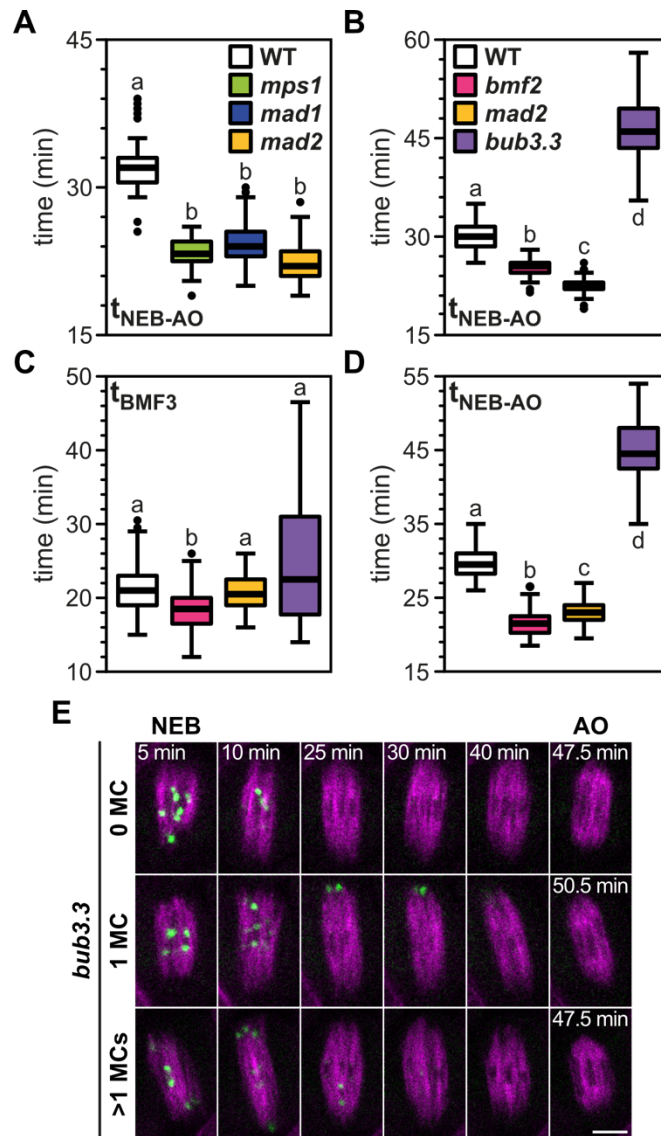
Figure 4 *bub3.3* **mutants exhibit prolonged metaphase I duration and delayed homologous chromosome pair congression to the metaphase plate. (A, B)** Quantification of metaphase I duration of WT and several SAC mutants whose proteins are either on the kinetochore **(A)** or presumably part of the MCC **(B)**. **(C, D)** Quantification of BMF3 kinetochore signal **(C)** and metaphase I **(D)** duration in the WT and SAC mutants. **(E)** Representative *bub3.3* cells with 0, 1 or multiple mislocalizing chromosome pairs (MCs) in metaphase I. BMF3 is fused to GFP (green) and TUA5 to TagRFP (magenta). 2D movies were recorded with a frame rate of 30 seconds. Scale bar: 5 μm. For **(A)**, we quantified 68-98 cells from 11-16 anthers per genotype. For **(B)**, we quantified 67-86 cells from 16-17 anthers per genotype. For **(C, D)**, we quantified 62-154 cells from 10-28 anthers per genotype. Different letters indicate significance (P < 0.01; pairwise comparison using Kruskal-Wallis test for independent samples with Bonferroni correction for multiple tests).

As expected, all three mutants of SAC components that encode for kinetochore-bound proteins had an ~ 30 % shorter metaphase I duration compared to the WT (Fig. 4A). Metaphase I duration in *bmf2* was ~ 20 % shorter compared to the WT (Fig. 4B). In striking contrast to all other SAC mutants, in *bub3.3* metaphase I was ~ 50 % longer compared to the WT (Fig. 4B). After confirming that *bub3.3* is a null allele, we also observed the prolonged metaphase I duration in a second null allele of *BUB3.3*, i.e., *bub3.3-2*, as well as an F1 cross between homozygous *bub3.3* and

bub3.3-2 plants (Fig. EV4B, L, M). Furthermore, metaphase I duration could be rescued to WT levels by the introgression of genomic *BUB3.3* expressed under its own promoter in the *bub3.3* background in three independent lines (Fig. EV4H).

We became particularly interested in *BUB3.3* due to the contradictory role of its homolog Bub3 observed in yeasts. Both in budding and fission yeast, *bub3-*depleted mitotic cells exhibited a prolonged AO delay because of – but not limited to – inefficient APC/C activation (Cairo et al., 2023; Vanoosthuyse et al., 2009; Yang et al., 2015). Intriguingly, in budding yeast, *bub3-*depleted meiotic cells have a shorter metaphase I and II duration than WT due to a disruption of the phosphorylation-dephosphorylation balance at the kinetochore (Cairo et al., 2020, 2023).

Considering that Bub3 has been implicated in proper chromosome segregation both in yeast (Cairo et al., 2020, 2023; Vanoosthuyse et al., 2009; Yang et al., 2015) and human cells (Logarinho et al., 2008), we scored pollen viability in *bub3.3* and found that it was the lowest among the WT, *bmf2*, and *mad2* (Fig. EV5A). To start untangling the function of *BUB3.3 in planta*, we, then, generated double mutants between *bub3.3* and mutants in core SAC components. Similar experiments in yeast mitosis have revealed a diversified role of Bub3. In fission yeast, the *mad2* mutation is epistatic, while in budding yeast, the *bub3* mutation is epistatic in the *bub3 mad2* double mutant (Vanoosthuyse et al., 2009; Yang et al., 2015). Hence, we chose to cross *bub3.3* with *mad1*, *mad2*, and *bmf2* mutants to test which of the mutations is either epistatic or additive in Arabidopsis. Notably, we could not obtain any viable double homozygous mutant with *bub3.3* (Fig. EV5B). Genotyping the progeny of *bub3.3 -/- mad2 +/-* and *bub3.3 +/- mad2 -/-*, we obtained a ratio of 89 : 150 WT : Heterozygous seedlings indicating that the double mutant is most probably sporophytic (embryonic) lethal. Consistent with a predominant sporophytic defect, we found that the transmission of the *bub3.3* allele was neither reduced when using the mutant as a male (1 : 1.48 WT : *bub3.3* T-DNA) nor as a female (1 : 1.53 WT : *bub3.3* T-DNA) parent in reciprocal crosses between *bub3.3 +/- mad2 -/-* and the WT (Fig. EV5C).
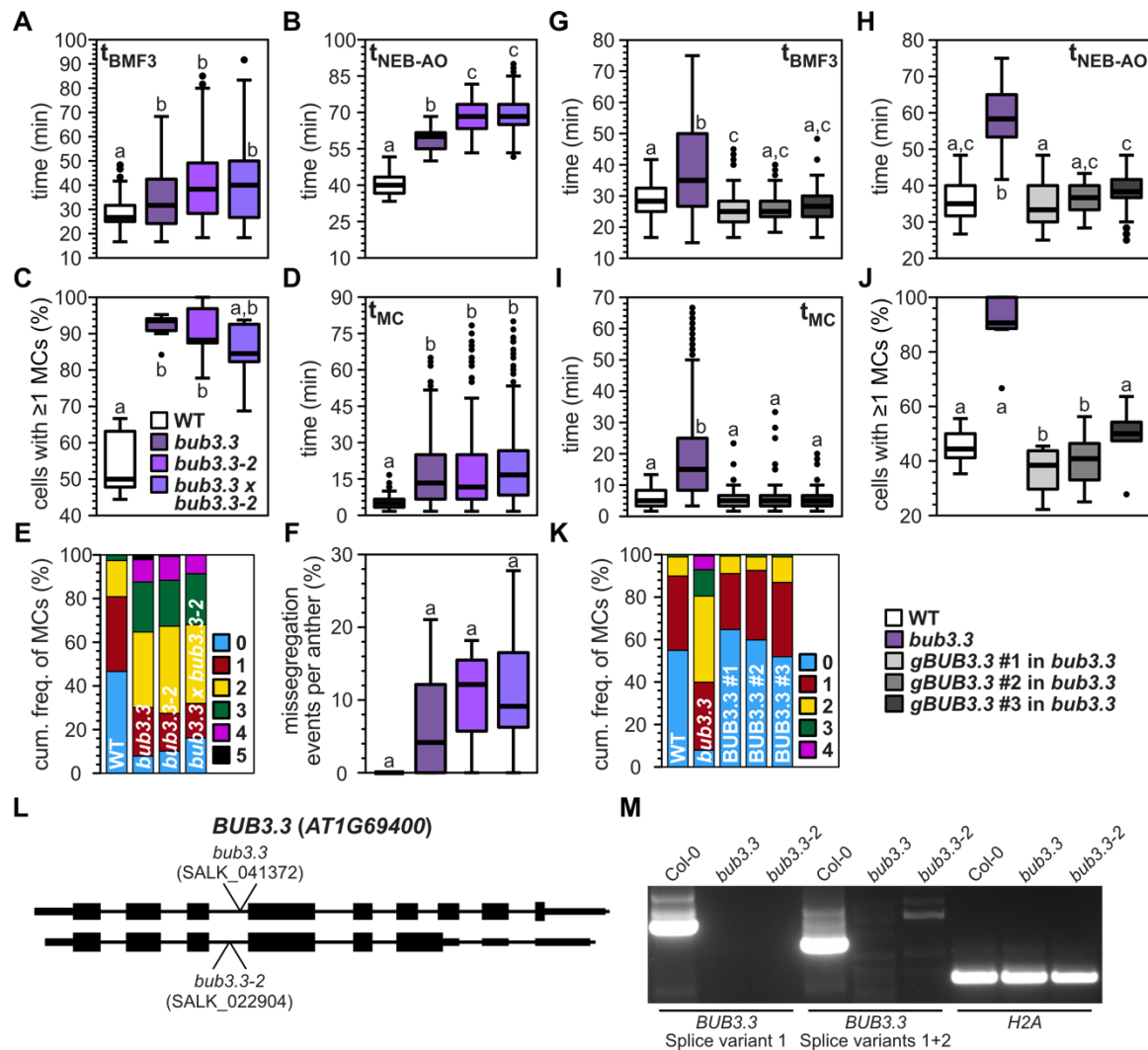
Figure EV4 gBUB3.3 rescues the aberrant meiotic phenotype of *bub3.3* in metaphase I, which is further confirmed by a second *bub3.3* allele. (A-F) Both *bub3.3-2* and the double heterozygous F1 cross *bub3.3 +/- x bub3.3-2 +/-* exhibit identical phenotypical defects to *bub3.3*. We quantified the duration of the BMF3 signal on kinetochores **(A)**, duration of metaphase I **(B)**, duration of chromosome pairs mislocalizing to the pole(s) **(C)**, percentage of cells per anther with at least one MC **(D)**, the cumulative frequency of the maximum number of MCs per cell **(E)**, and the percentage of missegregation events per anther **(F)**. **(G-K)** Three independent *BUB3.3::gBUB3.3* insertion lines in the *bub3.3* background were genetically crossed with the line expressing BMF3 and TUA5 in the *bub3.3* background. We quantified the duration of the BMF3 signal on kinetochores **(G)**, duration of metaphase I **(H)**, duration of chromosome pairs mislocalizing to the pole(s) **(I)**, percentage of cells per anther with at least one MC **(J)**, and the cumulative frequency of the maximum number of MCs per cell **(K)**. **(L)** Gene model of the two splice variants of *BUB3.3*. The arrows indicate the left border insertion site of the respective T-DNA. **(M)** RT-PCR of the full-length cDNA for either the large or both splice variants. We used *H2A* as a positive control. For **(A-F)**, we quantified 114-128 cells from 6-8 anthers per genotype. For **(G-K)**, we quantified 109-138 cells from 6-8 anthers per genotype. 3D movies were recorded with a frame rate of 100 seconds. Different letters indicate significance (P < 0.01; pairwise comparison using Kruskal-Wallis test for independent samples with Bonferroni correction for multiple tests).

A

pollen viability (%)

WT
bmf2
mad2
bub3.3

B

	mad1 -/-	*mad2 -/-*	*bmf2 -/-*
mad1 -/-		Viable	Viable
mad2 -/-	Viable		Viable
bmf2 -/-	Viable	Viable	
bub3.3 -/-	Lethal	Lethal	Lethal

C

Line (Female x Male)	*BUB3.3 +/+*	*bub3.3 +/-*	Ratio
Col-0 x *mad2 -/-; bub3.3 +/-*	126	187	1 : 1.48
mad2 -/-; bub3.3 +/- x Col-0	161	247	1 : 1.53

D

t_{NEB-AO}

time (min)

bmf2
mad1
mad2
bmf2 x mad1
bmf2 x mad2
mad1 x mad2

E

bub3.3

WT | 0 MC | 1 MC | 2 MC same pole | 2 MC different pole

F

relative frequency (%)

WT
bmf2
mad2
bub3.3

< 13 | 13-15.5 | 16-18.5 | 19-21.5 | 22-24.5 | ≥ 25

t_{BMF3} (min)
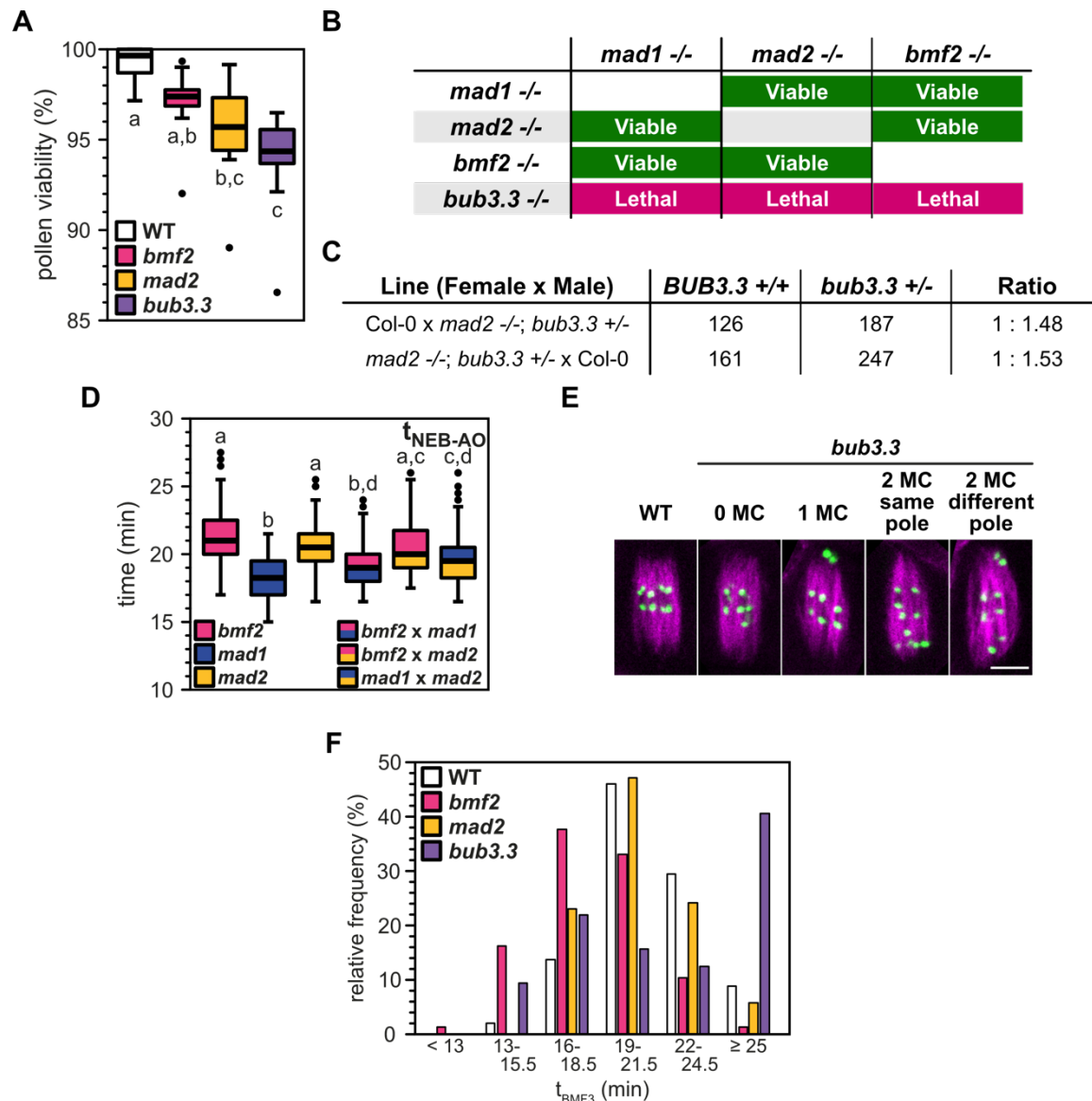
Figure EV5 Phenotypic description of SAC single and double mutants. (A) Pollen viability of the WT and several SAC mutants. **(B)** Summary of successful and failed double mutant combinations. **(C)** Genotyping results of the F1 progeny of reciprocal crosses between the WT (Col-0) and *mad2 -/-; bub3.3 +/-*. **(D)** Quantification of metaphase I duration of viable double mutants. We introgressed the *TagRFP:TUA5* reporter in the double mutants through crossing. 2D movies were recorded with a frame rate of 30 seconds. We quantified 79-120 cells from 13-22 anthers per genotype. Different letters indicate significance (P < 0.01; pairwise comparison using Kruskal-Wallis test for independent samples with Bonferroni correction for multiple tests). **(E)** Representative images of WT and *bub3.3* metaphase I. BMF1 is fused to GFP (green) and TUA5 to TagRFP (magenta). From left to right: WT, *bub3.3* with 0 MCs, *bub3.3* with 1 MC, *bub3.3* with 2 MCs on the same spindle pole, and *bub3.3* with 2 MCs on opposite spindle poles. Scale bar: 5 μm. **(F)** Relative frequency of the BMF3 kinetochore signal duration in the different groups for each genotype. We quantified the same 64-154 cells from 10-28 anthers per genotype as in Fig. 4C, D.

In contrast to double mutants of SAC components with *bub3.3*, we found that the combinations of other SAC mutants did not result in lethality (Fig. EV5B). We could

successfully obtain all homozygous double mutant combinations between *mad1*, *mad2*, and *bmf2*, i.e., *mad1* x *bmf2*, *mad2* x *bmf2*, and *mad1* x *mad2* (Fig. EV5B). We then measured metaphase I duration in these double mutants as it has been shown in HeLa cells that double knock-down of BubR1 and Mad2 has an additive effect suggesting that these proteins might inhibit the APC/C through parallel pathways (Meraldi et al., 2004). However, this does not seem to be the case for Arabidopsis as no additive effect on metaphase I duration could be observed in any of the double mutant combinations we generated (Fig. EV5D).

Prolonged metaphase I duration in *bub3.3* correlates with mislocalizing chromosome pairs to the spindle pole

The synthetic lethality of *bub3.3* with other SAC mutants, which has never been observed in any other system, prompted us to hypothesize that BUB3.3 might not be a core SAC component in Arabidopsis. In mammals and yeast, Bub3 interacts with both Bub1 and BubR1 and recruits them to the kinetochore via its recognition of and interaction with phosphorylated MELT motifs in Knl1/Spc105 (London et al., 2012; Overlack et al., 2015; Primorac et al., 2013; Shepperd et al., 2012; Vleugel et al., 2013, 2015). Both Bub1 and BubR1 have been implicated in the establishment of K-MT attachments and chromosome congression through distinct pathways (Lampson & Kapoor, 2005; Logarinho et al., 2008; Meraldi & Sorger, 2005). However, in plants BMF1 and BMF2, the respective homologs of Bub1 and BubR1, as well as BMF3 have lost the Gle2-binding sites (GLEBS domain), via which they interact with Bub3 (Larsen et al., 2007; Taylor et al., 1998; Wang et al., 2001). Consistently, it was recently shown in maize (*Zea mays*), that ZmBub3 does not interact in a yeast-two-hybrid assay neither with ZmKnl1 nor with ZmBmf1/2/3 (Su et al., 2021). Matching these interaction data, we found that the localization of both BMF1 and BMF3 in *bub3.3* was indistinguishable from the WT in metaphase I (Fig. 4E, EV5E).

To approach the question of what the function of BUB3.3 could be, we followed the BMF3 reporter in the *bub3.3* background and compared the phenotype to *bmf2* and *mad2*. In agreement with our previous results (Fig. 4B), the metaphase I

duration of *mad2* and *bmf2* were shorter while in *bub3.3* it was longer than in the WT (Fig. 4D). In contrast to metaphase I, the BMF3 kinetochore signal duration in *bub3.3* was not consistently longer than in the WT and exhibited a large variation in comparison to the other genotypes (Fig. 4C). We recognized that the *bub3.3* cells fall into two groups, with ~ 60 % of the cells having a similar distribution with the other genotypes and ~ 40 % having a prolonged BMF3 kinetochore signal persistence (Fig. EV5F). Upon closer inspection, we realized that *bub3.3* cells with a prolonged BMF3 kinetochore signal persistence exhibited a characteristic chromosome mislocalization phenotype, with individual or multiple homologous chromosomes mislocalizing to the spindle pole(s) (Fig. 4E). The two paired kinetochores tended to be at an almost right angle to the long axis of the spindle, indicating that most probably these kinetochores were unattached, poorly attached or syntelically attached to spindle MTs. This would also explain why these kinetochores were persistently highlighted by BMF3 in contrast to kinetochores that aligned efficiently in the metaphase plate. We did not observe a similar defect neither in *bmf2* nor *mad2*, suggesting that it is specific to *bub3.3*. All these observations were confirmed with a BMF1 reporter, introgressed in *bub3.3* as well *bmf2* and *mad2*, that labels the kinetochore independently of K-MT attachment status (Fig. EV5E).

Based on the synthetic lethality of *bub3.3* with all other SAC mutants tested and its unique chromosome mislocalization phenotype, BUB3.3 does not seem to be primarily involved in the plant SAC, but in a different pathway.

BUB3.3 is not a *bona fide* SAC component

Although, we could observe mislocalizing chromosome pairs in ~ 40 % of *bub3.3* cells, all of them had a comparatively equally long metaphase I (Fig. 4B, D, EV4B, H). So, we hypothesized that in our 2D movies we were likely underestimating the number of cells with aberrant chromosome behavior in *bub3.3*. Thus, we proceeded to generate 3D movies of WT, *bub3.3*, *mad2*, and *bmf2* to capture the entire cell volume. Our results regarding BMF3 kinetochore signal and metaphase I duration in 3D movies (Fig. 5A, B, EV4A, B) mirrored almost perfectly the results

obtained in 2D movies (Fig. 4C, D), confirming the large variation of SAC activity in *bub3.3* cells. Then, we quantified the proportion of cells exhibiting at least one mislocalizing chromosome pair (MC). This was the case for ~ 75 % of *bub3.3* cells compared to ~ 10 % for all other genotypes (Fig. 5B) and the ~ 40 % of *bub3.3* we had obtained from the 2D movies (Fig. EV5F). The MCs in *bub3.3* stayed at the spindle pole from several minutes to > 1 hour while in the other mutants they averaged out at ~ 5 minutes (Fig 5B). This reflected fully and essentially explained the large variation in SAC activity in *bub3.3* and reinforced the notion that the lack of proper chromosome-spindle MT attachment seems to be a stochastic, cell-autonomous process. Additionally, the distribution of the number of MCs per cell revealed that most *bub3.3* cells had only 1 MC in metaphase I, however, a substantial amount had 2 or more, which was rarely – if ever – the case in the WT, *mad2*, and *bmf2* (Fig. 5B). We consistently observed MCs both on the same or opposite spindle poles with no clear preference, suggesting that this process is also stochastic (Fig. 5A). Finally, with the exception of a single missegregation event observed in a *mad2* cell, missegregation events were regularly observed in *bub3.3* meiocytes (Fig. 5B).

All defects observed in *bub3.3* in metaphase I were recapitulated in *bub3.3-2* as well as the F1 cross between homozygous *bub3.3* and *bub3.3-2* plants in 3D movies (Fig. EV4A-F). Moreover, in 3D movies of metaphase I in the three rescue lines, the genomic *BUB3.3* construct brought the quantified parameters back to WT levels corroborating that loss of *BUB3.3* and not any other gene caused the above-described chromosome segregation defects (Fig. EV4G-K).

Similar results were obtained for metaphase II (Fig 5C). Here, we analyzed the two spindles in each cell individually, because (1) it was not always possible to capture both spindles due to their angle relative to our imaging axis and (2) in cells, where we could image both spindles, we did not find any apparent correlation between the behavior of the two spindles with regard to MCs. In metaphase II, we observed for all genotypes a higher proportion of spindles with at least one MC compared to

metaphase I. A similar trend was observed for the missegregation events per cell, which were more abundant compared to metaphase I (Fig. 5C).

Having analyzed the *bub3.3* phenotype in metaphase I and II, we asked whether this phenotype is also found in mitosis. This is especially interesting considering that partially opposing phenotypes in mitotic and meiotic *bub3*-depleted cells were described in budding yeast (Cairo et al., 2020, 2023; Yang et al., 2015). For this, we recorded 3D movies of mitotic root epidermal cells in the WT and *bub3.3* background. Recapitulating essentially our observations in meiosis, *bub3.3* cells stayed much longer in metaphase than the WT, exhibiting a prolonged BMF3 kinetochore signal due to MCs which persisted for up to ~ 1 hour (Fig. 5D, E). Additionally, in all observed *bub3.3* cells, we found at least two MCs. Given the progressive worsening of the *bub3.3* phenotype from metaphase I through metaphase II over to mitosis, it is tempting to speculate that perhaps kinetochore size, which becomes progressively smaller in these divisions, might play a role in that. It would be an interesting line of research to follow in the future, for instance in mutants with reduced centromere size (Capitao et al., 2021), considering similar work in animal cells (Drpic et al., 2018).

Conclusion

Surveillance of faithful chromosome segregation in meiosis is of key importance for fertility and transgenerational genome stability. Thus, studying the SAC is of great relevance to understand not only fundamental aspects of plant reproduction and evolution but is also highly relevant for plant breeding. Importantly, male meiocytes are a powerful model system to study the SAC due to their high level of synchronicity and their accessibility through an established live-cell imaging approach (Prusicki et al., 2019) together with the possibility to apply drugs such as the MT poison oryzalin (Sofroni et al., 2020; Chapter 1). Here, we have quantitatively assessed key parameters and properties of the SAC, such as the timing of its assembly and disassembly, setting the foundation for future studies of this checkpoint (Fig. 6). Our work has also allowed us to assign BUB3.3 a novel role in K-MT attachment and chromosome congression instead of a function in the

SAC (Fig. 6). These observations led us to a refined and temporally resolved model of the composition and regulation of the Arabidopsis core SAC comprising AUR1/2/3, BMF1, BMF2, BMF3, MAD1, MAD2, and MPS1 (Fig. 6).
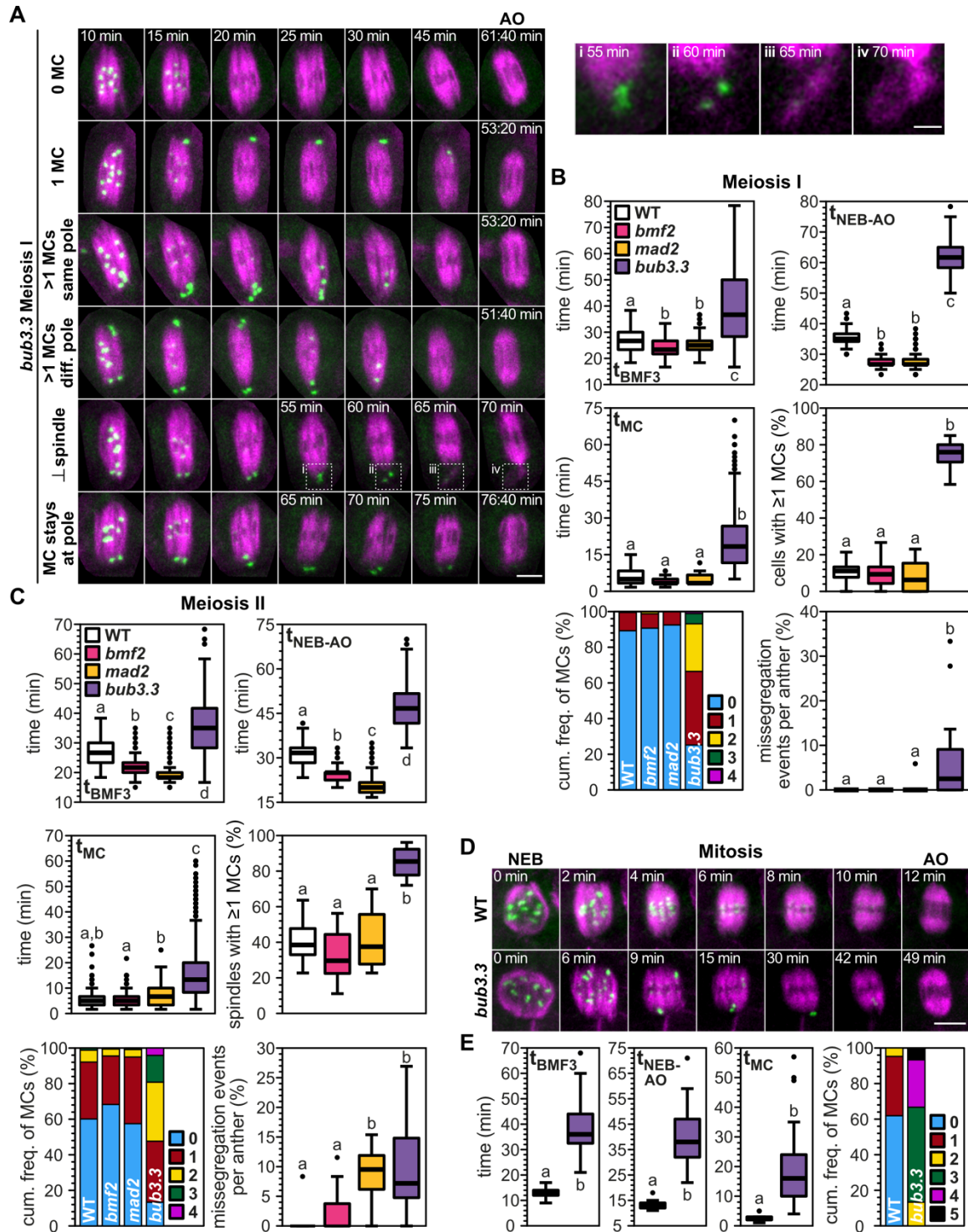
Figure 5 *bub3.3* **cells exhibit similar chromosome congression defects in meiosis and mitosis. (A-C)** We recorded 3D movies of WT, *bmf2*, *mad2*, and *bub3.3* anthers in meiosis I **(A, B)** and meiosis II **(C)** as well as movies of WT and *bub3.3* in mitosis **(D, E)**. **(A)** Representative maximum projections of *bub3.3* cells with 0, 1 or multiple mislocalizing chromosome pairs (MCs) in

metaphase I. BMF3 is fused to GFP (green) and TUA5 to TagRFP (magenta). In cells, where chromosome pairs persistently stay at the spindle pole, they missegregate either through the formation of a perpendicular (⊥) spindle or by staying at the spindle pole. In both cases, the BMF3 signal slowly fades indicating a silencing of the SAC. **(i-iv)** Insets highlight the formation of a perpendicular spindle. **(B, C, E)** We quantified the duration of the BMF3 signal on kinetochores, duration of metaphase, duration of chromosome pairs mislocalizing to the pole(s)**,** and the cumulative frequency of the maximum number of MCs per cell. For **(B, C)**, we quantified the percentage of cells per anther with at least one MC and that of missegregation events per anther. **(D)** Representative maximum projections of WT and *bub3.3* cells. 3D movies were recorded with a frame rate of 100 seconds **(A-C)** or 1 minute **(D, E)**. For **(B)**, we quantified 195-263 cells from 13-18 anthers per genotype. For **(C)**, we quantified 341-459 spindles from 15-22 anthers per genotype. Different letters indicate significance (P < 0.01; pairwise comparison using Kruskal-Wallis test for independent samples with Bonferroni correction for multiple tests). For **(E)**, we quantified 15-21 cells per genotype. Different letters indicate significance (P < 0.01; Mann-Whitney U test for independent samples). Scale bars: 5 μm **(A, D)** and 2 μm **(i-iv)**.

56
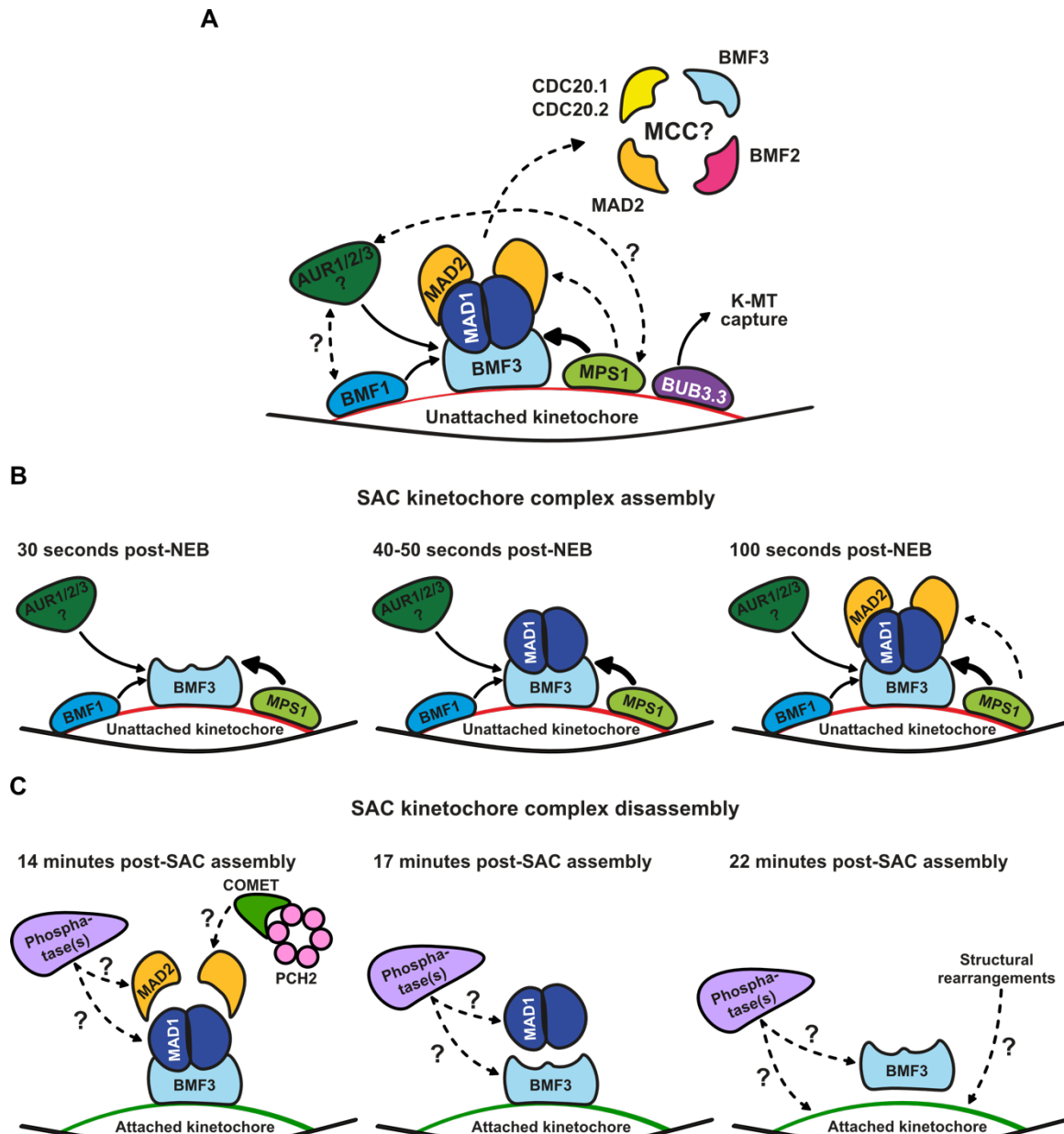
Figure 6 A revised model of the Arabidopsis SAC and the function of BUB3.3. Solid line arrows indicate conclusions from this study, dotted line arrows indicate conclusions from Komaki & Schnittger (2017), while dotted line arrows with question marks indicate hypotheses. **(A)** The timing as well as the protein amount of BMF3 recruited to the kinetochore is influenced by AURORA kinases, BMF1, and MPS1. Most probably, AUR3 – and not AUR1/2 – is responsible for the timely and sufficient recruitment of BMF3 to the kinetochore as it is localized at the kinetochore and/or centromere during metaphase. It remains to be determined whether AURORA kinase(s), BMF1, and MPS1 cross-regulate each other like in mammalian cells. Finally, BUB3.3 is probably not a *bona fide* SAC component and this is why it is probably not a component of the MCC in plants. The composition of the plant MCC still remains to be resolved. Additionally, BUB3.3 is not mediating the kinetochore anchorage of BMF1 or BMF3 in Arabidopsis. Thus, we hypothesize that, similarly to other organisms, BUB3.3 sits at the outer kinetochore, but has evolved novel functions. BUB3.3 is probably involved in K-MT attachment formation and chromosome congression. Conclusively, *BUB3.3* appears to have evolved a novel function in plants and, in contrast to other organisms, to not be a SAC component. **(B)** BMF3, MAD1, and MAD2 are recruited to the kinetochore in a stepwise fashion, where BMF3 comes first, followed by MAD1, and finally, MAD2. According to our data, this process is most probably regulated either directly or indirectly through multiple kinases. **(C)** The disassembly of the complex happens in the opposite order. Phosphatases have been shown to counteract the action of kinases and promote SAC silencing (Lara-Gonzalez et al., 2021). Their combined action fine-tunes SAC activity and eventually silences the SAC. The PCH2-COMET, complex which is present in Arabidopsis (Balboni et al., 2020), might be involved in removing MAD2 from the MCC and/or kinetochore-localized MAD1-MAD2 complex, since it has been shown to be involved in SAC silencing in mammalian cells (Lara-Gonzalez et al., 2021). Finally, outer kinetochore components undergo structural rearrangements upon K-MT attachment formation (Magidson et al., 2016; Roscioli et al., 2020), which might play a role in the disassociation of SAC components from the outer kinetochore.

Materials and Methods

Plant materials

We used the *Arabidopsis thaliana* (Arabidopsis) accession Columbia-0 (Col-0) as the wild type (WT) throughout this research and all mutant lines are in the Col-0 background. We used the following T-DNA insertion lines, which we obtained from the Nottingham Arabidopsis Stock Center (NASC) (http://arabidopsis.info/): SALK_122554 (*bmf1*), SAIL_303_E05 (*bmf2*), GABI_084G06 (*bmf3*), SALK_041372 (*bub3.3*), SALK_022904 (*bub3.3-2*), SALK_073889 (*mad1*), SAIL_191G06 (*mad2*), GABI_663H07 (*mps1*). All lines, except for *bub3.3-2*, were previously used in Komaki & Schnittger (2017). For *bub3.3-2*, we used the same genotyping primers as for *bub3.3* (Komaki & Schnittger, 2017).

For mitosis imaging, seedlings were grown for 4 days on a solid medium containing half-strength Murashige and Skoog (MS) medium, 1 % (w/v) sucrose, 0.8 % (w/v) agar, and pH 5.8 in a growth chamber (16 hours light at 21 °C / 8 hours dark at 18 °C). For imaging and phenotypic analyses of meiosis, 7- to 10-day old seedlings grown on plate as described above were transferred to soil and grown for 5-6 weeks in growth chambers (16 hours light at 21 °C / 8 hours dark at 18 °C).

Genotyping, T-DNA mapping, and RT-PCR

Primers for genotyping of T-DNA insertion lines are described in Komaki & Schnittger (2017). For, *bub3.3-2* we used the same genotyping primers as for *bub3.3* (Komaki & Schnittger, 2017). To map the T-DNA insertion in *bub3.3* and *bub3.3-2*, we used the left border primer SALK_Lb1.3 (ATTTTGCCGATTTCGG AAC).

For the reverse transcription-polymerase chain reaction (RT-PCR), we isolated RNA from ∼ 200 9-day old seedlings per genotype grown as described above. The seedlings were collected in an Eppendorf tube, flash frozen in liquid nitrogen and RNA was isolated according to the manual of the RNA-isolation kit (innuPREP Plant RNA Kit, Analytik Jena AG). cDNA synthesis was performed according to the manual of the cDNA synthesis kit (Thermo Scientific RevertAid Reverse Transcriptase, Thermo Fisher Scientific) using the Oligo(dT)18 primer. According to The Arabidopsis Information Resource (TAIR, https://www.arabidopsis.org/), there are two splice variants of *BUB3.3*, a long (Splice variant 1) and a short (Splice variant 2) variant. We performed two PCR reactions for each genotype using primers TCGGAATTCGAAATTGGGGA (fwd) and TGGTTGACACGAGTCAGTT CT (rev) to amplify the full-length of Splice variant 1 and primers TCTCCTCGTTGCTTCTTGGG (fwd) and GGCCAAGAGTTCTCCAGTGT (rev) to amplify both splice variants simultaneously. We used histone *H2A* as a positive control and primers ATGGCGGGTCGTGGTAAAACACTCGGATCT (fwd) and TC AATCGTCTTCAGCAGATGGCTTGGAAGCACC (rev).

Plasmid construction and line generation

All constructs – except for *BUB3.3::gBUB3.3* – were previously generated in Komaki & Schnittger (2017). To generate the *BUB3.3::gBUB3.3* construct, the *BUB3.3* gene, including 2 kb upstream of the start codon and 0.5 kb downstream of the stop codon, was amplified by PCR and cloned into *pDONR221*, followed by LR recombination reaction with the destination vector *pGWB501*. We used the following primers: GGGGACAAGTTTGTACAAAAAAGCAGGCTGCTCT AGATTTGCTTGTT (forward) and GGGGACCACTTTGTACAAGAAAGCTGGGT GATTCAGCGAAATCGGAA (reverse). The underlined part of the sequence indicates the *attB*-sites.

We introgressed all reporters from the WT into the mutant backgrounds through genetic crossing. We wanted to ensure that all lines carry the same reporter insertion(s), thus eliminating the possibility that variation in expression level due to insertion site would influence our observations.

Pollen viability

We used the Peterson staining protocol to score pollen viability (Peterson et al., 2010). Three mature flowers with dehisced anthers were dipped in 20 μl Peterson staining solution (10 % ethanol, 0.01 % malachite green, 25 % glycerol, 0.05 % fuchsin, 0.005 % orange G, and 4 % glacial acetic acid) and incubated for 1 hour at 95 °C. The samples were analyzed the same day.

Live-cell imaging

Live-cell imaging of anthers was performed using the protocol described in Prusicki et al. (2019) with slight variations. 40-80 flower buds were detached from the inflorescence stem keeping the pedicel intact and were placed on live-cell imaging medium as described in Prusicki et al. (2019). For 2D live-cell imaging, samples were prepared either on the same day or the day before and incubated overnight in the dark. For 3D live-cell imaging, samples were prepared on the day before and incubated overnight in the dark.

2D live-cell imaging of anthers was performed on a Zeiss LSM780 upright confocal laser scanning microscope (CLSM) equipped with a GaAsP-detector and a W-plan-Apochromat 40x/1.0 DIC M27 or a W-plan-Apochromat 63x/1.0 DIC water-dipping lens. 8-bit images were acquired using bi-directional scanning every 5 seconds to 2 minutes with 100-120 nm lateral pixel resolution, 4 times line average, 1.3-2.7 μs pixel dwell time, and a pinhole size of 1-2 AU (for the GFP detection channel). GFP was excited at 488 nm and emission was detected at 489-550 nm. TagRFP was excited at 561 nm and emission was detected at 565-650 nm. GFP and TagRFP were detected either sequentially using line-scan mode or simultaneously to increase the frame rate. In the latter case, to prevent crosstalk, TagRFP emission was detected at 576-655 nm.

3D live-cell imaging of anthers was performed on a Zeiss LSM880 upright CLSM equipped with a GaAsP-detector and a W-plan-Apochromat 40x/1.0 DIC M27 water-dipping lens. 16-bit images were acquired using bi-directional scanning every 100 seconds to 2 minutes with 84-96 nm lateral pixel resolution, 2 times line average, 1.04-1.18 μs pixel dwell time, and a pinhole size of 1.51 AU (for the GFP detection channel). z-stacks were acquired with a step-size of 0.93 μm. GFP and TagRFP were excited at 488 nm and emission was detected simultaneously at 490-553 nm and 579-651 nm, respectively.

For imaging of mitosis, we used 4-day old seedlings grown vertically as described above. Before imaging, the seedlings were carefully lifted from the growth medium and placed in a drop of liquid half-strength MS-medium on a glass-bottom dish. 5-8 seedlings were placed on each dish and then, the roots were covered with a strip of solid half-strength MS-medium.

3D live-cell imaging of mitotic root epidermal cells was performed on a Leica TCS SP8 inverted CLSM equipped with three hybrid photodetectors (Leica HyD™) and a HC PL APO 63x/1.2 W motCORR CS2 water-immersion objective. 12-bit images were acquired using bi-directional scanning every 1 min with 99 nm lateral pixel resolution, 4 times line average, at a speed of 700 Hz, and a pinhole size of 1.5

AU (for 510 nm emission wavelength). z-stacks were acquired with a step-size of 0.52 μm. GFP and TagRFP were excited at 488 nm and emission was detected simultaneously at 493-555 nm and 575-655 nm, respectively.

Oryzalin and hesperadin treatment

For the oryzalin treatment, we followed the protocol described in Sofroni et al. (2020) with slight variations. A 10 mM oryzalin (Duchefa Biochemie) stock solution was prepared in dimethyl sulfoxide (DMSO) and stored at -20 °C. 1:10,000 (v/v) stock solution or the equivalent amount of DMSO was added to the medium used for live-cell imaging. We always used freshly prepared plates. Flowers were incubated minimum 4-5 hours in the medium prior to live-cell imaging.

For the hesperadin treatment, we prepared a 10 mM hesperadin (Sigma-Aldrich) stock solution in DMSO and stored it at -20 °C. The appropriate amount of the stock solution was added to the live-cell imaging medium. As a mock treatment, we added 1:1000 (v/v) DMSO to the medium. We always used freshly prepared plates. Flowers were incubated for at least 12 hours in the medium prior to live-cell imaging.

Post-processing of movies and measurement of fluorescence intensity

We performed all post-processing operations and fluorescence intensity (FI) quantifications of our movies in Fiji (Schindelin et al., 2012).

For 2D movies, we only adjusted the brightness and contrast settings and extracted single cells manually using the rectangle selection tool.

For 3D movies, we performed two different protocols of post-processing for the BMF3 and the TUA5 channel, due to the different nature of the signal (spheres vs complex 3D structure of the spindle). For the BMF3 channel, we used the command "Gaussian blur 3D" with a sigma radius of 1 for x, y, and z. For the TUA5 channel, we followed a variation of the protocol presented in Krüger (2017). We, first, duplicated the movie using the command "Duplicate" with the setting

"Duplicate hyperstack". We renamed the two stacks as "GB_15" and "GB_0.5".
Next, we used the command "Gaussian blur 3D" with a sigma radius of 15 for x, y,
and z on "GB_15" and with a sigma radius of 0.5 for x, y, and z on "GB_0.5". Using
the command "Image calculator" we subtracted "GB_0.5" from "GB_15". This
operation removes the sharper signal from the blurred background and generates
the image "Background". Then, using again the command "Image calculator" we
subtracted "Background" from "GB_0.5", resulting in the image "TUA5_final". After
removing the background noise through these mathematical operations, we used
the command "Gaussian blur 3D" with a sigma radius of 0.5 for all dimensions on
"TUA5 final" to smoothen the image. Upon post-processing the two channels, we
extracted single cells manually using the polygon selection tool, the "duplicate"
command for the appropriate z-slice range for each cell, and then, the "clear
outside" command for each z-slice. Finally, we applied the "Z Project" command
with the setting "Max Intensity" for each cell and channel and adjusted the
brightness and contrast settings.

To measure the maximum BMF3 reporter FI, we manually drew an ellipse using
the elliptical selection tool in a way that all kinetochores labeled with BMF3 were
within the ellipse's boundaries throughout the movie. The FI was measured in all
frames from NEB to AO and normalized to the frame of the NEB, which we
designated as t_0. All other timepoints were designated as t_n, where n is the number
of the frame post-NEB. We used the following equation for normalizing the signal
intensity: $[FI(t_n) - FI(t_0)] / FI(t_0)$ and plotted the maximum normalized FI.

Statistics and figure design

All graphs and statistical operations were generated in IBM SPSS Statistics
Version 28 (IBM Corporation).

The boxplots highlight the 25th and 75th percentile indicated by the lower and upper
border of the box, respectively, the median with a thick line and the outliers within
1.5 times the interquartile range with the whiskers. Outliers outside this range are
indicated by dots above and below the whiskers.

We performed exclusively non-parametric statistical tests and our significance threshold was always $P < 0.01$. For comparisons between two genotypes, we performed a Mann-Whitney U test. For comparisons between multiple genotypes and/or treatments, we performed pairwise comparisons using a Kruskal-Wallis test for independent samples with Bonferroni correction for multiple tests.

The figures were assembled in Affinity Designer v. 1.10 (Serif).

Chapter 2

A KIN7O-BUB3.3 module promotes the establishment of kinetochore-microtubule attachments and chromosome congression in *Arabidopsis thaliana*

Konstantinos Lampou[1], Shinichiro Komaki[2], Maren Köhler[1], Arp Schnittger[1]

[1] Department of Developmental Biology, Institute for Plant Sciences and Microbiology, University of Hamburg, 22609 Hamburg, Germany

[2] Graduate School of Science and Technology, Nara Institute of Science and Technology, Nara, 630-0192 Japan

Contributions of authors

All experiments were performed exclusively by me, Konstantinos Lampou, unless stated explicitly below. I am deeply indebted to Dr. Shinichiro Komaki and Maren Köhler for their significant contribution to this work.

Dr. Shinichiro Komaki has generated and transformed all reporters used in this study. They were published in Komaki & Schnittger (2017). Additionally, he has cloned the yeast-two-hybrid constructs and performed the yeast-two-hybrid experiment.

Maren Köhler has performed the semi-qRT expression analyses of Col-0, *kin7n-1*, *kin7n-2*, *kin7o-1*, *kin7o-2*, and *kin7o-3* seedlings.

Chapter organization

The chapter is written in the form of a manuscript, including the following sections: Abstract, Introduction, Results, Discussion, and finally, Materials and Methods. The main figures are designated as "Figure *X*", where *X* is the corresponding number starting at 1, and the supplementary figures are designated as "Figure EV*X*", where *X* is the corresponding number starting at 1, and "EV" stands for "expanded view". The main figure and the supplementary figure(s) under the same sub-heading represent a thematical unit.

Abstract

Error-free chromosome segregation relies on the establishment and maintenance of bipolar kinetochore-microtubule (K-MT) attachments. The spindle assembly checkpoint (SAC) monitors K-MT attachments and prevents anaphase onset until all kinetochores are attached in a bipolar fashion to spindles MTs. SAC proteins, such as human Bub3, have been also implicated in regulating the formation of end-on K-MT attachments. We have previously observed chromosome mislocalisation and alignment defects in *bub3.3* cells in Arabidopsis, *BUB3.3* being one of the homologs of *Bub3*, and proposed that BUB3.3 is not a *bona fide* SAC protein. Here, we expand on this work and show that BUB3.3 physically interacts with KINESIN-7O, an Arabidopsis CENP-E homolog. We propose that both proteins work in the same pathway suggesting that – contrary to Bub3 in yeast and humans – BUB3.3 in Arabidopsis and likely other plants regulates the formation of K-MT attachments and chromosome alignment. BUB3.1 and BUB3.2 are not involved in this process, but rather regulate interphase MTs in meiosis. Finally, we hypothesize that chromosomes/kinetochores might act as spindle organizing centers in plants, because mini-spindles formed consistently around chromosomes mislocalizing beyond the spindle pole.

Introduction

Error-free chromosome segregation during mitosis and meiosis is a prerequisite for (transgenerational) genomic stability. This requires the establishment and maintenance of stable, bipolar attachments of kinetochores to spindle micro-tubules, so that during anaphase sister chromatids in mitosis and meiosis II and homologous chromosomes in meiosis I are divided equally. The search and capture model was initially proposed to explain the process of establishing kinetochore-microtubule (K-MT) connections during prometaphase (Kirschner & Mitchison, 1986). According to this model, the dynamic instability of MTs allows them to explore the cellular space, eventually getting "captured" by a kinetochore, which in turn suppresses their dynamic instability and generates a stable K-MT attachment. Since then, many studies have refined this model and have discovered parallel pathways facilitating the search and capture, without ever contradicting the basic principles of this elegant mechanism (reviewed in Heald & Khodjakov, 2015; Prosser & Pelletier, 2017).

Since the establishment of K-MT connections is a stochastic, error-prone process, the resulting mistakes, i.e., unattached or erroneously attached kinetochores, must be recognized and corrected to avoid unequal chromosome segregation. The spindle assembly checkpoint (SAC) is a surveillance mechanism that recognizes incorrect K-MT attachments or the lack thereof and halts the onset of anaphase until these errors are fixed (reviewed in Lara-Gonzalez et al., 2021; McAinsh & Kops, 2023; Musacchio, 2015). While the SAC is a highly conserved mechanism found in evolutionarily distant branches of the eukaryotic tree, both the proteins involved as well as the mechanism itself have undergone major diversification in different lineages (Kops et al., 2020; Vleugel et al., 2012). However, there are some core principles shared at least among metazoan, yeast, and plant model organisms, referred to as a canonical SAC (Kops et al., 2020). Briefly, in a canonical SAC, an array of proteins assembles on kinetochores that have not achieved bipolar attachment and catalyze the formation of a diffusible inhibitor of the anaphase promoting complex/cyclosome (APC/C), called the mitotic

checkpoint complex (MCC). The MCC prevents the APC/C, a multi-protein ubiquitin E3 ligase complex, from ubiquitinating downstream targets, thereby licensing their destruction and the transition from metaphase to anaphase (Lara-Gonzalez et al., 2021; London & Biggins, 2014; Musacchio, 2015).

The formation of stable, bipolar, end-on K-MT attachments is the ultimate goal of the error correction machinery which the SAC sets in motion. Several studies have shown though that during the search and capture process kinetochores interact with the lattice rather than with the tip of MTs, i.e., lateral and not end-on attachments are frequently formed (Kalinina et al., 2013; Magidson et al., 2011; Tanaka et al., 2005). Additionally, in metazoans, monotelic attachments, i.e., only one kinetochore is attached to spindle MTs, are formed during prometaphase, because the two sister chromatids do not form K-MT attachments synchronously (Roos, 1976) and end up localizing close to the spindle poles (Rieder & Alexander, 1990). These erroneous attachments must be rectified before the cell proceeds with anaphase. In metazoans, polar chromosomes congress towards the metaphase plate predominantly with the help of kinesin-7/CENP-E while moving on the lattice of adjacent kinetochore MTs (Barisic et al., 2014; Kapoor et al., 2006). An additional role of CENP-E is to convert lateral to end-on attachments with the help of the MT depolymerase MCAK/Kif2c (Shrestha & Draviam, 2013; Sikirzhytski et al., 2018) as well as to maintain bipolar attachments in human cells (Gudimchuk et al., 2013). BubR1, a pseudokinase that is a core component in the SAC, is one of the mechanisms recruiting CENP-E to the kinetochore in human cells (Craske & Welburn, 2020; Legal et al., 2020).

In contrast to yeast and metazoan model organisms, little is known about K-MT establishment, correction, and maintenance in plants. Especially little is known about the regulation and process of chromosome congression. In Chapter 1, we discovered that BUB3.3, a protein previously hypothesized to be part of the plant SAC (Komaki & Schnittger, 2017), is most probably not a *bona fide* SAC component, but rather involved in the formation of K-MT attachments and chromosome congression. Similarly, Bub3, the BUB3.3 homolog in human cells,

was proposed to contribute to the establishment of end-on K-MT attachments (Logarinho et al., 2008). However, in contrast to BUB3.3, Bub3 is a core component of the SAC (Taylor et al., 1998). More specifically, knock-down of Bub3 caused the excessive formation of syntelic and lateral K-MT attachments, which was distinctive from knock-down of CENP-E (Logarinho et al., 2008). We provide evidence that this is not the case in plants and that BUB3.3 and KIN7O, one of the 15 *KINESIN-7* family members in Arabidopsis (Richardson et al., 2006), act in the same pathway to promote the formation of stable, bipolar K-MT attachments and the congression of chromosomes to the metaphase plate. Furthermore, we show that neither BUB3.1 nor BUB3.2, the two closest homologs of BUB3.3, are involved in the establishment of K-MT attachments, but rather regulate MTs during interphase. Finally, we propose that chromosomes act as spindle organizing centers in plants, as we and others have observed the formation of mini-spindles around chromosomes that mislocalize beyond the spindle pole.

Results

Low concentration of oryzalin aggravates the spindle and missegregation defects in *bub3.3*

In Chapter 1, we proposed a role for BUB3.3 in the establishment of K-MT attachments and chromosome congression. To test this hypothesis, we treated *bub3.3* anthers with a low concentration of oryzalin, i.e., an inhibitor of MT polymerization. Our rationale was that a treatment with a MT-destabilizing drug would disrupt the already weakened and/or defective K-MT connections, thus, exacerbating the instances of chromosome mislocalization and missegregation as well as the spindle defects. In fact, mutants affected in MT organization often exhibit hypersensitivity to MT-destabilizing drugs as for instance seen in plants with reduced CYCLIN B1 and CYCLIN B3;1 activity (Romeiro Motta et al., 2022; Sofroni et al., 2020). For this experiment, we used the kinetochore-bound kinase BMF1, allowing us to track the chromosomes independently of K-MT attachment status (Komaki & Schnittger, 2017; Chapter 1), and the tubulin subunit TUA5, allowing us

to visualize MTs and monitor the timing from nuclear envelope breakdown (NEB) until anaphase onset (AO).

Similarly to Sofroni et al. (2020), a treatment with 400 nM oryzalin caused an ~ 20 % decrease in spindle length in the wild type (WT) and an ~ 17 % decrease in *bub3.3* indicating that the oryzalin treatment was working (Fig. 1A, B). Metaphase I duration increased by ~ 17 % in the WT and by ~ 18.5 % in *bub3.3* (Fig. 1C). The similar increase in metaphase I duration in the WT and *bub3.3* is in full agreement with the conclusion from our previous work that *BUB3.3* is not a *bona fide* SAC component (Chapter 1). We observed a slight and non-significant (P > 0.01) increase in missegregation defects in the WT under oryzalin (Fig. 1D). We found more than 1 spindle in only 2 out of 248 oryzalin-treated WT cells (~ 0.75 %) that eventually led to missegregation (Fig. 1E). In contrast, *bub3.3* exhibited both highly increased missegregation (Fig. 1D) and strong spindle defects (Fig. 1A, E), which were not observed in the mock treatment of *bub3.3* with DMSO or in the WT (Fig. 1A, D, E). More specifically, we often observed the formation of 2 or more spindles in *bub3.3* cells which were formed either (i) when the chromosome pairs moved away from the future midzone during prometaphase but eventually the 2 or more spindles fused back together (Fig. 1A second row) or (ii) when the chromosome pairs mislocalized for a prolonged time (over 1 hour) beyond or adjacent to the spindle pole and eventually 1 or more perpendicular spindles formed around the 1 or more mislocalizing chromosome pairs (MCs) (Fig. 1A third and fourth row). Indeed, the *bub3.3* cells exhibiting severe spindle defects increased from ~ 2 % with DMSO to ~ 27 % with 400 nM oryzalin (Fig. 1E). Finally, the size of the perpendicular spindles scaled with the number of chromosome pairs that they formed around (compare the second and fourth row with the third row in Fig. 1A).
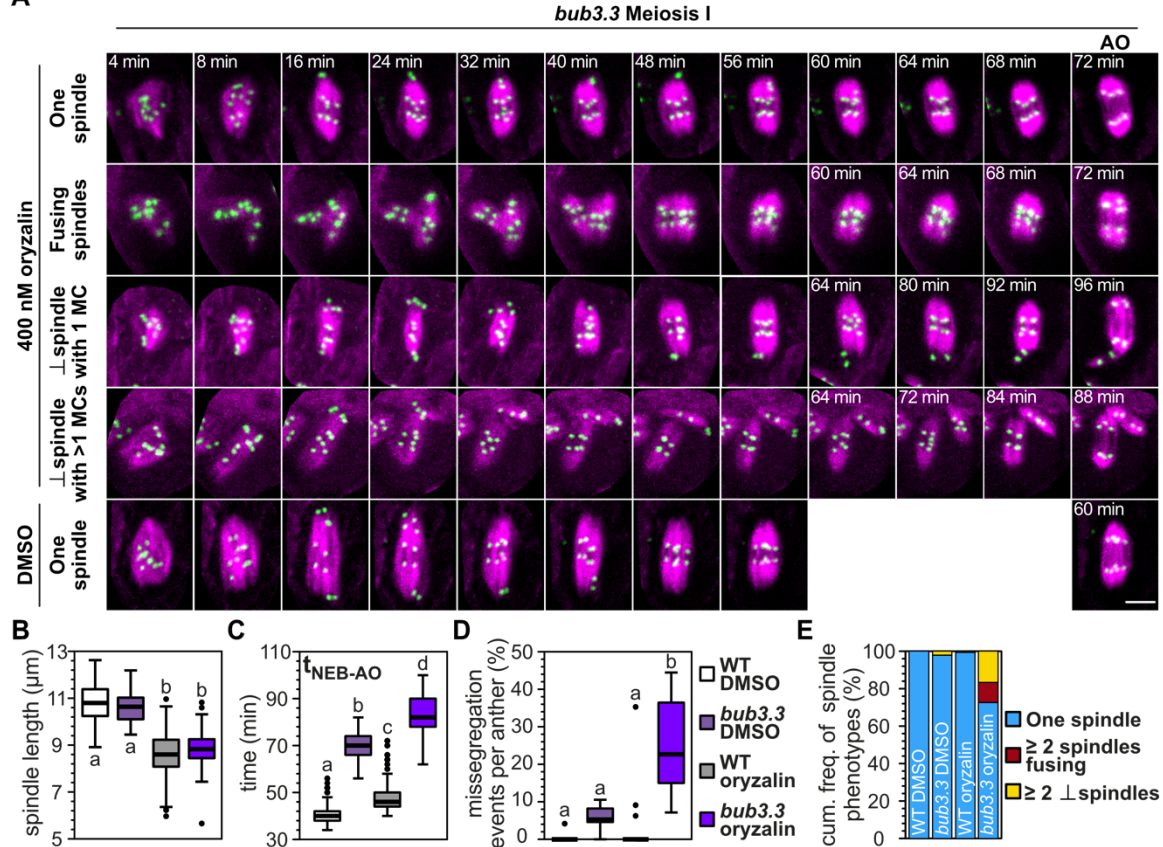
Figure 1 400 nM oryzalin causes spindle and missegregation defects in *bub3.3* but not the WT. (A) Representative maximum projections of *bub3.3* cells in metaphase I with a single spindle, two spindles that split and then fuse together, and two perpendicular (⊥) spindles with ≥1 MCs leading to missegregation. The anthers were treated either with 400 nM oryzalin or the equivalent amount of DMSO. BMF1 is fused to GFP (green) and TUA5 to TagRFP (magenta). 3D movies were recorded with a frame rate of 2 minutes. Scale bar: 5 µm. **(B-E)** Quantification of spindle length **(B)**, metaphase I duration **(C)**, the percentage of missegregation events per anther **(D)**, and the cumulative frequency of spindle phenotypes **(E)**. For **(B-E)**, we quantified 65-248 cells from 7-14 anthers per genotype. Different letters indicate significance (P < 0.01; pairwise comparison using Kruskal-Wallis test for independent samples with Bonferroni correction for multiple tests).

BUB3.1 and BUB3.2 do not act in the same or in a parallel pathway to BUB3.3

In mitosis, BUB3.1 and BUB3.2 were shown to initially bind the MT bundle in the spindle midzone and then, became progressively concentrated towards the future position of the phragmoplast (Komaki & Schnittger, 2017; H. Zhang et al., 2018). Their physical interaction with MAP65-3, the binding of cortical MTs by the BUB3.1-MAP65-3 complex heterologously expressed in tobacco leaf epidermal cells, and their localization in Arabidopsis root epidermal cells (H. Zhang et al., 2018), led us to hypothesize that potentially BUB3.1 and BUB3.2, which share a very high

74

sequence identity with each other (88 %), but not with BUB3.3 (37 %) (Lermontova et al., 2008), might act in the same or a parallel pathway to BUB3.3.

Initially, we utilized the BUB3.1 and BUB3.2 reporters, developed previously by Komaki & Schnittger (2017), to observe their localization pattern from pre-NEB in meiosis I till the tetrad stage (Fig. 2A, B). We observed a weak association with nuclear envelope MTs for BUB3.1 and a stronger association for BUB3.2 and upon NEB a weak association with spindle MTs for both. The association with spindle MTs became particularly apparent during AO. Throughout interphase, BUB3.1 and BUB3.2 accumulated in the midzone similarly to what has been observed in mitosis (Komaki & Schnittger, 2017; H. Zhang et al., 2018). Towards late interphase BUB3.1 accumulated weakly in the two nuclei like in mitosis (Komaki & Schnittger, 2017; H. Zhang et al., 2018), while BUB3.2 was only found in the midzone. Finally, in meiosis II and tetrad, stage we observed a similar localization pattern as in meiosis I and interphase, respectively. Generally, both proteins exhibited a strikingly similar localization pattern to MAP65-3 in meiosis (Sofroni et al., 2020), which is in agreement with the shown interaction of BUB3.1 with MAP65-3 (H. Zhang et al., 2018).

The weak association of BUB3.1 and BUB3.2 with spindle MTs led us to hypothesize that higher order *BUB3* family mutants might aggravate the chromosome mislocalization phenotype and perpendicular spindle formation observed in *bub3.3* (Fig.1; Chapter 1). Despite our best efforts, we could not obtain double mutants between *bub3.2* and *bub3.3* as well as triple mutants between *bub3.1 bub3.2* and *bub3.3* for reasons that are not readily apparent to us. Hence, we decided to take advantage of the *bub3.3-2* allele, which shows identical defects to *bub3.3* (Chapter 1), and finally, obtained the desired double and triple mutant combinations. In all quantified parameters, the *bub3.1 bub3.2* double mutant was identical to the WT (Fig. 2C-H, EV1), suggesting that neither BUB3.1 nor BUB3.2 are involved in the SAC, as previously reported (Komaki & Schnittger, 2017), or regulate K-MT formation in any way, meaning that most likely they do not act in the same pathway as BUB3.3. Similarly, the *bub3.2 bub3.3-2* double and *bub3.1*

bub3.2 bub3.3-2 triple mutant were identical in all aspects with *bub3.3-2* (Fig. 2C-H, EV1), suggesting that BUB3.1 and BUB3.2 are also not involved in a parallel pathway to or act redundantly with BUB3.3.
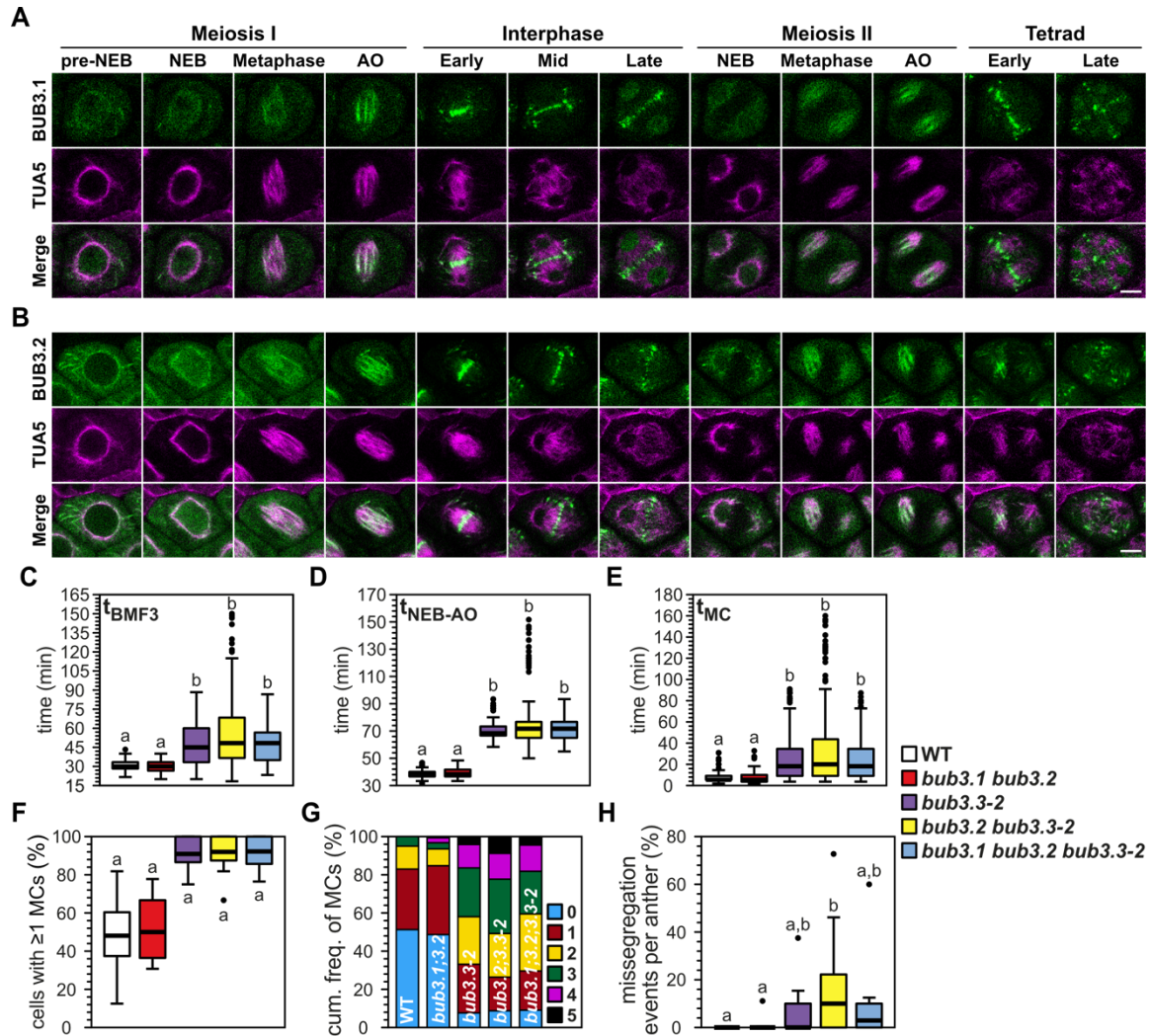
Figure 2 *bub3.2 bub3.3-2* **and** *bub3.1 bub3.2 bub3.3-2* **are phenotypically indistinguishable from** *bub3.3-2*. **(A, B)** Localization of BUB3.1 **(A)** and BUB3.2 **(B)** fused to GFP (green) together with TUA5 fused to TagRFP (magenta) in a representative cell. Movies were recorded with a frame rate of 20 seconds. Scale bars: 5 μm. **(C-H)** We recorded 3D movies of WT, *bub3.1 bub3.2*, *bub3.3-2*, *bub3.2 bub3.3-2*, and *bub3.1 bub3.2 bub3.3-2* anthers in metaphase I. Movies were recorded with a frame rate of 100 seconds. Quantification of the BMF3 kinetochore signal duration **(C)**, metaphase I duration **(D)**, duration of chromosome pairs mislocalizing to the pole(s) **(E)**, percentage of cells per anther with at least one mislocalizing chromosome pair (MC) **(F)**, cumulative frequency of the maximum number of MCs per cell **(G)**, and percentage of missegregation events per anther **(H)**. We quantified 145-198 cells from 12-18 anthers per genotype. Different letters indicate significance (P < 0.01; pairwise comparison using Kruskal-Wallis test for independent samples with Bonferroni correction for multiple tests).
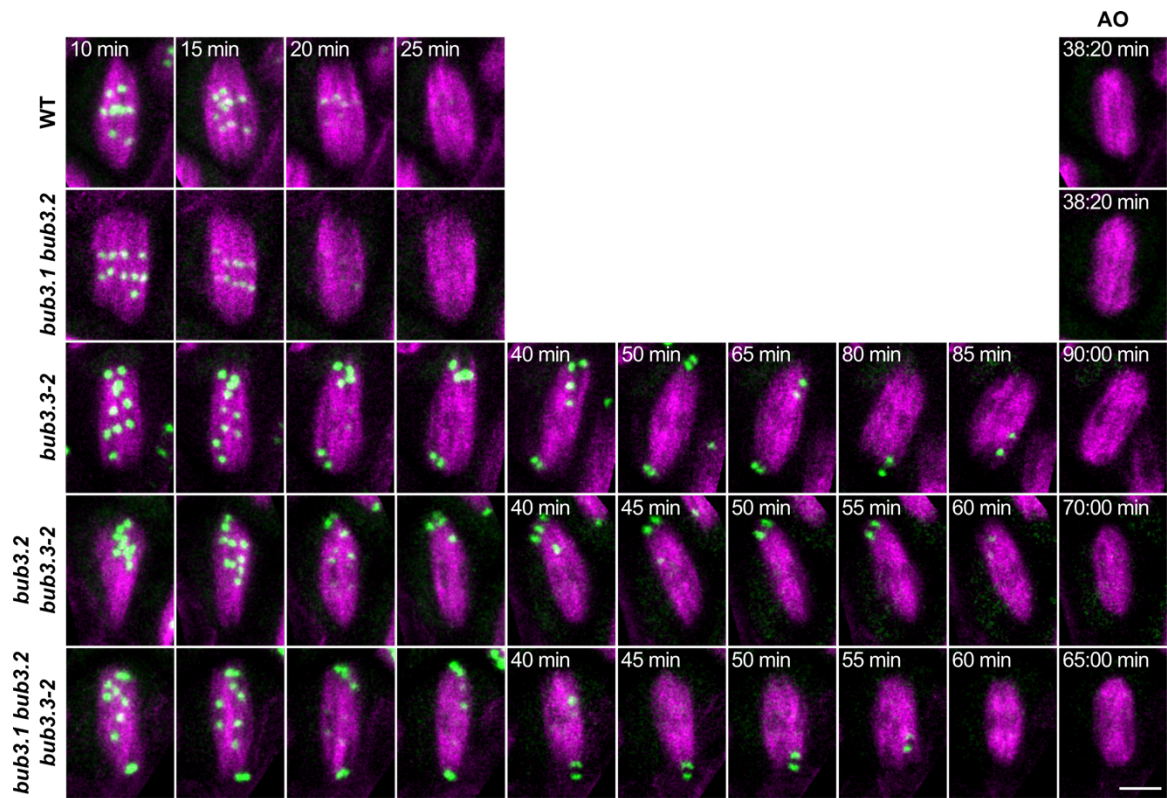
Figure EV1 WT, *bub3.1 bub3.2*, *bub3.3-2*, *bub3.2 bub3.3-2*, and *bub3.1 bub3.2 bub3.3-2* cells in metaphase I. Representative maximum projections of 3D movies of male meiocytes recorded with a frame rate of 100 seconds and quantified in Fig. 2C-H. Scale bar: 5 μm.

Interestingly, we noticed in *bub3.1 bub3.2* and *bub3.1 bub3.2 bub3.3-2* cells that the MTs normally extending in the midzone in interphase started disappearing after telophase I till eventually only few midzone MTs and the MTs around the two new nuclei were left (Fig. EV2). The latter MTs were also less tightly organized around the nucleus and appeared to be "spikier". This indicates that BUB3.1 and BUB3.2 – but not BUB3.3 – are involved in midzone MT organization during interphase, which mirrors somewhat their function in phragmoplast organization in mitosis (H. Zhang et al., 2018).
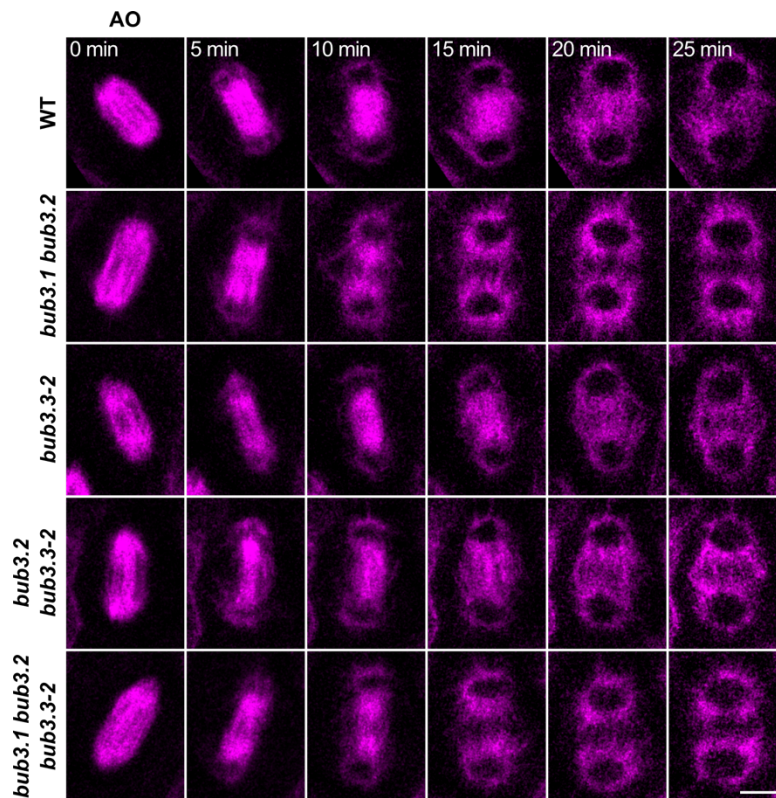
Figure EV2 Aberrant midzone MT organization during interphase in *bub3.1 bub3.2* and *bub3.1 bub3.2 bub3.3-2* cells. Representative z-slices of 3D movies of male meiocytes recorded with a frame rate of 100 seconds and quantified in Fig. 2C-H. Only the TUA5 signal is shown. Scale bar: 5 μm.

kin7o mutants exhibit similar phenotypic defects to *bub3.3*

Since our inquiry into a potential role of BUB3.1 and BUB3.2 in or parallel to the BUB3.3 pathway did not yield a positive outcome, we decided to look for potential interaction partners of BUB3.3. We looked into the cell-cycle interactome generated by Van Leene et al. (2010), as they used BUB3.3, which they called BUB3-like 1, as a bait in their pull-down assay. Interestingly, they identified KINESIN-7O (KIN7O; AT3G10180), a member of the Arabidopsis *KINESIN-7* (*KIN7*) family, as an interactor of BUB3.3. KIN7O was a very promising candidate for further inquiry, because (i) knock-down of CENP-E, the human kinesin-7, caused a *bub3.3*-like phenotype with several chromosomes mislocalizing at and tightly associated with the spindle poles as well as a SAC-dependent metaphase delay (McEwen et al., 2001; Schaar et al., 1997), and (ii) we confirmed the interaction of BUB3.3 with the C-terminus of KIN7O via yeast-two-hybrid (Fig. EV3). More, specifically, BUB3.3 interacted with the very distal C-terminus of KIN7O, namely with the last 84 amino acids, i.e., amino acids 1190-1273 (Fig. EV3).
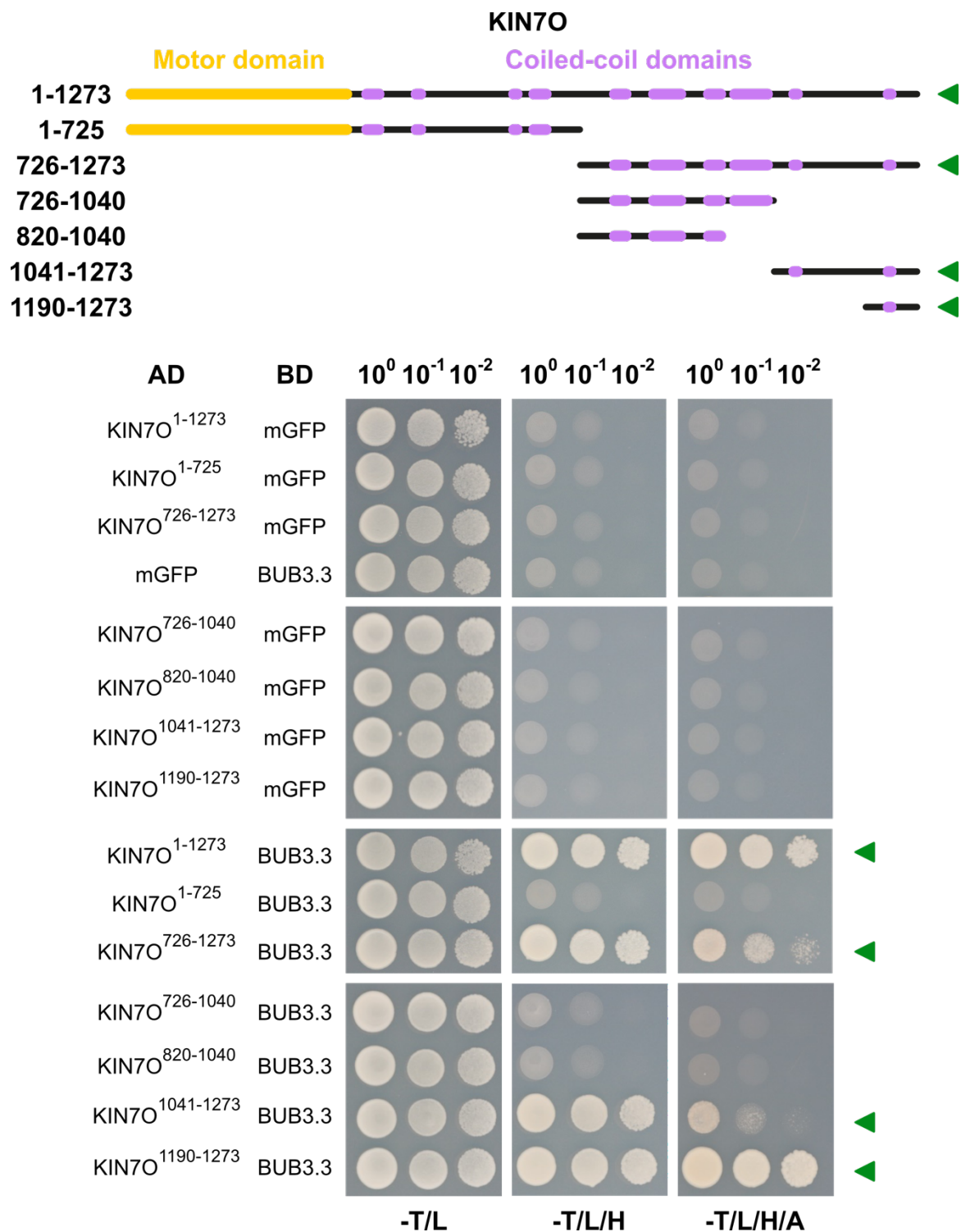
Figure EV3 BUB3.3 interacts with the very distal C-terminus of KIN7O. Yeast-two-hybrid assay of BUB3.3 with KIN7O. Green arrows highlight positive interactions.

First, we identified two null T-DNA insertion lines in *KIN7O*, i.e., *kin7o-1* (WiscDsLox_359Co06) and *kin7o-2* (GABI_242H04), with the T-DNA in the 8th intron and the 16th exon, respectively (Fig. EV4). A third T-DNA insertion line,

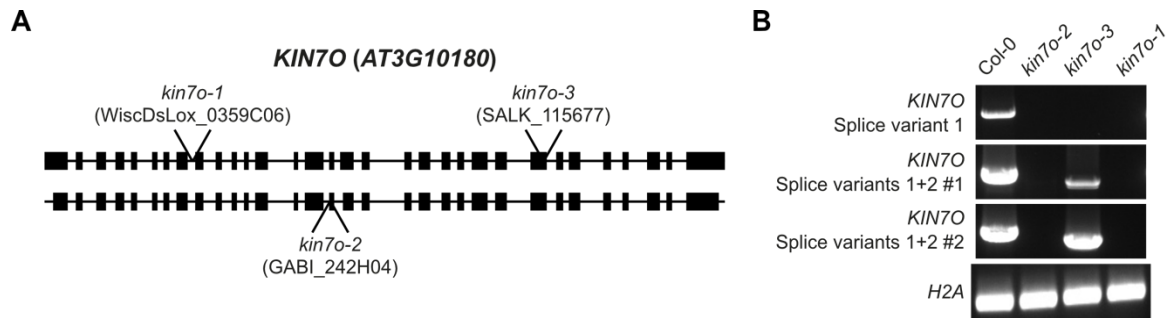namely *kin7o-3* (SALK_115677), with the T-DNA in the 25th exon, produced a truncated mRNA (Fig. EV4). In preliminary experiments, all mutants exhibited an overall similar phenotype to *bub3.3* with chromosome pair mislocalization and metaphase I delay. For further experiments, we decided to use only *kin7o-1* and *kin7o-2*.

A

KIN7O (AT3G10180)

kin7o-1
(WiscDsLox_0359C06)

kin7o-3
(SALK_115677)

kin7o-2
(GABI_242H04)

B

Col-0   kin7o-2   kin7o-3   kin7o-1

KIN7O
Splice variant 1

KIN7O
Splice variants 1+2 #1

KIN7O
Splice variants 1+2 #2

H2A

Figure EV4 Both *kin7o-1* and *kin7o-2* are null mutants, while *kin7o-3* produces a truncated mRNA. (A) Gene model of the two splice variants of *KIN7O* (*AT3G10180*). The left border of the respective T-DNA is highlighted by the arrow. **(B)** RT-PCR of the full-length cDNA for either the longer (splice variant 1) or both splice variants. For the latter, we used two different sets of primers. We used *H2A* as a positive control.

We recorded male meiocytes in 4D, to describe the *kin7o* mutant phenotype in full detail. Confirming our preliminary experiments, we observed *bub3.3*-like chromosome pair alignment defects and consequently prolonged metaphase I duration in both *kin7o-1* and *kin7o-2* (Fig. 3A; Chapter 1). More specifically, the BMF3 kinetochore signal (Fig. 3B) and metaphase I (Fig. 3C) duration were increased in *kin7o-1* and *kin7o-2* due to mislocalizing chromosome pairs (MCs) staying at the spindle poles for up to ~ 80-83 minutes compared to maximum ~ 17 minutes in the WT (Fig. 3D). On average ~ 88-95 % *kin7o* cells had MCs compared to ~ 60 % of WT cells (Fig. 3E). While in the WT we observed predominantly 1 or 2 MCs per cell, in *kin7o* cells we often observed 2 or 3 MCs, reaching up to 5 MCs, meaning that in ~ 1-5 % of *kin7o* cells none of the chromosome pairs formed bipolar attachments with spindle MTs during prometaphase (Fig. 3F). Finally, we observed an increase in the percentage of missegregation events per anther from 0 % in the WT to ~ 8-10 % on average in the *kin7o* mutants. Similar to *bub3.3* (Chapter 1), MCs that stayed at the spindle pole(s) for > 1 hour eventually missegregated in two different ways: (i) they stayed at the spindle pole and the BMF3 signal slowly faded

after AO (Fig. 3A sixth row) or (ii) a perpendicular spindle appeared when MCs moved beyond the spindle pole, K-MT attachments presumably formed as indicated by the fading of the BMF3 signal, and the mini-spindle with this/these homologous chromosome pair(s) underwent AO together with the main spindle (Fig. 3A fifth row and insets (i-iv)). Conclusively, *kin7o* mutants phenocopied *bub3.3* in all quantified aspects.
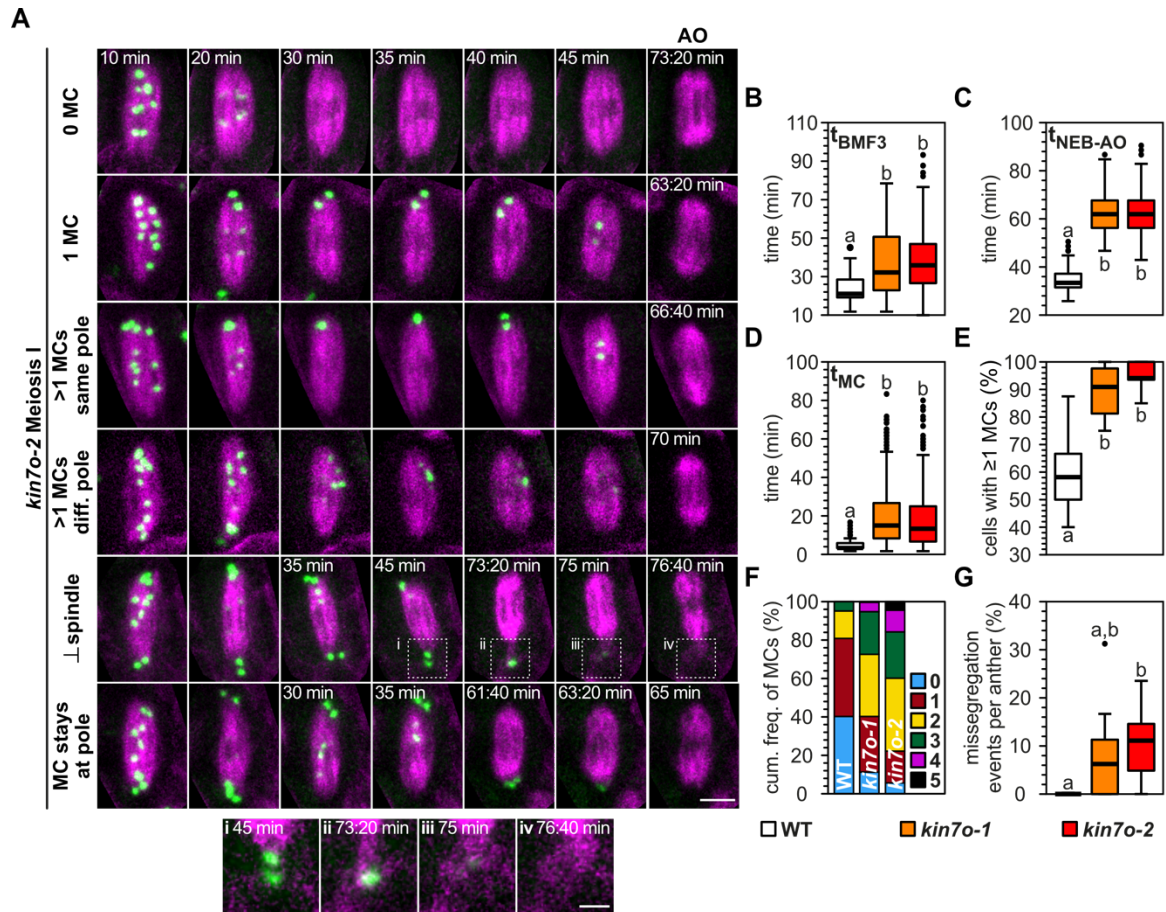
Figure 3 Prolonged metaphase I duration and delayed homologous chromosome pair congression to the metaphase plate in *kin7o* mutants. (A) Representative maximum projections of *kin7o-2* cells in metaphase I with 0, 1 or multiple MCs and MCs that missegregate either through a perpendicular (⊥) spindle or by staying at the pole. **(i-iv)** Insets highlight the formation of a perpendicular spindle. BMF3 is fused to GFP (green) and TUA5 to TagRFP (magenta). 3D movies were recorded with a frame rate of 100 seconds. Scale bars: 5 μm **(A)** and 2 μm **(i-iv)**. **(B-G)** We quantified the BMF3 kinetochore signal duration **(B)**, metaphase I duration **(C)**, duration of chromosome pairs mislocalizing to the pole(s) **(D)**, percentage of cells per anther with at least one MC **(E)**, the cumulative frequency of the maximum number of MCs per cell **(F)**, and the percentage of missegregation events per anther **(G)**. We quantified 157-182 cells from 10-11 anthers per genotype. Different letters indicate significance (P < 0.01; pairwise comparison using Kruskal-Wallis test for independent samples with Bonferroni correction for multiple tests).

KIN7N has a minor role in chromosome congression in meiosis I

Since Arabidopsis has 15 members in the *KIN7* family (Richardson et al., 2006), we wondered whether other members might be involved in chromosome congression. The phylogeny of the *KIN7* family, suggests that *KINESIN-7N* (*KIN7N*) is the closest one to *KIN7O* (Richardson et al., 2006). Additionally, the *KIN7N* transcript – but not that of *KIN7O* or of any other *KIN7* family member – was found to be upregulated in tissue culture cells during mitosis (Vanstraelen et al., 2006). Hence, we hypothesized that KIN7N might also be involved in chromosome congression.

To test this, we first identified two T-DNA insertion lines in *KIN7N*, i.e., *kin7n-1* and *kin7n-2*, with the T-DNA in the 8th and 13th exon, respectively (Fig. EV5). *kin7n-2* seems to be a null, while for *kin7n-1*, we observed a very faint band in the RT-PCR for splice variants 1+2, suggesting that it is a rather strong knock-down. *kin7n* mutants were indistinguishable from the WT in the BMF3 kinetochore signal, metaphase I, and MC duration (Fig. 4A-C, EV6). We observed only an uptick in the average percentage of cells with at least 1 MC from ~ 44 % in the WT to ~ 62-70 % in *kin7n* mutants (Fig. 4D). This was also reflected in the distribution of MCs, where we saw a higher percentage of *kin7n* cells exhibiting 2 or more MCs (Fig. 4E).
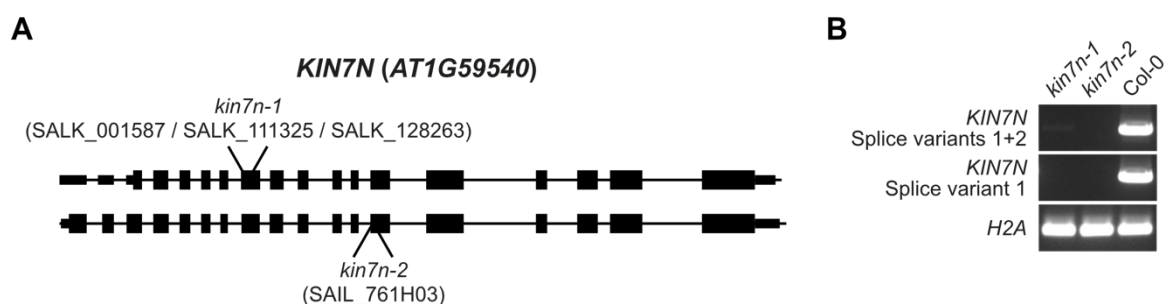
Figure EV5 *kin7n-1* is a strong knock-down and *kin7n-2* is a null mutant. (A) Gene model of the two splice variants of *KIN7N* (*AT1G59540*). The left border of the respective T-DNA is highlighted by the arrow. **(B)** RT-PCR of the full-length cDNA for either the longer (splice variant 1) or both splice variants. Note the faint band observed for *kin7n-1* in the PCR for both splice variants, suggesting that it is a strong knock-down mutant. We used *H2A* as a positive control.

To assess a redundant function of KIN7O with KIN7N, we generated *kin7o-1 kin7n* double mutants. However, in all quantified parameters *kin7o-1* single and *kin7o-1 kin7n* double mutants were nearly indistinguishable (Fig. 4F-K, EV7). We noticed a non-significant (P > 0.01) increase of ~ 8-11 % on the average percentage of cells with at least 1 MC (Fig. 4I) and a slightly elevated percentage of cells exhibiting 3 or more MCs (Fig. 4J). Generally, in *kin7o-1 kin7n-2,* the defects seemed enhanced compared to *kin7o-1* and *kin7o-1 kin7n-1*, in agreement with *kin7n-2*, but not *kin7n-1*, being a null mutant. Conclusively, our results suggest a minor role of KIN7N in chromosome congression in meiosis I, as this function seems to be performed predominantly by KIN7O.
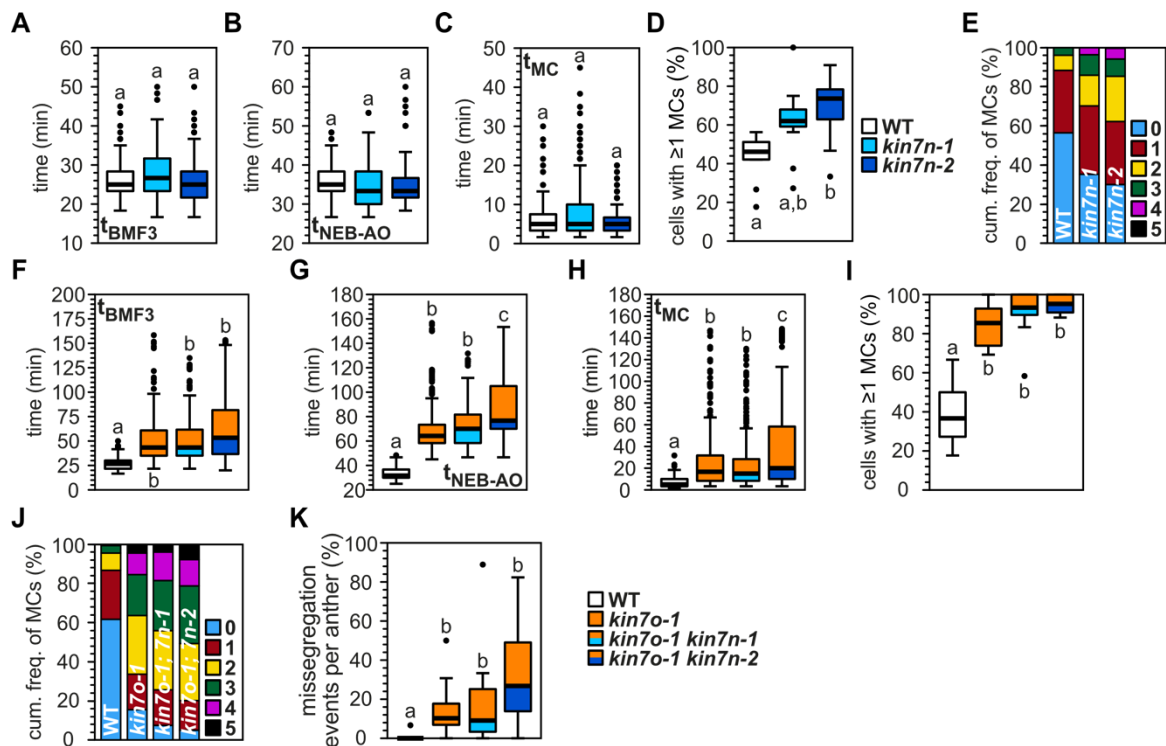
Figure 4 *kin7o-1 kin7n-1* and *kin7o-1 kin7n-2* exhibit no clear additive phenotype compared to *kin7o-1*. (A-E) We recorded 3D movies of WT, *kin7n-1*, and *kin7n-2* anthers in metaphase I with a frame rate of 100 seconds. **(F-K)** We recorded 3D movies of WT, *kin7o-1*, *kin7o-1 kin7n-1*, and *kin7o-1 kin7n-2* anthers in metaphase I with a frame rate of 100 seconds. We quantified the BMF3 kinetochore signal duration **(A, F)**, metaphase I duration **(B, G)**, duration of chromosome pairs mislocalizing to the pole(s) **(C, H)**, percentage of cells per anther with at least one MC **(D, I),** the cumulative frequency of the maximum number of MCs per cell **(E, J)**, and the percentage of missegregation events per anther **(K)**. For **(A-E)**, we quantified 181-223 cells from 10-16 anthers per genotype. For **(F-K)**, we quantified 178-200 cells from 12-16 anthers per genotype. Different letters indicate significance (P < 0.01; pairwise comparison using Kruskal-Wallis test for independent samples with Bonferroni correction for multiple tests).

Figure EV6 WT, *kin7n-1*, and *kin7n-2* cells in metaphase I. Representative maximum projections of 3D movies recorded with a frame rate of 100 seconds and quantified in Fig. 4A-E. Scale bar: 5 μm.
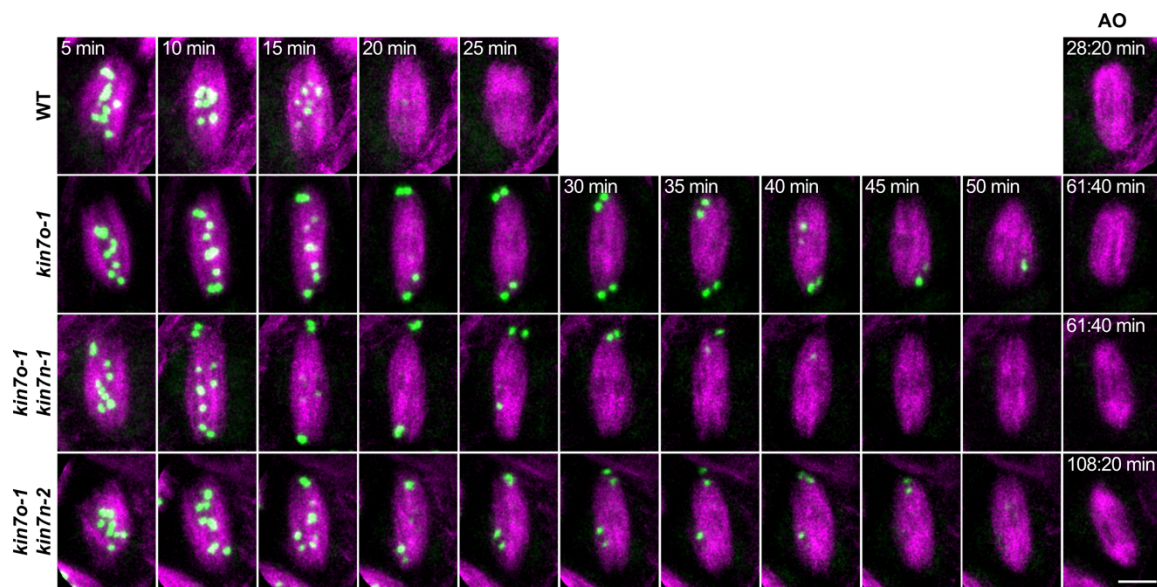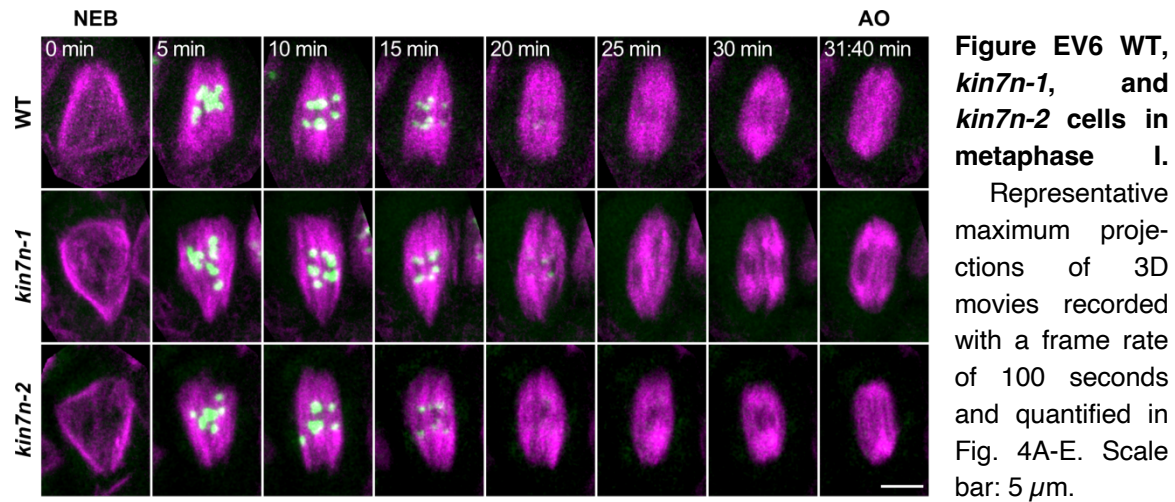
Figure EV7 WT, *kin7o-1*, *kin7o-1 kin7n-1*, and *kin7o-1 kin7n-2* cells in metaphase I. Representative maximum projections of 3D movies of male meiocytes recorded with a frame rate of 100 seconds and quantified in Fig. 4F-K. Scale bar: 5 μm.

KIN7O is involved in chromosome congression in mitosis

Since specifically the *KIN7N* transcript was upregulated in tissue culture cells in mitosis (Vanstraelen et al., 2006), we wondered whether there are tissue-specific roles for KIN7N and KIN7O in chromosome congression. Thus, we recorded mitotic root epidermal cells in 4D. We observed that *kin7o* mitotic root cells exhibited similar defects with *kin7o* and *bub3.3* male meiocytes as well as *bub3.3* mitotic root cells (Fig. 3; Chapter 1), while *kin7n* mitotic root cells were WT-like (Fig. 5A). More specifically, *kin7o* – but not *kin7n* – mitotic root cells showed prolonged BMF3 kinetochore signal (Fig. 5B), metaphase (Fig. 5C), and MC (Fig. 5D) duration.

Additionally, all of *kin7o* mitotic root cells had at least one MC and we observed up to 7 MCs per cell (Fig. 5E). Although we cannot exclude a minor role of KIN7N also in mitosis, we suggest that KIN7O is the major functional equivalent of CENP-E both in meiosis I and mitosis.
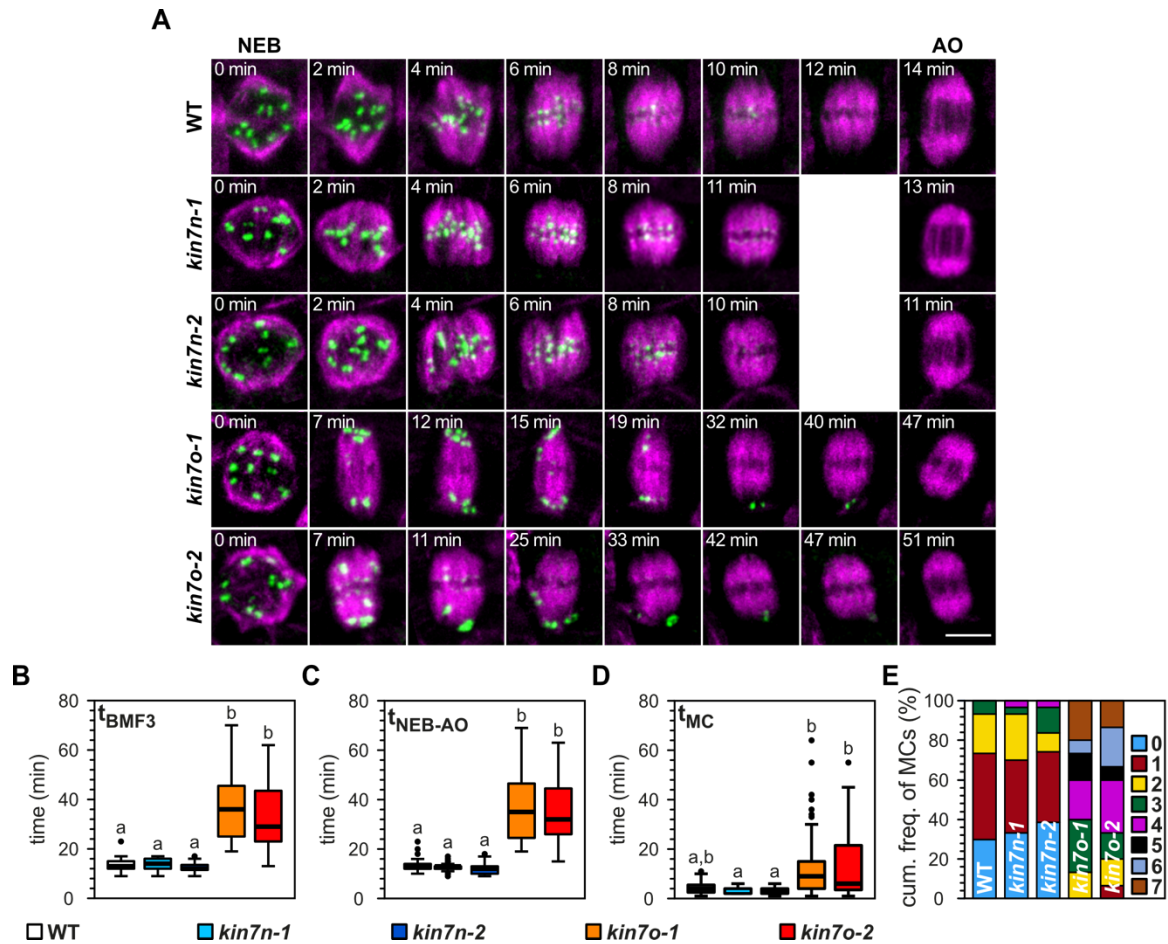
Figure 5 Mitotic *kin7o* cells exhibit similar defects to *kin7o* male meiocytes. (A) Representative maximum projections of WT, *kin7n-1*, *kin7n-2*, *kin7o-1*, and *kin7o-2* mitotic root epidermal cells. BMF3 is fused to GFP (green) and TUA5 to TagRFP (magenta). 3D movies were recorded with a frame rate of 1 minute. Scale bar: 5 μm. **(B-F)** We quantified BMF3 kinetochore signal duration **(B)**, metaphase duration **(C)**, duration of chromosome pairs mislocalizing to the pole(s) **(D)**, and the cumulative frequency of the maximum number of MCs per cell **(F)**. We quantified 15-31 cells per genotype. Different letters indicate significance ($P < 0.01$; pairwise comparison using Kruskal-Wallis test for independent samples with Bonferroni correction for multiple tests).

BUB3.3 and KIN7O act in the same pathway

Considering that *kin7o* mutants showed identical phenotypical defects to *bub3.3* (Fig. 3, 5; Chapter 1) and the two proteins physically interacted (Fig. EV3; Van Leene et al., 2010), we hypothesized that BUB3.3 and KIN7O might act in the same pathway. Thus, we generated *bub3.3 kin7o* double mutants. Indeed, in all quantified parameters we observed that the *bub3.3*, *kin7o-1*, and *kin7o-2* single mutants were identical with their *bub3.3 kin7o-1* and *bub3.3 kin7o-2* double mutant counterparts in metaphase I (Fig. 6A-F, EV8). We conclude that BUB3.3 and KIN7O act in the same pathway.
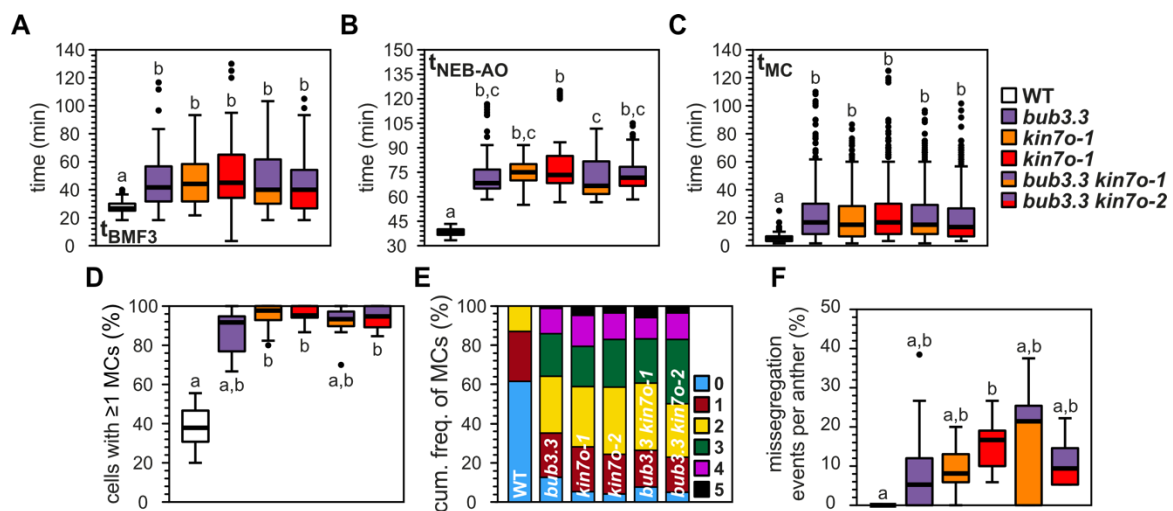
Figure 6 The defects in *bub3.3 kin7o* double mutants are identical to *bub3.3* and *kin7o* single mutants. (A-F) We recorded 3D movies of WT, *bub3.*3, kin7o-*1*, *kin7o-2*, *bub3.3 kin7o-1*, and *bub3.3 kin7o-2* anthers in metaphase I with a frame rate of 100 seconds. We quantified the BMF3 kinetochore signal duration **(A)**, metaphase I duration **(B)**, duration of chromosome pairs mislocalizing to the pole(s) **(C)**, percentage of cells per anther with at least one MC **(D)**, the cumulative frequency of the maximum number of MCs per cell **(E)**, and the percentage of missegregation events per anther **(F)**. We quantified 102-166 cells from 7-10 anthers per genotype. Different letters indicate significance (P < 0.01; pairwise comparison using Kruskal-Wallis test for independent samples with Bonferroni correction for multiple tests).
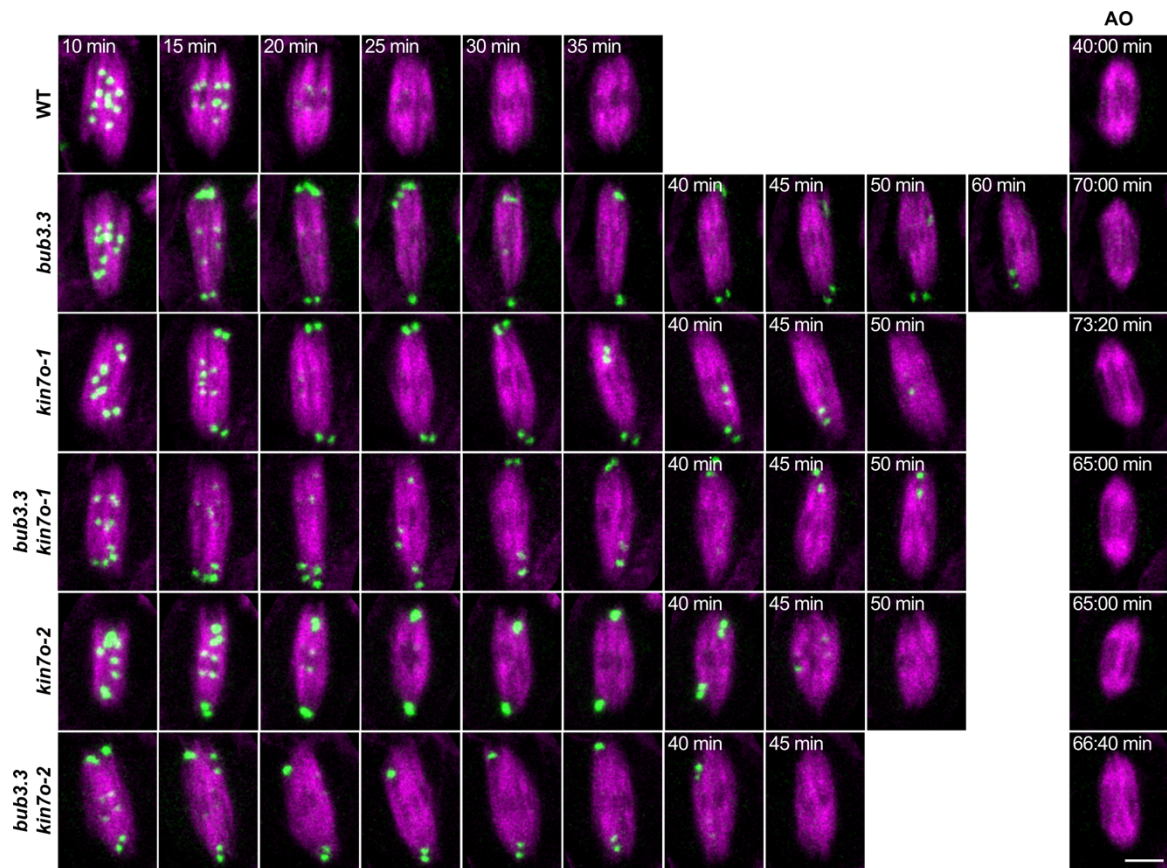
Figure EV8 WT, *bub3.3*, *kin7o-1*, *bub3.3 kin7o-1*, *kin7o-2*, and *bub3.3 kin7o-2* cells in metaphase I. Representative maximum projections of 3D movies of male meiocytes recorded with a frame rate of 100 seconds and quantified in Fig. 6A-F. Scale bar: 5 μm.

Discussion

BUB3.1, BUB3.2, and BUB3.3 – Same same, but different

Arabidopsis, in contrast to most organisms not belonging to the plant lineage, possesses three genes in the *BUB3* family. Rice has at least two *BUB3* genes (Lermontova et al., 2008) while maize seems to have only one (Su et al., 2017). Thus, this expansion might be found only in part of the plant lineage and might be the consequence of independent whole-genome duplication (WGD) or smaller scale duplication events. Alternatively, this expansion might have been the result of a WGD event at least prior to the split of monocots and dicots and have been lost secondarily in maize. BUB3.1 and BUB3.2 have 88 % amino acid sequence identity, while BUB3.3 shares only 37 % of its amino acids with the other two members (Lermontova et al., 2008). Interestingly, phylogenetic analysis of the

BUB3 family on the protein level grouped BUB3.1 and BUB3.2 of Arabidopsis and rice together and in a separate clade from the Arabidopsis BUB3.3, which was grouped together with the Bub3 proteins from non-plant organisms (Lermontova et al., 2008). This might suggest that BUB3.3 is also functionally closer to the ancestral *BUB3* gene, while BUB3.1 and BUB3.2 are potentially the outcome of a WGD or smaller scale duplication event specific to the plant lineage. This would explain both the larger sequence as well as the functional similarity between BUB3.1 and BUB3.2 and divergence from BUB3.3, as duplicated genes often sub- or neofunctionalize. However, this would raise the question of why the two BUB3s in rice group together with BUB3.1 and BUB3.2 and whether they fulfill the function of BUB3.3 in rice or whether there is at least one more BUB3 that could not be identified due to low sequence identity and/or similarity. It is noteworthy that structurally all three Arabidopsis BUB3s as well as the human and budding yeast Bub3 are nearly identical forming seven-bladed WD40 β-propellers as predicted by Alphafold (Jumper et al., 2021). This means that despite their divergence in sequence and function, their predicted 3D structure remained essentially unchanged.

BUB3.1 and BUB3.2 are probably functionally redundant, as the double mutant exhibited more severe defects than the single mutants, which are essentially WT-like (H. Zhang et al., 2018; Chapter 2). More specifically, BUB3.1 and BUB3.2 shared a similar localization pattern in mitosis (Komaki & Schnittger, 2017; H. Zhang et al., 2018) and meiosis (Fig. 2A, B). In mitosis, they were concentrated on MT bundles in the spindle midzone after AO, where the phragmoplast would be later formed (Komaki & Schnittger, 2017; H. Zhang et al., 2018). In meiosis, we observed a weak association with MTs already before NEB and during metaphase I and II, though the strongest association was – similarly to mitosis – on MT bundles in the spindle midzone after AO in meiosis I and II as well as during interphase and the tetrad stage (Fig. 2A, B). Interestingly, we observed the loss of MT bundles connecting the two nuclei in interphase in *bub3.1 bub3.2* and *bub3.1 bub3.2 bub3.3-2*, but not *bub3.2 bub3.3-2* (Fig. EV2). This supports the notion that BUB3.1 and BUB3.2 are functionally redundant and that they are important for the MT

organization post-AO. Finally, the hypothesis that BUB3.1 and BUB3.2 are involved in post-AO MT organization in meiosis is supported by the observation that the MTs around the nuclei in *bub3.1 bub3.2* and *bub3.1 bub3.2 bub3.3-2* appeared "spikier" compared to the other genetic backgrounds (Fig. EV2).

We conclude that despite their near-identical 3D structure, the expanded BUB3 family in Arabidopsis has allowed for BUB3.1 and BUB3.2 to sub- or neofunctionalize, while BUB3.3 has maintained the most ancestral function.

A KIN7O-BUB3.3 module is required for efficient K-MT attachment formation and chromosome congression

We have previously suggested that BUB3.3 is most probably not a *bona fide* SAC component, but rather involved in K-MT attachment formation and chromosome congression through an unknown mechanism (Chapter 1). Human Bub3, on the other hand, seems to have at least two functions: (i) it is involved in the SAC by forming a constitutive complex with Bub1 and BubR1, recruiting them to the kinetochore (Taylor et al., 1998), as well as by being part of the MCC (Sudakin et al., 2001), and (ii) it is important for the efficient establishment of end-on K-MT attachments (Logarinho et al., 2008). Bub1 and Bub3 depletion caused chromosome misalignment in metaphase due to an increased ratio of syntelic and lateral rather than bipolar, end-on K-MT attachments (Logarinho et al., 2008; Meraldi & Sorger, 2005). Compelling evidence, such as distinctive defects in chromosome alignment and K-MT attachments, suggested that the effect of Bub1 and Bub3 depletion is CENP-E-independent in human cells (Logarinho et al., 2008; Meraldi & Sorger, 2005). The most characteristic function of CENP-E is the transport of mono-oriented chromosomes along adjacent kinetochore MTs in a plus-end directed fashion towards the metaphase plate (Barisic et al., 2014; Kapoor et al., 2006). Additionally, CENP-E converts lateral K-MT attachments onto end-on attachments (Shrestha & Draviam, 2013; Sikirzhytski et al., 2018). CENP-E is recruited to unattached kinetochores partly by BubR1, although there are also other pathways (Chan et al., 1998; Ciossani et al., 2018; Johnson et al., 2004; Legal et al., 2020), and the two proteins cross-regulate each other (Guo et al.,

2012; Huang et al., 2019; Mao et al., 2003). Nonetheless, BubR1 knock-down causes more severe alignment defects than CENP-E knock-down, suggesting that BubR1 regulates chromosome congression through other pathways as well (Lampson & Kapoor, 2005). Hence, the Bub1-Bub3 and BubR1-CENP-E pathways appear to have distinct functions in human cells (Logarinho et al., 2008; Meraldi & Sorger, 2005).

The situation in Arabidopsis is different from the one observed in human cells. First, the kinetochore localization of BMF1, the Bub1 homolog, and other SAC proteins does not depend on BUB3.3 and vice versa, the localization of BUB3.3 is independent of BMF1 or other SAC proteins (unpublished data from the Liu lab; Chapter 1). Next, using a functional reporter, we could not observe binding of BMF2, the BubR1 homolog, to the kinetochore, but rather a diffuse cytosolic signal, which we interpreted to mean that BMF2 is only part of the MCC and not the kinetochore-bound complex (Komaki & Schnittger, 2017; Chapter 1). Furthermore, neither *bmf1* nor *bmf2* exhibited MCs in mitosis or meiosis I (Komaki & Schnittger, 2017; Chapter 1), suggesting that these proteins are most probably not involved in correcting, establishing and/or maintaining K-MT attachments. This is not surprising, considering that neither BMF1 nor BMF2 interacted with BUB3 in maize (Su et al., 2021), while both Bub1 and BubR1 interact with Bub3 in human cells (Taylor et al., 1998). On the contrary, *bub3.3* and *kin7o* single as well as *bub3.3 kin7o* double mutants exhibited similar K-MT establishment and metaphase plate alignment defects in meiosis I (Fig. 3, 7) and mitosis (Fig. 6; Chapter 1), suggesting that BUB3.3 and KIN7O, which directly physically interact (Fig. EV3; Van Leene et al., 2010), work in the same pathway in Arabidopsis. Although we cannot formally exclude a redundant or synergistic role of KIN7N in the KIN7O-BUB3.3 pathway, we propose that KIN7O is the major CENP-E functional equivalent *in planta*.

We observed that most of the homologous chromosome pairs in meiosis I and chromosomes in mitosis aligned at the metaphase plate presumably in a bipolar configuration as indicated by the extinguishing of the BMF3 signal, suggesting satisfaction of the SAC (Fig. 3, 5). We interpret this to mean that *bub3.3* and *kin7o*

mutants do not exhibit defects in maintaining stable, bipolar attachments. Additionally, we think that error correction is not affected. We frequently observed that MCs with BMF3 positive kinetochores seemed to be bound MTs as indicated by the parallel orientation to the long axis of the spindle and were pulled towards the metaphase plate, only to be found again close to the spindle pole in the next couple of minutes, suggesting that presumably aberrant K-MT connections were severed. Finally, MCs with BMF3 positive kinetochores often stayed close to the pole despite being bound by spindle MTs, as indicated by the parallel orientation to the long axis of the spindle, suggesting that the K-MT connections were not maturing into stable, end-on K-MT attachments that would satisfy the SAC. Thus, we conclude that the KIN7O-BUB3.3 pathway is most probably important for establishing end-on K-MT connections and promoting chromosome metaphase plate alignment in plants. The observation that both kinetochores of MCs were BMF3 positive, indicating lack of end-on K-MT attachments for both, is in full agreement with a defective K-MT establishment pathway and a resulting overly active error correction machinery. Whether the KIN7O-BUB3.3 pathway is closer to the human Bub1-Bub3 or BubR1-CENP-E pathway or a mix and match of both remains to be elucidated in the future. Based on our observations, we believe that the two distinct pathways in humans have fused into one in plants. Nevertheless, considering that ~ 90 % of MCs in *bub3.3* and *kin7o* single and double mutants were eventually pulled towards and aligned at the metaphase plate with the BMF3 signal extinguishing, plants clearly possess redundant mechanisms and/or pathways for establishment of stable, bipolar K-MT attachments and chromosome alignment.

Do chromosomes and/or kinetochores act as spindle-organizing centers in plants?

Spindle assembly is a highly coordinated, intricate process that has been covered in detail by recent reviews both for animals (Prosser & Pelletier, 2017) and plants (Lee & Liu, 2019; Yamada & Goshima, 2017). It is well documented that chromosomes and kinetochores act as MT-polymerizing hotspots in animals (Prosser & Pelletier, 2017), but similar studies have not been performed in plants.

We (Chapter 1, 2) and others (Falconer et al., 1988; unpublished data from the Liu lab) have observed the formation of mini-spindles forming around chromosomes isolated from the chromosome mass in meiotic and mitotic plant cells. Falconer et al. (1988) observed mini-spindles around isolated chromosomes during recovery from treatment with a MT depolymerizing agent, a process that was enhanced by taxol, a MT stabilizing chemical. Similarly, mini-spindles were observed in the *bub3.3* and *kin7o* backgrounds when chromosomes stayed persistently at the spindle pole(s), which was further enhanced by a low concentration oryzalin treatment (unpublished data from the Liu lab; Chapter 1, 2). When MT polymerization is weakened in a genetic background deficient in the establishment of K-MT connections, then there is a higher probability that chromosomes can escape from the chromosome mass and consequently, lead to the formation of one or more mini-spindles. Finally, the oryzalin treatment revealed that mini-spindles scaled in size with the number of chromosome pairs included. Based on these observations, we hypothesize that chromosomes and/or kinetochores act as MT nucleation and/or spindle organization centers in plants. The factors promoting, but also inhibiting multiple spindle formation in a cell, indicated for instance by the fusion of spindles we observed under oryzalin treatment, remain to be identified in the future.

Materials and Methods

Plant materials and line generation

The *Arabidopsis thaliana* (Arabidopsis) accession Columbia-0 (Col-0) was used as the wild type (WT) reference in this work and all T-DNA insertion lines are in the Col-0 background. We obtained the T-DNA insertion lines from the Nottingham Arabidopsis Stock Center (NASC) (http://arabidopsis.info/) and used the following ones: SK29246 (*bub3.1*) and SALK_151687C (*bub3.2*) from H. Zhang et al. (2018); SALK_041372 (*bub3.3*) from Komaki & Schnittger (2017); SALK_022904 (*bub3.3-2*) from Chapter 1; SALK_001587/SALK_111325/SALK_128263 (*kin7n-1*), SAIL_761H03 (*kin7n-2*), WiscDsLox_359Co06 (*kin7o-1*), GABI_242H04 (*kin7o-2*), and SALK_115677 (*kin7o-3*) (Chapter 2).

All plants used for our experiments were grown vertically on plate with a solid medium containing half-strength Murashige and Skoog (MS) medium, 1 % (w/v) sucrose, 0.8 % (w/v) agar, and pH 5.8 and grown in a 16 hours light at 21 °C / 8 hours dark at 18 °C cycle. For imaging mitosis, we used 4-day old seedlings. For imaging meiosis, 7- to 10-day old seedlings were transferred to soil and grown for another 5-6 weeks.

All reporter constructs were generated in Komaki & Schnittger (2017) and were genetically crossed from the WT into the different mutant backgrounds (Chapter 1, 2).

Genotyping, T-DNA mapping and RT-PCR

The primers for genotyping *bub3.1, bub3.2, bub3.3*, and *bub3.3-2* are described in the respective publications. We always used the LP+RP primer combination to detect the WT allele and the left border primers GABI_LB, SAIL_LB3, SALK_Lb1.3 or WiscDsLox_LB together with RP to detect the T-DNA insertion. For *kin7n-1*, we used ATTTGGAGGTTGGTTTGGATC (LP), GCAGACCTCATTCACTTGAGC (RP), and ATTTTGCCGATTTCGGAAC (SALK_Lb1.3); for *kin7n-2,* we used TATGCACTATCGCACCAGAAG (LP), ATTGACATTGCATAGCCCATC (RP), and TAGCATCTGAATTTCATAACCAATCTCGATACAC (SAIL_LB3); for *kin7o-1*, we used GGTCAGAGTGAGAAGTCTGCG (LP), TGAAGGTGTTGGAAATTCCTG (RP), and AACGTCCGCAATGTGTTATTAAGTTGTC (WiscDsLox_LB); for *kin7o-2*, we used TCCCTGGCACATATATTCTGC (LP), TTGAATACTCTTGTTGG CGATG (RP), and ATATTGACCATCATACTCATTGC (GABI_LB); for *kin7o-3*, we used CGCTACAGGGAGTTCATTCTG (LP), AATGTTGGAAATGCAAAGTCG (RP), and SALK_Lb1.3. The respective left border primer was also used to map the *kin7n-1, kin7n-2, kin7o-1, kin7o-2*, and *kin7o-3* T-DNA insertions.

RNA from ~ 200 8-day old seedlings per genotype was extracted to perform the reverse transcription-polymerase chain reaction (RT-PCR). We put the seedlings of each genotype in an Eppendorf tube, flash froze them in liquid nitrogen, and upon pulverizing them, we isolated RNA according to the manual of the RNA-

isolation kit (innuPREP Plant RNA Kit, Analytik Jena AG). For synthesizing cDNA, we used the Oligo(dT)18 primer and followed the manual of the cDNA synthesis kit (Thermo Scientific RevertAid Reverse Transcriptase, Thermo Fisher Scientific). Since both *KIN7N* and *KIN7O* have two splice variants according to The Arabidopsis Information Resource (TAIR, https://www.arabidopsis.org/), we performed two PCR reactions for each genotype. For *KIN7N*, we amplified full-length Splice variant 1 with CACGCTTTTGATCATGTGTTCG (fwd) + AGATTTGT GCCTGGTAGCGA (rev), and full-length Splice variants 1+2 with GTCGCAGTCA GGGTAAGACC (fwd) + AGATTTGTGCCTGGTAGCGAA (rev). For *KIN7O*, we amplified full-length Splice variant 1 both with GCGAAGACAAGTCCCTGGAA (fwd) + AACTGGAAGACCAAGAGCGG (rev) and AGCGCGATTGTCTGGTGTAT (fwd) + CTGGAAGACCAAGAGCGGTG (rev), and Splice variants 1+2 with GGTCTTACT TTGTTCGCCGGA (fwd) + AGAGAGTTGCTTCTTGAGGTCG (rev). Histone *H2A* was used as a positive control and its transcript was amplified with primers ATGGCGGGTCGTGGTAAAACACTCGGATCT (fwd) + TCAATCGTCTTC AGCAGATGGCTTGGAAGCACC (rev).

Yeast-two-hybrid assay

Initially, we amplified full-length cDNAs by PCR using gene-specific primers for BUB3.3 (aaaagcaggctccaccatgAGCGGAGATAGACTTGAATTTGAAAACC (fwd) and ctgggtctagatatctcgaTCAAAGCCTGTGTATGAACACTTGAGG (rev)) and KIN7O (aaaagcaggctccaccatgGAGAGAATCCATGTCTCAGTCAGAGC (fwd) and ctgggtctagatatctcgaTCACATTGTTCTTGAAGAAGCAGAGAG (rev)). Then, we linearized the entry vector pENTR4 (tcgagatatctagacccagctttcttg (fwd) and catggtggagcctgcttttttgtac (rev)) and subcloned the fragments into pENTR4. Finally, the fragments were cloned via recombination into the destination vector pGBT9 (BD) or pGAD424 (AD) by LR recombination reaction. The final constructs were transformed into the AH109 yeast strain, and transformants were spotted on SD plates without tryptophan and leucine (-TL) as a control, and without tryptophan, leucine, and histidine (-TLH), as well as without tryptophan, leucine, histidine, and alanine (-TLHA) for selection. Photographs were taken after incubation for 2 days at 30 °C.

The primer pairs for the KIN7O truncations are listed below. KIN7O$^{1-725}$ (aaaagcaggctccaccatgGAGAGAATCCATGTCTCAGTCAGAGC (fwd) and ctgggt ctagatatctcgatcaCGGAGAGAAGAAAGCAAAATCTTGG (rev)), KIN7O$^{726-1273}$ (ctg ggtctagatatctcgaTCACATTGTTCTTGAAGAAGCAGAGAG (fwd) and aaaagcaggc tccaccatgTTGATACATGATTTCACATTGTTTGTGC (rev)), KIN7O$^{726-1040}$ (aaaagc aggctccaccatgTTGATACATGATTTCACATTGTTTGTGC (fwd) and ctgggtctagatat ctcgatcaTTCCTCCACAGCCTCTGTCAAAGC), KIN7O$^{820-1040}$ (aaaagcaggctccacc atgGGGAGTCTGTCATCCTCTTCCTTG (fwd) and ctgggtctagatatctcgatcaTTCCT CCACAGCCTCTGTCAAAGC (rev)), KIN7O$^{1041-1273}$ (aaaagcaggctccaccatgAAGA TCAGACTATATAAAAATATAC (fwd) and ctgggtctagatatctcgaTCACATTGTTCTT GAAGAAGCAGAGAG (rev)), and KIN7O$^{1190-1273}$ (aaaagcaggctccaccatgAGCCAA GAAACCAATCTGCACAAGG (fwd) and ctgggtctagatatctcgaTCACATTGTTCTTG AAGAAGCAGAGAG (rev)).

Live-cell imaging

We performed 3D live-cell imaging of male meiocytes on a Zeiss LSM880 upright CLSM equipped with a GaAsP-detector and a W-plan-Apochromat 40x/1.0 DIC M27 water-dipping lens as described in Chapter 1. We placed 60-80 flower buds with intact pedicels on live-cell imaging medium (Prusicki et al., 2019) on the day before imaging and incubated them in the dark overnight. We recorded 16-bit images with 96 nm lateral pixel resolution, bi-directional scanning, 2 times line average, 1.18 μs pixel dwell time, pinhole size of 66.5 μm or 1.51 AU (for GFP), and 0.93 μm step size at a frame rate of 100 seconds to 2 minutes. Both GFP and TagRFP were excited at 488 nm. Emission was detected simultaneously at 490-553 nm for GFP and 579-651 nm for TagRFP.

We performed 3D live-cell imaging of mitotic root epidermal cells on a Leica TCS SP8 inverted CLSM equipped with three hybrid photodetectors (Leica HyD™) and a HC PL APO 63x/1.2 W motCORR CS2 water-immersion objective as described before (Chapter 1). Directly before imaging, 6-10 4-day old seedlings were placed in liquid medium in a glass bottom dish. The liquid medium had the same composition with the solid medium minus agarose. Finally, the roots were covered with a strip of solid medium. We recorded 12-bit images with 99 nm lateral pixel

resolution, bi-directional scanning, 4 times line average, 475 ns pixel dwell time (700 Hz), pinhole size of 147.04 μm or 1.5 AU at 510 nm, and 0.52 μm step-size. Both GFP and TagRFP were excited at 488 nm. Emission was detected simultaneously at 493-555 nm for GFP and 575-655 nm for TagRFP.

Oryzalin treatment

The oryzalin treatment was performed as described in Sofroni et al. (2020) and Chapter 1 with minor modifications. We prepared a 1 mM oryzalin (Duchefa Biochemie) stock solution in dimethyl sulfoxide (DMSO) (stored at -20 °C). We added 1:2,500 (v/v) stock solution for a 400 nM final concentration or the equivalent amount of DMSO to the live-cell imaging medium. The plates were always freshly prepared on the day before the experiment and the flowers were incubated in the medium overnight for a minimum of 12 hours before imaging.

Post-processing of movies and spindle length measurement

We used Fiji for all our post-processing operations and measurement of the spindle length (Schindelin et al., 2012).

The post-processing protocol for the 3D movies is presented in detail in Chapter 1. Briefly, we applied two different post-processing protocols for the BMF3 and TUA5 channels. We applied the "Gaussian Blur 3D" command with sigma radius 1 in x, y, and z on the BMF3 channel. For TUA5, we adapted a protocol from Krüger (2017). We, initially, duplicated the movie using the "Duplicate" command and the setting "Duplicate hyperstack". The two stacks were designated as "GB_15" and "GB_0,5", because as a next step we applied the "Gaussian Blur 3D" command with sigma radius 15 and 0.5 in x, y, and z, respectively. "GB_0,5" was then subtracted from "GB_15" using the "Image calculator", generating the image "Background". "Background" was subsequently subtracted from "GB_0,5" using the "Image calculator" and generated the image "TUA5_final", on which we applied the "Gaussian Blur 3D" command with sigma radius 0.5 in x, y, and z.

For further analysis, single cells were extracted manually using the polygon selection tool and the "duplicate" command with the "Duplicate hyperstack" setting with the desired z-slice range for each cell. After applying the "clear outside" command for all z-slices, we used the "Z Project" command with the setting "Max Intensity". As a final step, we adjusted the brightness and contrast settings.

The spindle orientation in meiosis I can be variable depending on the cell shape, orientation of the cell within the anther as well the angle of the anther relative to the imaging axis. Thus, for the spindle length measurement, we only chose cells whose spindle was flat, i.e., the long axis of the spindle was (near-)perpendicular to the imaging axis. We measured spindle length 5 minutes before AO, when (most) chromosome pairs are aligned at the metaphase plate, because mislocalization of chromosome pairs to the pole(s) caused stretching of the spindle in *bub3.3*. Finally, we did not measure spindle length in cells that had more than one spindle, because spindle size correlated with the number of chromosome pairs encapsulated by the spindle.

We followed the protocol of Herrmann et al. (2021) for measuring the length of the long and short axis of the spindle. Briefly, single z-planes of flat spindles, that were 5 min prior to AO, were extracted using the "duplicate" command. The image was transformed into 8-bit, an appropriate threshold was applied to segment the spindle from the background, and then, the "Analyze particles" command was applied with a minimum particle size of 25 pixel units and the settings "Show Outlines", "Add to manager", and "Include holes". Finally, we used the command "measure" on the resulting ROI after choosing the "Fit ellipse" setting in "Set measurements".

Statistics and figure design

We used IBM SPSS Statistics Version 28 (IBM Corporation) to generate all graphs and perform statistical tests. The lower and upper border of the boxplot highlight the 25th and 75th percentile, respectively. The median is shown by a thick black line. The outliers that are within 1.5 times the interquartile range are indicated by the whiskers and finally, the dots represent outliers outside this range. We applied

a Kruskal-Wallis test for independent samples with Bonferroni correction for multiple tests, a non-parametric test for pairwise comparisons. The significance threshold was set at $P < 0.01$.

We used Affinity Designer v. 1.10 (Serif) to assemble the graphs and images into figures.

Chapter 3

Impaired chromosome bi-orientation seems to be causing a SAC-dependent metaphase I delay in tetraploid *Arabidopsis thaliana*

Konstantinos Lampou[1], Franziska Böwer[1], Shinichiro Komaki[2], Arp Schnittger[1]

[1] Department of Developmental Biology, Institute for Plant Sciences and Microbiology, University of Hamburg, 22609 Hamburg, Germany

[2] Graduate School of Science and Technology, Nara Institute of Science and Technology, Nara, 630-0192 Japan

Contributions of authors

All experiments were performed exclusively by me, Konstantinos Lampou, unless stated explicitly below. I am deeply indebted to Franziska Böwer and Dr. Shinichiro Komaki for their significant contribution to this work.

Franziska Böwer performed the meiotic chromosome spreads of F3 tetraploid wild type and *mad2* plants.

Dr. Shinichiro Komaki has generated and transformed all reporters used in this study. They were published in Komaki & Schnittger (2017). Additionally, he performed virus-induced gene silencing treatment of wild type and *mad2* plants expressing the BMF3 and TUA5 reporters and harvested the F1 seeds.

Chapter organization

The chapter is written in the form of a manuscript, including the following sections: Abstract, Introduction, Results and Discussion, and finally, Materials and Methods. The main figures are designated as "Figure *X*", where *X* is the corresponding number starting at 1, and the supplementary figure is designated as "Figure EV*X*", where "EV" stands for "expanded view" and *X* is the corresponding number starting at 1.

Abstract

Polyploidy, i.e., having three or more complete sets of chromosomes, occurred frequently in the plant lineage, especially among angiosperms. Its prevalence and evolutionary significance have sparked renewed interest in the last decades in studying the advantages and disadvantages of polyploidy as well as the molecular and cell biological adaptations that (neo-)polyploids have to undergo. For example, neo-polyploids face severe issues in meiosis due to aberrant chromosome pairing as well as chromosome entanglement during prophase I, leading eventually to chromosome missegregation and reduced fertility. The molecular mechanisms underlying these defects have attracted a lot of attention considering also the agricultural significance of polyploids in times of severe environmental challenges such as global warming. However, subsequent phases of meiosis have received little to no attention. Using live-cell imaging of male meiocytes, we found that metaphase I duration is noticeably longer in *Arabidopsis thaliana* neo-autotetraploids. We did not observe any delay in metaphase II as well as metaphase in mitosis, where no homologous chromosome pairing takes place. Based on spindle and cell size quantifications, we propose that improper kinetochore orientation in multivalents or entangled chromosomes probably caused the observed delay in metaphase I.

Introduction

Organisms possessing three or more complete chromosome sets are polyploid. We can distinguish between two types of polyploids. Autopolyploids are the result of whole-genome duplication (WGD) within a single species. Allopolyploids are the result of hybridization between different species followed by genome doubling. The evolutionary significance of polyploidization has been a subject of fierce debate (D. E. Soltis et al., 2014), there is, however, no doubt that polyploidy is very common in the plant lineage. While estimates vary substantially, depending on the approach used to infer polyploidization, 30-80 % of angiosperms are currently estimated to be polyploid (Ramsey & Schemske, 1998; P. S. Soltis & Soltis, 2009).

Not only are many important agricultural plants, such as cotton, potato, rapeseed, wheat, and sugarcane, polyploids, but polyploids are multi-stress resilient, and thus, are a promising strategy for crop improvement in times of environmental instability such as global warming (Bomblies, 2020). Surprisingly, the view that polyploidy is an evolutionary "dead end" has been very influential and has shaped research in the field during the last century (D. E. Soltis et al., 2014). However, several recent studies have highlighted that, although polyploids might not be favorable under stable conditions, they are of great importance in times of severe environmental challenges or invasion of novel habitats by providing increased genetic variation to their diploid counterparts that enhances their short-term adaptation potential and eventually shapes their evolutionary trajectory in the long-term (Te Beest et al., 2012; Van De Peer et al., 2017). Indeed, palaeopolyploidization might have defined plant evolution in an unprecedented and underappreciated way. Multiple independent polyploidization events coincide with the Cretaceous-Paleogene boundary around 66 million years ago, the most recent and arguably most (in)famous extinction event that wiped out all non-avian dinosaurs (Fawcett et al., 2009; Vanneste et al., 2014; Wu et al., 2020). These studies and others suggest that polyploidization might have helped plants adapt to the harsh environment with global wildfires, leading to massive dust clouds and

subsequently, global cooling caused by the asteroid impact as well as a potential surge in volcanic activity (Van De Peer et al., 2017).

Despite these major advantages, polyploidy is also connected with a multitude of challenges, especially when it first arises, somewhat justifying the initial – albeit rather simplistic and incomplete – view of polyploidy being an evolutionary "dead end" (D. E. Soltis et al., 2014). For example, meiosis presents a major hurdle, especially for neo-autopolyploids, which typically exhibit missegregation of chromosomes in meiosis I due to multivalent formation and chromosome entanglement, eventually generating aneuploid gametes (Bomblies, 2023; Bomblies et al., 2016). In diploid meiosis, homologous chromosomes are physically connected in prophase I through the formation of at least one crossover (CO) between non-homologous sister chromatids forming bivalents. The sister chromatids of each homolog are also physically linked together and their two kinetochores are mono-oriented, meaning that they act as a single unit. Finally, multivalents arising from entanglement of chromosomes during prophase I are dissolved (Storlazzi et al., 2010). All of these factors together ensure the bi-orientation of bivalents and the proper segregation of homologs in metaphase I. Polyploids face, however, some challenges in this respect. On the one hand, allopolyploids must avoid pairing between homoeologous chromosomes, i.e., chromosomes of the two hybridizing species that were identical in the common ancestor but have diverged since, because this can result in deleterious chromosomal rearrangements and/or gene loss. On the other hand, since COs form based on sequence homology, autopolyploids, that possess four virtually identical homologous chromosomes, must either limit CO formation to no more than two homologous chromosomes forming bivalents or generate quadrivalents, i.e., COs among all four homologous chromosomes, in a configuration that promotes proper segregation. Indeed, both strategies have been reported in established autotetraploid species and many influential studies have been excellently summarized in Bomblies (2023), Bomblies et al. (2016), and Hollister (2015).

While the vast majority of (neo-)polyploid meiosis research has focused on prophase I, little to no attention has been paid to subsequent phases. Metaphase I is of particular interest in this respect as one can envision that the presence of univalents and/or multivalents probably interferes with the bi-orientation of homologous chromosomes. This would trigger the spindle assembly checkpoint (SAC), a safe-guarding mechanism that prevents the onset of anaphase before all kinetochores are attached to spindle microtubules (MTs) in a stable, end-on, bipolar configuration (Lara-Gonzalez et al., 2021; London & Biggins, 2014; McAinsh & Kops, 2023; Musacchio, 2015). We have attempted a first description of the *Arabidopsis thaliana* (Arabidopsis) meiotic SAC in our previous work and found that it is an active, but weak checkpoint that can be flexibly silenced (Chapter 1), not unlike the pachytene checkpoint in Arabidopsis (De Jaeger-Braet et al., 2021). Briefly, the Arabidopsis SAC consists of two major kinases, BMF1 and MPS1, a transient kinetochore-bound complex and a transient cytosolic complex, the mitotic checkpoint complex (MCC) (Komaki & Schnittger, 2017; Chapter 1). The Arabidopsis kinetochore-bound complex consists of BMF3, MAD1, and MAD2, while BMF2, MAD2, and CDC20 were hypothesized to form the MCC (Komaki & Schnittger, 2017; Chapter 1).

Here, we have set out to understand the implications of neo-tetraploidization on metaphase I. Utilizing our live-cell imaging platform of male meiocytes (Prusicki et al., 2019; Chapter 1), we observed a SAC-dependent metaphase I delay in neo-autotetraploid Arabidopsis. However, this was neither the case in metaphase II nor metaphase in mitosis. Our work suggests that the SAC in metaphase I might be triggered by incorrect kinetochore orientation in multivalents and/or entangled chromosomes preventing sufficient kinetochore-microtubule (K-MT) occupancy and timely SAC silencing.

Results & Discussion

Metaphase I duration is increased in a SAC-dependent manner in autotetraploids

Unpublished work from our lab has found that meiosis progresses more slowly in tetraploid wild type (WT) male meiocytes compared to their diploid counterpart. To understand this process better, we wanted to test whether there are any differences in SAC activity and/or metaphase I duration in tetraploid versus diploid plants. For this, we generated two independent neo-autotetraploid Arabidopsis WT lines expressing the BMF3 and TUA5 reporters (Komaki & Schnittger, 2017; Chapter 1) using a virus-induced gene silencing approach (VIGS) we have previously published in Calvo-Baltanás et al. (2022). We confirmed the chromosome number with chromosome spreads of male meiocytes (Fig. EV1).
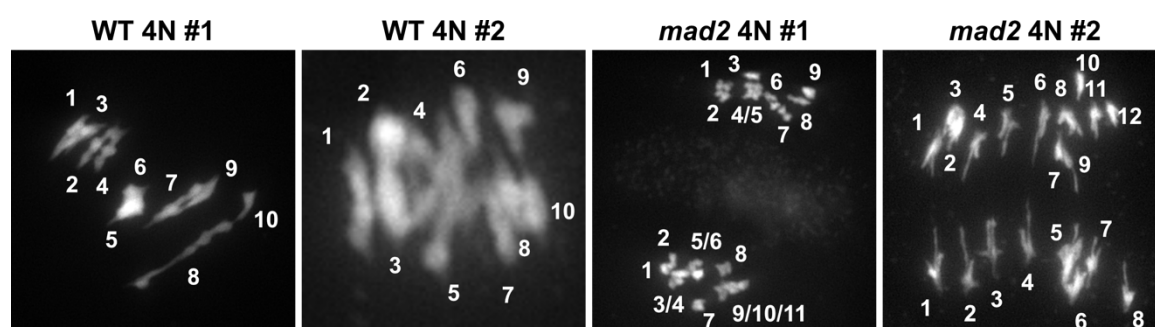
Figure EV1 Representative chromosome spreads of male meiocytes of the autotetraploid WT and *mad2* lines. For ease of counting the chromosomes were numbered due to multivalents and chromosome entanglements often observed in neo-autotetraploid plants.

We, then, proceeded with more detailed cell biological analysis and imaged male meiocytes in meiosis I from nuclear envelope breakdown (NEB) until anaphase onset (AO) as previously described (Prusicki et al., 2019; Chapter 1). In two independent autotetraploid WT lines, we observed an ~ 50-60 % prolonged BMF3 localization to the kinetochore (Fig. 1A, B) and an ~ 40-55 % longer metaphase I duration (Fig. 1A, C) compared to the diploid WT. This suggested that the SAC might be involved in delaying AO in the autotetraploid WT background.
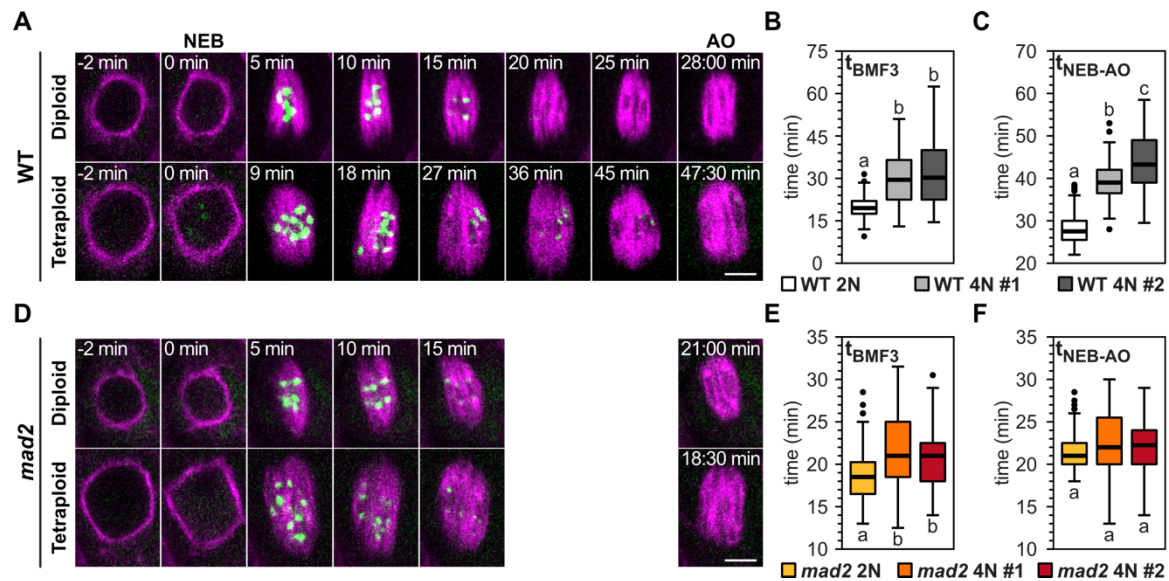
**Figure 1 Tetraploid male meiocytes exhibit a longer metaphase I duration than diploid cells in a SAC-dependent manner. (A)** Representative diploid and autotetraploid WT male meiocytes in metaphase I. **(B, C)** Quantification of BMF3 kinetochore signal **(B)** and metaphase I **(C)** duration in diploid and autotetraploid WT cells. **(D)** Representative diploid and autotetraploid *mad2* male meiocytes in metaphase I. **(E, F)** Quantification of BMF3 kinetochore signal **(E)** and metaphase I **(F)** duration in diploid and autotetraploid *mad2* cells. **(A, D)** BMF3 is fused to GFP (green) and TUA5 to TagRFP (magenta). Movies were recorded with a frame rate of 30 seconds. For **(B, C)**, we quantified 130-160 cells from 28-33 anthers per genotype. For **(E, F)**, we quantified 85-168 cells from 26-31 anthers per genotype. Different letters indicate significance (P < 0.01; pairwise comparison using Kruskal-Wallis test for independent samples with Bonferroni correction for multiple tests). Scale bars: 5 μm.

To test this, we, next, generated neo-autotetraploid *mad2* plants expressing the BMF3 and TUA5 reporters by VIGS (Calvo-Baltanás et al., 2022), confirmed the chromosome number with chromosome spreads of male meiocytes (Fig. EV1), and performed the same measurements in *mad2* autotetraploids, where SAC activity is abolished (Komaki & Schnittger, 2017; Chapter 1). Interestingly, BMF3 kinetochore signal duration in *mad2* autotetraploids was ~ 12-17 % longer compared to diploid *mad2* (Fig. 1 D, E). However, in the *mad2* background metaphase I duration was essentially identical in the diploid and the two independent autotetraploid lines (Fig. 1D, F).

Finally, we wanted to test the effects of autotetraploidy on fertility, especially in the *mad2* background with abolished SAC activity. Thus, we quantified pollen and seed viability in autotetraploid WT and *mad2* lines and compared them to their diploid

counterparts (Fig. EV2). Pollen and seed viability in both autotetraploid WT lines were on average lower than in their diploid counterpart by ∼ 3 % and ∼ 25-30 %, respectively (Fig. EV2A). Autotetraploid *mad2* lines were more severely affected with pollen viability dropping on average by ∼ 8-9 % and seed viability by ∼ 36-41 % (Fig. EV2B). Both in the WT and *mad2* the seed viability was more strongly affected than the pollen viability. There are probably two reasons for that. First, while scoring pollen viability, we cannot account for pollen aneuploidy that could subsequently lead to seed abortion. Secondly, while scoring seed viability, we are measuring a combination of aneuploid male and female gametophytes as well as aberrant seed development.

Thus, we conclude from these experiments that the delay in metaphase I in the autotetraploid WT background is SAC-dependent and that SAC activity enhances the fertility in neo-autotetraploids.
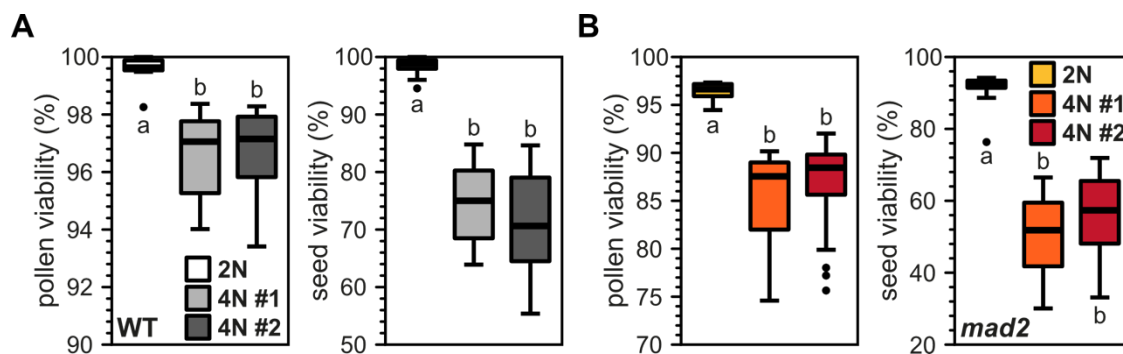
Figure EV2 Diploid and autotetraploid *mad2* lines exhibit more severe pollen and seed viability defects compared to their WT counterparts. Pollen and seed viability in diploid and autotetraploid WT **(A)** and *mad2* **(B)**. For **(A)**, we quantified 385-1232 pollen grains per plant from 26-28 plants per genotype and counted seeds from 3-9 siliques per plant from 26 plants per genotype. For **(B)**, we quantified 185-1061 pollen grains per plant from 14-17 plants per genotype and counted seeds from 6-11 siliques per plant from 16-18 plants per genotype.

The extension of metaphase in autotetraploids is specific to metaphase I

To test whether metaphase duration in mitosis is also sensitive to changes in ploidy, as previously reported for autotetraploid mammalian cells (Bloomfield et al., 2021; Kuznetsova et al., 2015; Paim & FitzHarris, 2019; Quinton et al., 2021), we imaged diploid and autotetraploid mitotic root epidermal cells (Fig. 2A). BMF3

kinetochore signal duration increased non-significantly (P > 0.01) by ~ 7 % in autotetraploid line # 1 and remained essentially identical in autotetraploid line # 2 compared to the diploid WT (Fig. 2B). Similarly, metaphase duration increased marginally, but not significantly (P > 0.01), by ~ 3-12 % in autotetraploid lines compared to the diploid WT (Fig. 2C). Thus, both BMF3 kinetochore signal and metaphase duration were not significantly (P > 0.01) different in autotetraploid versus diploid mitotic root cells.
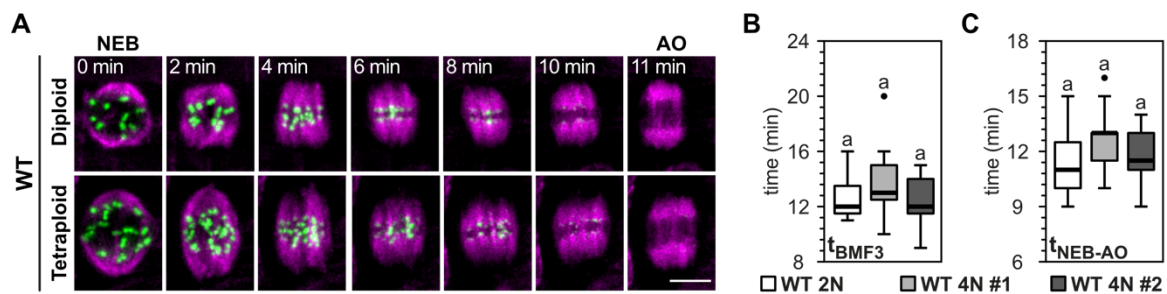
Figure 2 Metaphase duration is not significantly different between diploid and autotetraploid mitotic root cells. (A) Representative maximum projections of a diploid and autotetraploid WT mitotic root cell in metaphase. 3D movies were recorded with a frame rate of 1 min. Scale bar: 5 μm. **(B, C)** Quant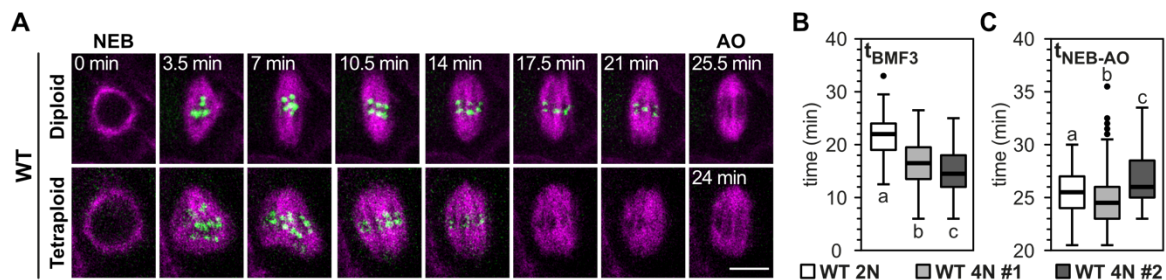ification of BMF3 kinetochore signal **(B)** and metaphase **(C)** duration in diploid and autotetraploid WT cells. For **(B, C)**, we quantified 19-20 cells per genotype. Different letters indicate significance (P < 0.01; pairwise comparison using Kruskal-Wallis test for independent samples with Bonferroni correction for multiple tests).

Considering that metaphase duration of meiosis I, but not mitosis, was prolonged by the increase in ploidy in a SAC-dependent manner, we wanted to measure BMF3 kinetochore signal and metaphase duration in meiosis II. Since sister chromatids are separated in meiosis II, it resembles a mitotic division. We, thus, imaged anthers of the two independent autotetraploid WT lines in meiosis II and compared them to their diploid counterpart (Fig. 3A). The BMF3 kinetochore signal duration was decreased significantly (P < 0.01) by ~ 24 % and ~ 32 % in autotetraploid line #1 and #2, respectively. However, the duration of metaphase II exhibited only an ~ 2 % decrease in autotetraploid line # 1, while we observed an ~ 5 % increase in autotetraploid line # 2 (Fig. 3C). Despite the fact that tetraploid metaphase II duration was significantly different (P < 0.01) from their diploid counterpart, the difference was rather marginal compared to what we have

observed in meiosis I (Fig. 1C). Our results suggested that metaphase II was also relatively unaffected by the doubling in chromosome numbers.

Figure 3 Autotetraploid male meiocytes do not exhibit a similar increase in metaphase II duration compared to metaphase I. (A) Representative diploid and autotetraploid WT male meiocytes in metaphase II. Movies were recorded with a frame rate of 30 seconds. Scale bar: 5 μm. **(B, C)** Quantification of BMF3 kinetochore signal **(B)** and metaphase II **(C)** duration in diploid and autotetraploid WT cells. For **(B, C)**, we quantified 122-207 spindles from 7-21 anthers per genotype. Different letters indicate significance (P < 0.01; pairwise comparison using Kruskal-Wallis test for independent samples with Bonferroni correction for multiple tests).

We conclude that the SAC-dependent extension of metaphase in WT autotetraploids was specific to metaphase I.

spo11-1 rec8 mutants exhibit a similar increase in metaphase I duration to autotetraploid WT male meiocytes

Considering our results, we next hypothesized that the SAC-dependent delay in metaphase I might have been caused by the increase in chromosome number and not by the formation of multivalents and/or entangled chromosomes frequently observed in neo-autotetraploids. To generate a first meiotic division with double the chromosome number, while preventing multivalent formation and chromosome entanglement, we took advantage of the *spo11-1 rec8* double mutant, which was previously shown to undergo a mitotic-like first meiotic division (Chelysheva et al., 2005). More specifically, SPO11-1 generates double-strand breaks in prophase I, an essential prerequisite towards the formation of COs, and REC8 is necessary to maintain the monopolar orientation of sister chromatid kinetochores. Hence, in the absence of COs, no bivalents are formed and without mono-orientation of sister chromatid kinetochores, sister chromatids and not homologous chromosomes are separated in meiosis I (Chelysheva et al., 2005).

We observed that metaphase I duration in *spo11-1 rec8* was increased by ~ 56 % in comparison to the WT (Fig. 4A, B), which is in a similar range to what we have measured in the autotetraploid WT lines before (Fig. 1C). Although we cannot exclude that the absence of SPO11-1 and/or REC8 negatively impacts the efficient K-MT capture or other processes that might have led to the observed delay, we are not aware of any work that would support such a hypothesis. Quite the opposite is the case, as overexpression of Spo11 or Rec8 in fission yeast was recently shown to dismantle centromeres and potentially impact kinetochore structure (Hou et al., 2021).
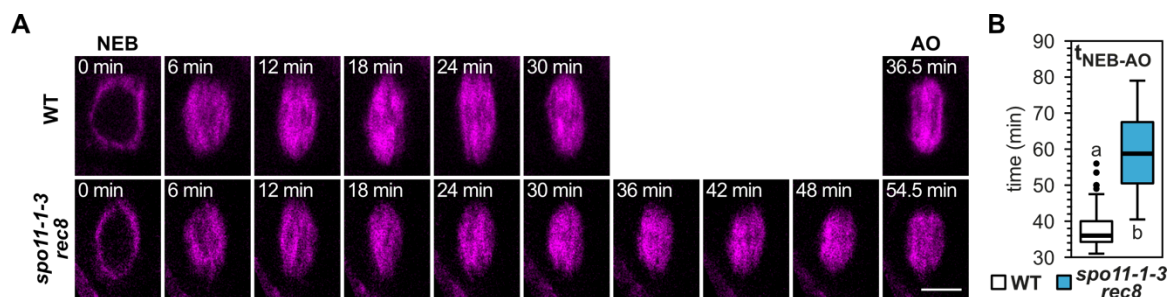
Figure 4 *spo11-1-3 rec8* **male meiocytes exhibit a similar metaphase I duration increase to autotetraploid WT male meiocytes in metaphase I. (A)** Representative WT and *spo11-1-3 rec8* male meiocytes in metaphase I. Movies were recorded with a frame rate of 30 seconds. Scale bar: 5 *µ*m. **(B)** Quantification of metaphase I duration in WT and *spo11-1-3 rec8* cells. We quantified 96-104 cells from 15 anthers per genotype. Different letters indicate significance (P < 0.001; Mann-Whitney U test for independent samples).

Distinct defects explain most probably the delayed metaphase I in *spo11-1 rec8* and autotetraploid WT

Experimental and modeling studies have suggested that a combination of factors including cell and spindle size as well as MT abundance influence metaphase duration through altering SAC signaling dynamics (Bloomfield et al., 2021; J. Chen & Liu, 2016; Galli & Morgan, 2016; Kyogoku & Kitajima, 2017). More specifically, studies in mouse oocytes (Kyogoku & Kitajima, 2017) and early *Caenorhabditis elegans* embryos (Galli & Morgan, 2016) showed that increased cell size weakened SAC signaling. Other studies have contested this, however, suggesting that cell size might be only one – but not the decisive – factor in weakening the SAC (Lane & Jones, 2017; Vázquez-Diez et al., 2019). Furthermore, modeling work suggested that both spindle scaling with cell size and the spindle width-to-

length aspect ratio were important for proper SAC silencing, and thus, essential for SAC signaling robustness (J. Chen & Liu, 2016). J. Chen & Liu (2016) provided some preliminary modeling data that increase in ploidy might weaken the SAC robustness even in plant cells. Though these results should be regarded with caution as they applied their metazoan-centric model to plant cells with minimal change in their modeling parameters.

With this in mind, we decided to measure and compare spindle dimensions in the different metaphases to test whether this correlated with the delay observed only in metaphase I. Spindle length increased by ~ 8-10 % in WT autotetraploid metaphase I and by ~ 6-16 % in WT autotetraploid metaphase II compared to the diploid control, while it was not significantly (P > 0.01) different in WT diploid versus tetraploid mitotic root cells as well as WT versus *spo11-1 rec8* meiocytes in metaphase I (Fig. 5A-E). On the other hand, spindle width increased by ~ 24-29 % in all WT autotetraploid metaphases compared to the diploid control, while it was not significantly (P > 0.01) different in WT versus *spo11-1 rec8* meiocytes in metaphase I (Fig. 5F-J). Accordingly, spindle area increased by ~ 31-50 % in all WT autotetraploid metaphases compared to the diploid control, while it was not significantly (P > 0.01) different in WT versus *spo11-1 rec8* meiocytes in metaphase I (Fig. 5K-O).

Next, we calculated the width-to-length aspect ratio of the spindles (Fig. 5P-T), as modeling work from J. Chen & Liu (2016) has shown that efficient SAC silencing is achieved in long and thin (low aspect ratio) or short and wide (high aspect ratio) spindles. WT autotetraploid spindles exhibited significantly (P< 0.01) increased aspect ratio by ~ 13-17 % in metaphase I and ~ 10-22 % in metaphase II (Fig. 5P-R), while in both cases the spindle length increased (Fig. 5A-C). On the other hand, mitotic spindle length was not significantly (P > 0.01) different between diploid and autotetraploid WT cells (Fig. 5A, D), while spindle width increased significantly (P < 0.01) (Fig. 5F, I), which was also reflected in the significant (P < 0.01) aspect ratio increase by ~ 26-29 % in WT autotetraploid cells (Fig. 5P, S). Finally, the aspect ratio remained unchanged between WT and *spo11-1 rec8* meiocytes in

metaphase I (Fig. 5P, T). Based on the modeling study of J. Chen & Liu (2016), the aspect ratios measured in all backgrounds relative to the observed spindle length were within the range of efficient SAC silencing. Although this should be regarded with caution, as one cannot simply compare experimental results from autotetraploid plant cells with a model built for diploid mammalian cells, if an incorrect aspect ratio would have been the underlying cause of the observed delay in metaphase I, then one would have expected that the aspect ratio should decrease for metaphase II spindles, which are significantly ($P < 0.01$) longer than their diploid counterpart (Fig. 5A, C). This was, however, not the case (Fig. 5P, R). Hence, we think that neither spindle size parameter correlated consistently with NEB-AO duration.

Finally, we wanted to see if the increase in spindle size positively correlated with cell size in autotetraploid meiocytes, as there is contradicting evidence coming from metazoan and yeast model systems regarding the scaling of the spindle relative to the cell volume (Bloomfield et al., 2021; Crowder et al., 2015; Storchová et al., 2006). More specifically, the cell volume of budding yeast cells scales with ploidy, but the metaphase spindle length does not and this does not seem to cause any delays in cell-cycle progression (Storchová et al., 2006). On the contrary, the size of the metazoan mitotic spindle scales linearly with cell size across many species, while female meiotic spindles do not, hinting at distinct regulatory mechanisms between mitotic cells and oocytes (Crowder et al., 2015). Similarly, a positive correlation between spindle and cell size has been observed in autotetraploid human cells as well, where smaller cells exhibit a stronger metaphase delay than larger cells (Bloomfield et al., 2021). Indeed, several studies reported that autotetraploid mammalian cells progressed more slowly through metaphase (Kuznetsova et al., 2015; Paim & FitzHarris, 2019; Quinton et al., 2021). Arabidopsis autotetraploid male meiocytes had on average ~ 54-56 % larger cell area compared to their diploid counterpart, confirming a positive correlation between the two factors. Since smaller rather than larger human autotetraploid cells exhibited prolonged metaphase duration (Bloomfield et al., 2021), the size of meiocytes did not seem to explain the observed phenotype either.
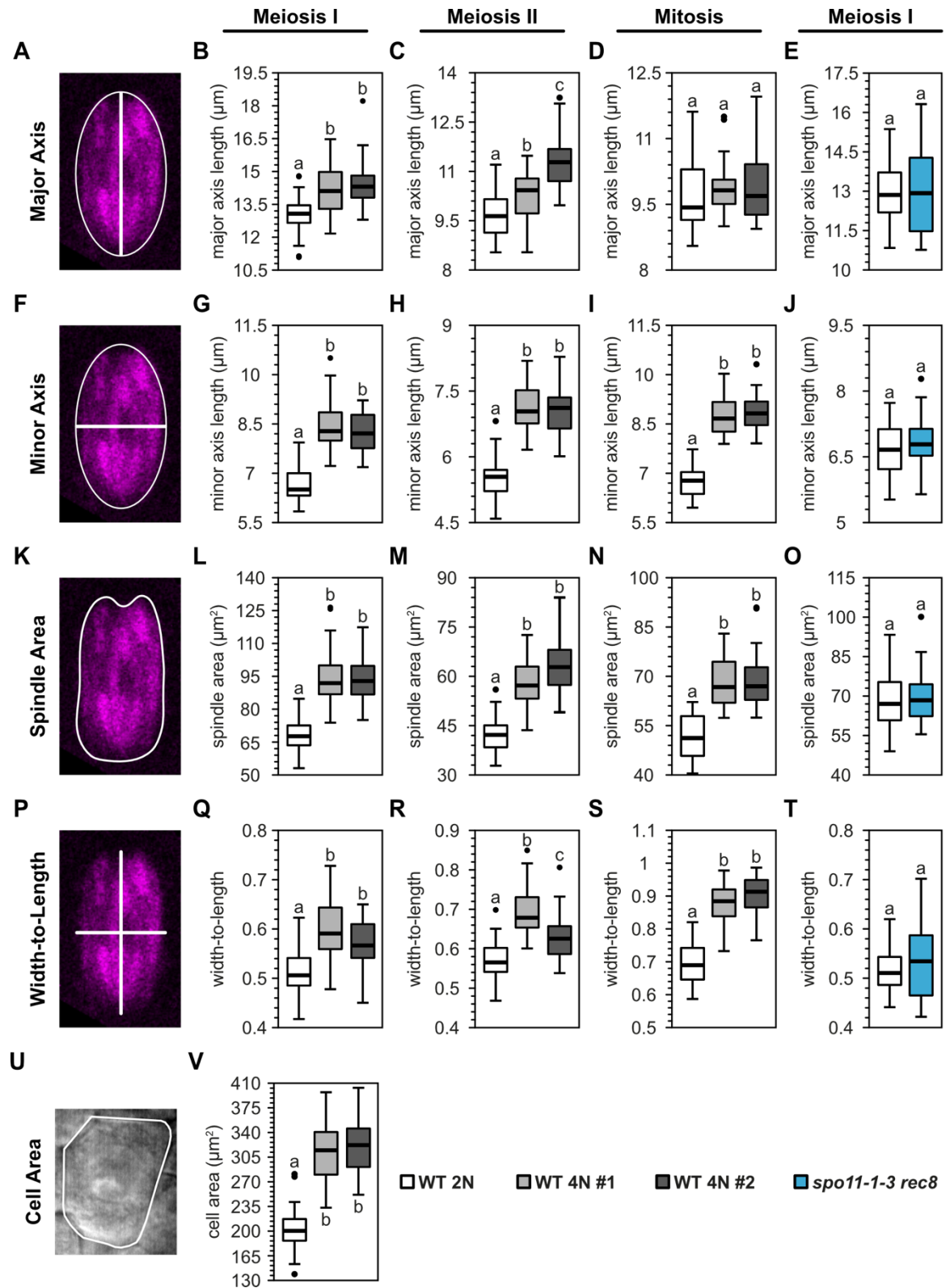
Figure 5 Neither changes in spindle dimensions nor cell area correlate consistently with metaphase duration. Quantification of spindle length **(A-E)**, spindle width **(F-J)**, spindle area **(K-O)**, spindle width-to-length aspect ratio **(P-T)**, and cell area **(U, V)**, as shown in representative images **(A, F, K, P, U)**, for metaphase I **(B, E, G, J, L, O, Q, T, V)**, metaphase II **(C, H, M, R)**, and metaphase in mitosis **(D, I, N, S)**. For **(B, G, L, Q)**, we quantified 39-60 spindles from 16-26 anthers per genotype. For **(C, H, M, R)**, we quantified 44-57 spindles from 7-21 anthers per genotype. For

(D, I, N, S), we quantified 19-20 spindles from equal number of mitotic root cells. For **(E, J, O, T)**, we quantified 30-46 spindles from 15 anthers per genotype. For **(V)**, we quantified the cell area of 31-48 cells from 16-26 anthers per genotype. For comparisons between multiple genotypes, different letters indicate significance ($P < 0.01$; pairwise comparison using Kruskal-Wallis test for independent samples with Bonferroni correction for multiple tests). For comparisons between two genotypes, different letters indicate significance ($P < 0.01$; Mann-Whitney U test for independent samples).

These measurements prompted us to entertain an alternative hypothesis, i.e., the increase in metaphase I duration was perhaps caused by multivalent formation and/or entangled chromosomes resulting in incorrect kinetochore orientation, which in turn led to insufficient K-MT occupancy resulting in prolonged SAC signaling. Multivalents and entangled chromosomes are frequently formed in neo-autotetraploids (Bomblies, 2023; Bomblies et al., 2016), and these aberrant configurations might lead to kinetochores being less accessible to spindle MTs. A careful re-examination of our movies showed that the prolonged SAC activation as quantified in Fig. 1B was caused mostly by one and less frequently by more homologous chromosome pairs that had either defective metaphase plate alignment or, despite the alignment at the metaphase plate, the BMF3 signal persisted on at least one of the kinetochores (Fig. 6), suggesting that the cells had trouble in efficiently aligning and bi-orienting their chromosomes. This would be consistent with multivalents and/or entangled chromosomes having formed in prophase I and their kinetochores being oriented in a way that prevented efficient bi-polar attachment or sufficient end-on K-MT interactions that would lead to SAC silencing. This hypothesis is also consistent with neither metaphase II nor metaphase in mitotic root cells being delayed in autotetraploids versus diploids, as these aberrant chromosomal arrangements are specific to meiosis I.
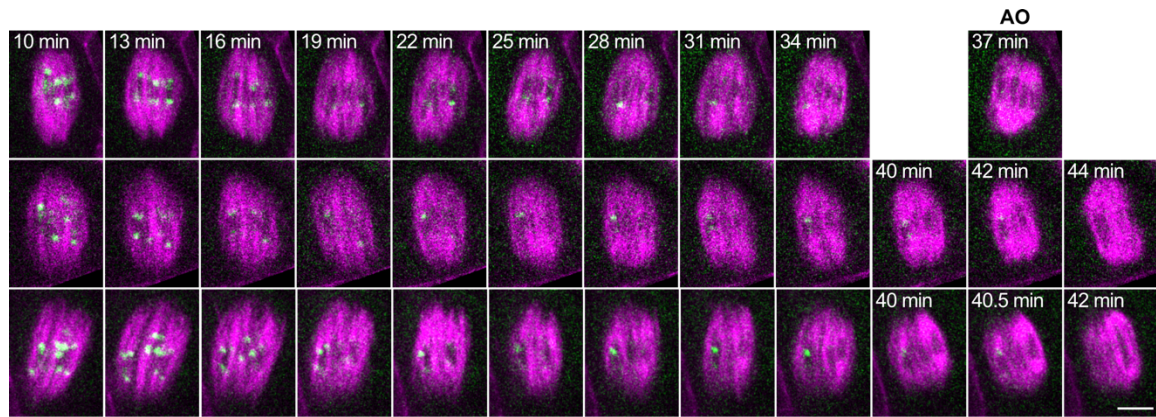
Figure 6 Representative autotetraploid spindles in metaphase I with persistent BMF3 kinetochore signal. Notice that only few kinetochores are labeled by BMF3, despite alignment at the metaphase plate suggesting that they are connected through erroneous K-MT attachments to spindle MTs. Scale bar: 5 μm.

On the other hand, in the case of *spo11-1 rec8*, spindle size remained unchanged in comparison to the WT (Fig. 6E, J, O), while in *spo11-1 rec8*, double the number of kinetochores need to be attached to spindle MTs in metaphase I in comparison to the WT. Since spindle size and possibly MT density did not scale with kinetochore number in this background, we propose that insufficient MTs are present in metaphase I to form enough end-on, bipolar K-MT attachments to silence the SAC in a timely manner. Although we cannot formally exclude this, it is most probably not the case in autotetraploid metaphase I, as one would expect a delay also in metaphase II and metaphase in mitotic root cells under this condition. Additionally, the surface area of the spindle in metaphase I averaged at ~ 94 μm^2 and at ~ 58-63 μm^2 in metaphase II (Fig. 5L, M). Based on our experience both spindles in metaphase II are of approximately the same dimensions and assuming that MT density is similar between spindles in metaphase I and II, the total surface area of the two spindles in autotetraploid metaphase II is larger than of the single spindle in metaphase I, suggesting that sufficient tubulin dimers are present in these meiocytes.

Conclusion

In contrast to tetraploid mammalian cells, that exhibit a metaphase delay already in mitosis (Bloomfield et al., 2021; Kuznetsova et al., 2015; Paim & FitzHarris, 2019; Quinton et al., 2021), this was the case only for metaphase I in Arabidopsis. We propose that multivalent formation and/or chromosome entanglement during prophase I resulting in incorrect kinetochore orientation are the most probable culprits causing the quantified delay in autotetraploid metaphase I. Ultrastructural analysis of K-MT connections (lateral versus end-on) as well as kinetochore orientation in autotetraploid metaphase I, metaphase II, and metaphase in mitosis might reveal the underlying cause of the observed delay in the future. Considering the propensity of plants for polyploidization, it is of particular interest to understand the mechanisms that allow tetraploid plant cells to efficiently capture chromosomes in metaphase II and metaphase in mitosis and how spindle architecture might influence this process.

Materials & Methods

Plant materials

We used the *Arabidopsis thaliana* (Arabidopsis) accession Columbia-0 (Col-0) as the wild type (WT) throughout this work. We used the T-DNA insertion lines SAIL_191G06 (*mad2*), SALK_146172 (*spo11-1-3*), and SAIL_807B08 (*rec8*) which we obtained from the Nottingham Arabidopsis Stock Center (NASC) (http://arabidopsis.info/). The primers for genotyping *mad2* are described in Komaki & Schnittger (2017), the ones for *spo11-1-3* in Grelon et al. (2001), and the ones for *rec8* are described in Bhatt et al. (1999).

For imaging mitosis, seedlings were grown in a growth chamber (16 hours light at 21 °C / 8 hours dark at 18 °C) for 4 days on a solid medium containing half-strength Murashige and Skoog (MS) medium, 1 % (w/v) sucrose, 0.8 % (w/v) agar, and pH 5.8. For imaging meiosis, 7- to 10-day old seedlings grown on plate as described above were transferred to soil and grown for 5-6 weeks in growth chambers (16 hours light at 21 °C / 8 hours dark at 18 °C).

Plasmid construction, line generation, and tetraploidization through virus-induced gene silencing (VIGS)

All reporter constructs were previously generated in Komaki & Schnittger (2017). We introgressed both reporters from the WT into *mad2* through genetic crossing.

For tetraploidization through VIGS-mediated silencing of *OSD1*, 3-week old WT or *mad2* plants expressing the BMF3 and TUA5 reporters were infiltrated with the TRV-*OSD1* vector mixed with TRV1 as described in Calvo-Baltanás et al. (2022). We targeted *OSD1* (*OMISSION OF SECOND DIVISION1*), because OSD1 is essential for the transition from meiosis I to meiosis II (D'Erfurth et al., 2009). Thus, *osd1* mutants exit meiosis after meiosis I and generate diploid gametes. We visually scored the seeds (F1) based on size and put the larger seeds on plate, because seed size in the Col-0 background positively correlates with ploidy (Calvo-Baltanás et al., 2022; Ravi et al., 2008). The plants that were exhibiting no signs of phenotypical defects and increased ratio of multi-branched trichomes, suggesting a higher ploidy (Z. Yu et al., 2009), were put on soil and their seeds were harvested. The progeny of F1 plants (F2) with a relatively low percentage of aberrant and dead seeds was grown on plate for 3 weeks to score for phenotypic defects. The ploidy of F2 plants was determined in a CyFlow® Ploidy Analyzer (Partec). We used non-infiltrated Col-0 plants as our diploid reference and F3 tetraploid Col-0 plants produced through VIGS-mediated silencing of *OSD1* and confirmed through meiotic chromosome spreads as our tetraploid reference. All experiments were performed in the F3 in two independent WT and *mad2* autotetraploid lines.

Meiotic chromosome spreads

Chromosome spreads of F3 autotetraploid male meiocytes were performed essentially as previously described in Ross et al. (1996). Briefly, fresh flower buds of 5-6 week-old plants were incubated for ≥ 48 hours in a 3:1 ethanol:acetic acid fixative solution at 4 °C. Upon being washed twice with fresh fixative solution, they were stored for further use in a 70 % ethanol solution at 4 °C. To prepare them for chromosome spreading, the flower buds were digested in a 10 mM citrate, 1.5% cellulose, 1.5 % pectolyase, and 1.5 % cytohelicase solution for 3 hours at 37 °C.

Flower buds were screened based on size and those deemed to be at the right stage were transferred onto a glass slide, and crashed with a bended needle in a 12 μl 45 % acetic acid solution. Finally, for chromosome spreading, the slide was incubated for 2 minutes on a hot plate at 48 °C, subsequently washed with fixative solution, and incubated over night at 37 °C in Vectashield with DAPI (Vector Laboratories).

Pollen and seed viability

To score pollen viability, we used the Peterson staining protocol (Peterson et al., 2010). Three to five mature flowers with dehisced anthers were dipped in 20 μl Peterson staining solution (10 % ethanol, 0.01 % malachite green, 25 % glycerol, 0.05 % fuchsin, 0.005 % orange G, and 4 % glacial acetic acid) and incubated for 1 hour at 95 °C. The samples were analyzed the same day.

To score seed viability, we opened mature siliques using a sharp needle and counted plump and aborted seeds.

Live-cell imaging

Live-cell imaging of male meiocytes was performed using the protocol described in Prusicki et al. (2019) with slight variations described in Chapter 1. Briefly, 60-80 flower buds were detached from the inflorescence stem and were placed on live-cell imaging medium as described in Prusicki et al. (2019). For 2D live-cell imaging, samples were prepared either the same day or the day before and incubated overnight in the dark.

2D live-cell imaging of male meiocytes was performed on a Zeiss LSM780 upright confocal laser scanning microscope (CLSM) equipped with a GaAsP-detector and a W-plan-Apochromat 40x/1.0 DIC M27 or a W-plan-Apochromat 63x/1.0 DIC water-dipping lens. 8-bit images were acquired using bi-directional scanning every 30 seconds with 100-113 nm lateral pixel resolution, 4 times line average, 1.36-1.62 μs pixel dwell time, and a pinhole size of 44.5 μm (1 AU for the GFP detection channel). GFP was excited at 488 nm and emission was detected at 489-550 nm.

TagRFP was excited at 561 nm and emission was detected at 565-650 nm. GFP and TagRFP were detected sequentially using line-scan mode.

For imaging mitosis, seedlings were grown vertically for 4 days as described above. Before imaging, we carefully lifted the seedlings from the growth medium and placed them one-by-one in a drop of liquid half-strength MS-medium on a glass-bottom dish. We put 6-10 seedlings on each glass-bottom dish and then covered the roots with a strip of solid half-strength MS-medium.

3D live-cell imaging of mitotic epidermal root cells was performed on a Leica TCS SP8 inverted CLSM equipped with three hybrid photodetectors (Leica HyD™) and a HC PL APO 63x/1.2 W motCORR CS2 water-immersion objective as described before (Lampou er al., 2023). We recorded 12-bit images at a 99 nm lateral pixel resolution using the bi-directional scan setting with a frame rate of 1 min, 4 times line averaging, at a speed of 700 Hz, and a pinhole size of 1.5 AU (for 510 nm emission wavelength). We used a step-size of 0.52 μm for acquiring the z-stack. GFP and TagRFP were excited at 488 nm and emission was detected simultaneously at 493-555 nm and 575-655 nm, respectively.

Post-processing of movies and quantifications

All post-processing operations and quantifications of our movies were performed in Fiji (Schindelin et al., 2012).

For 2D movies, we only adjusted the brightness and contrast settings and extracted single cells manually using the rectangle selection tool.

For 3D movies, we applied two different protocols for the BMF3 and the TUA5 signal. For BMF3, we used the command "Gaussian blur 3D" with a sigma radius of 1 for x, y, and z. For TUA5, we followed a variation of the protocol presented in Krüger (2017) and a detailed account can be found in Chapter 1.

Spindle and cell size measurement

To ensure comparable results between the different metaphases, we decided to quantify spindle dimensions after ≥ 90 % of NEB-AO time has passed. This cut-off was determined by previous observations that at this late point in metaphase, cells with intact SAC signaling and chromosome congression machinery have aligned their chromosomes at the metaphase plate. For measuring spindle length and width, an outline of flat spindles, i.e., their long axis was (near-)perpendicular to the imaging axis, was designed with the "polygon selections" tool, and added to the ROI manager in Fiji (Schindelin et al., 2012). As described in Herrmann et al. (2021), we used the command "measure" on the ROI after choosing the "Fit ellipse" setting in "Set measurements". The major axis of the ellipse corresponds to the length and the minor axis to the width of the spindle. We measured the area of the hand-designed outline for quantifying spindle and cell area.

Statistics and figure design

All graphs were generated and statistical tests were performed in IBM SPSS Statistics Version 28 (IBM Corporation).

In the boxplots, the 25th and 75th percentile are indicated by the lower and upper border of the box, respectively, the median is represented by a thick line and the outliers which are within 1.5 times the interquartile range are highlighted with the whiskers. Outliers outside this range are shown as dots above and below the whiskers.

For comparisons between two genotypes, we performed a Mann-Whitney U test. For comparisons between multiple genotypes, we performed pairwise comparisons using a Kruskal-Wallis test for independent samples with Bonferroni correction for multiple tests. Both statistical tests are non-parametric and we used a significance threshold of $P < 0.01$ or $P < 0.001$.

The images and graphs were arranged into figures in Affinity Designer v. 1.10 (Serif).

General Discussion and Outlook

Our understanding of the SAC architecture and function in plants falls short compared to what is already known in other model organisms, especially metazoans and yeast. Since every chapter included a discussion of the data presented, to avoid repeating similar discussion points, I decided to provide mostly an outlook with the most pressing research questions born out of this work, which are feasible with the currently rather limited methods available in plant meiosis and mitosis research. Additionally, I present some new experiments that did not fit in any other chapter and can provide a basis upon which future studies can build upon.

Dynamic assembly and disassembly of SAC components at the kinetochore

In Chapter 1, I set out to generate a cytological and functional framework of the Arabidopsis SAC. Timing the stepwise assembly of BMF3, MAD1, and MAD2 to the kinetochore, as well as the subsequent stepwise disassembly, is a novel aspect in SAC research as I am not aware of similar efforts in other organisms. To elucidate further the dynamics of the kinetochore SAC components, fluorescence recovery after photobleaching experiments could uncover which of these proteins cycle through unattached kinetochores in plants (Howell et al., 2004; Shah et al., 2004), thus potentially revealing whether they function in a similar way to their metazoan counterparts. Considering that the SAC response in human cells is graded (Collin et al., 2013; Dick & Gerlich, 2013) and dependent on how many active complexes are formed to generate the diffusible MCC inhibitor (C. Chen et al., 2019), maybe this rapid cycling is a way to finetune SAC activity.

Similarly, the stepwise disassembly suggests a strict hierarchy and regulation. In metazoans, the Pch2/TRIP13-p31^{comet} complex regulates SAC activation during early prometaphase and SAC silencing in later phases by catalyzing conformational changes in the HORMA domain protein Mad2 (Alfieri et al., 2018; Brulotte et al., 2017; Ma & Poon, 2016, 2018; Westhorpe et al., 2011; Ye et al., 2015). Briefly, Mad2 can adopt two different conformations, an "open" (O-Mad2) and a "closed" (C-Mad2) one. C-Mad2 can interact with Mad1 and Cdc20, become

part of the MCC, and subsequently inhibit the APC/C, while O-Mad2 cannot (Luo et al., 2002, 2004; Sironi et al., 2002). Hence, to initiate and maintain a SAC response, it is necessary to produce C-Mad2-Mad1 and C-Mad2-Cdc20 complexes, while conversion to O-Mad2 would lead to SAC silencing. The catch lies in the fact that most cytosolic Mad2 is initially in the closed conformation as it spontaneously converts from O-Mad2 to C-Mad2 (Ye et al., 2015), but to be effectively recruited to the kinetochore and form complexes with Mad1 and Cdc20 it first needs to be converted to O-Mad2 (Ma & Poon, 2016, 2018). The Pch2/TRIP13-p31^{comet} complex catalyzes this conversion, creating and replenishing a pool of O-Mad2 (Ma & Poon, 2016, 2018). Simultaneously, the Pch2/TRIP13-p31^{comet} complex assists in the turnover of MCC by removing Mad2, thus contributing also to SAC inactivation (Eytan et al., 2014; D. H. Kim et al., 2018; Ma & Poon, 2016, 2018). Essentially, the two opposing functions of the Pch2/TRIP13-p31^{comet} complex finetune the SAC response by tipping the balance in the one or the other direction. Our group has previously shown the importance of the Arabidopsis PCH2-COMET complex in regulating another HORMA domain protein, ASY1, (Balboni et al., 2020), opening up the possibility for exploring the role of this complex in the plant SAC. Indeed, the PCH2 reporter (Balboni et al., 2020) localized temporarily to kinetochores and/or centromeres from before NEB till ~ 13 minutes post-AO on average (Fig. 1). Studies in human (Arnst, 2019) and *Caenorhabditis elegans* (Nelson et al., 2015) mitotic cells have also reported localization of TRIP13/Pch2 to unattached kinetochores, suggesting that PCH2 could act in converting C-MAD2 to O-MAD2 at the kinetochore and/or centromere in Arabidopsis as well.
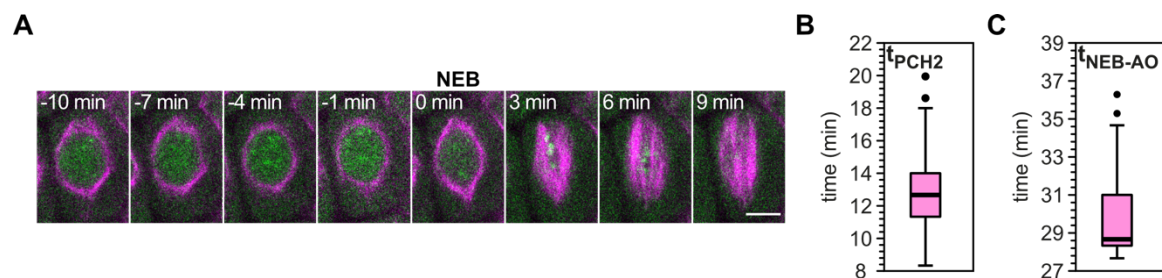
Figure 1 PCH2 localizes to the kinetochore and/or centromere prior to NEB and during metaphase I. (A) Localization of PCH2 fused to GFP (green) together with TUA5 fused to TagRFP

(magenta) in metaphase I. **(B, C)** Quantification of PCH2 kinetochore signal duration post-NEB **(B)** and duration of metaphase I **(C)**. I quantified 33-35 cells from 9 anthers.

Finally, since three major kinases, i.e., AURORA, BMF1, and MPS1, appeared to promote BMF3 kinetochore recruitment, it raises the question of whether they phosphorylate BMF3 directly and/or recruit BMF3 through phosphorylation of other kinetochore components, like KNL1. Indeed, the recruitment of BMF3 by direct or indirect MPS1-dependent phosphorylation would be a variation of the mechanism observed in metazoans (Hiruma et al., 2015; Ji et al., 2015). There, Bub3 recognizes phosphorylated proteins by Mps1 and brings Bub1 and BubR1 to the kinetochore (Primorac et al., 2013; Vleugel et al., 2013, 2015). Upon Mps1-dependent Bub1 phosphorylation, Mad1-Mad2 complexes bind on Bub1, thus completing the kinetochore-bound SAC complex (Ji et al., 2017; G. Zhang et al., 2017). In maize, ZmBUB3 did not interact with ZmBMF1/2/3 and neither ZmBMF3 nor ZmBUB3, but ZmBMF1, interacted with ZmKNL1 in yeast-two-hybrid experiments (Su et al., 2021). In Arabidopsis, BMF3 interacted with BUB3.3 in yeast-two-hybrid experiments, but the kinetochore localization of neither protein was dependent on the other, hinting at the Arabidopsis kinetochore SAC complex architecture being quite different from the one observed in metazoan and yeast model systems (unpublished data from the Liu lab; Chapter 1). So, maybe BMF3 binds through an unidentified interactor onto KNL1 or interacts with another kinetochore protein in plants which could be potentially identified through immunoprecipitation of BMF3-GFP followed by mass spectrometry or the tandem affinity purification (TAP-tag) pipeline (Van Leene et al., 2010). Importantly, I also observed a strongly decreased BMF3 recruitment in *mps1* mitotic epidermal root cells in preliminary experiments not included here, suggesting that this recruitment is conserved both in meiosis and mitosis. This also raises the possibility that MPS1 does not recruit MAD2 directly, as previously proposed in Komaki & Schnittger (2017), but rather the MAD2 kinetochore signal is not bright enough to stand out from the strong MAD2 cytosolic signal in live-cell imaging experiments. To settle this, it would be sufficient to perform immunofluorescence detection of MAD2 in *mps1*. Nonetheless, I cannot currently discount the hypothesis that MPS1 might directly and/or indirectly recruit both BMF3 and MAD2 to the kinetochore. Hence,

it remains to be elucidated with which kinetochore proteins BMF3 interacts as well as how phosphorylation by the three major kinases regulates these interactions in a cell-cycle dependent manner and ultimately, finetunes SAC activity.

Does BMF2 act as an internal timer of SAC signaling and metaphase duration?

I reported that meiotic SAC signaling could not be sustained for longer than 6 hours under severe MT-destabilizing conditions (Chapter 1), which is comparable to previous observations in mitotic root cells (Komaki & Schnittger, 2017). Interestingly, I observed that the BMF2 reporter started getting degraded ~ 8 minutes prior to AO and continued for ~ 10 minutes post-AO (Fig. 2A-C) with comparable metaphase I duration to other SAC reporter lines (compare Fig. 2D with Fig. 1E in Chapter 1), prompting us to hypothesize that maybe BMF2 acts as a molecular timer. Indeed, a plethora of studies from yeast and human cells have highlighted the importance of Mad3 and BubR1, the BMF2 yeast and human homolog, respectively, in inhibiting the APC/C by acting as a pseudosubstrate (Burton & Solomon, 2007; Choi et al., 2009; Elowe et al., 2010; E. M. J. King et al., 2007; Lara-Gonzalez et al., 2011; Lischetti et al., 2014; Malureanu et al., 2009; Rahmani et al., 2009; Sczaniecka et al., 2008; Sewart & Hauf, 2017; Zich et al., 2016). More specifically, both in yeast and human cells the two KEN-boxes of Mad3/BubR1 are important for interacting with Cdc20-Mad2 complexes generated at the kinetochore and for inhibiting the APC/C both through Cdc20 and independently of it by blocking substrate binding to the APC/C (Fig. 2A). Additional motifs such as D-boxes in Mad3/BubR1 and ABBA motifs in BubR1 further contribute to their interaction with Cdc20-Mad2 complexes and regulate checkpoint signaling (Fig. 2A) (Burton & Solomon, 2007; Choi et al., 2009; Di Fiore et al., 2015, 2016; Izawa & Pines, 2015; Sewart & Hauf, 2017). In contrast to the budding yeast Mad3, which is not degraded by the APC/C through its KEN- and D-boxes (Burton & Solomon, 2007), human BubR1 is degraded prior to AO via ubiquitination-mediated proteolysis, a process that is regulated through acetylation of lysine 250 (K250) (Fig. 2A) (Choi et al., 2009). This extra layer of regulation allows the cell to prevent APC/C-mediated Cyclin B destruction as long as unattached or poorly

attached kinetochores exist, as well as rapidly and irreversibly silence the SAC and ramp up APC/C activity upon de-acetylation and degradation of BubR1.
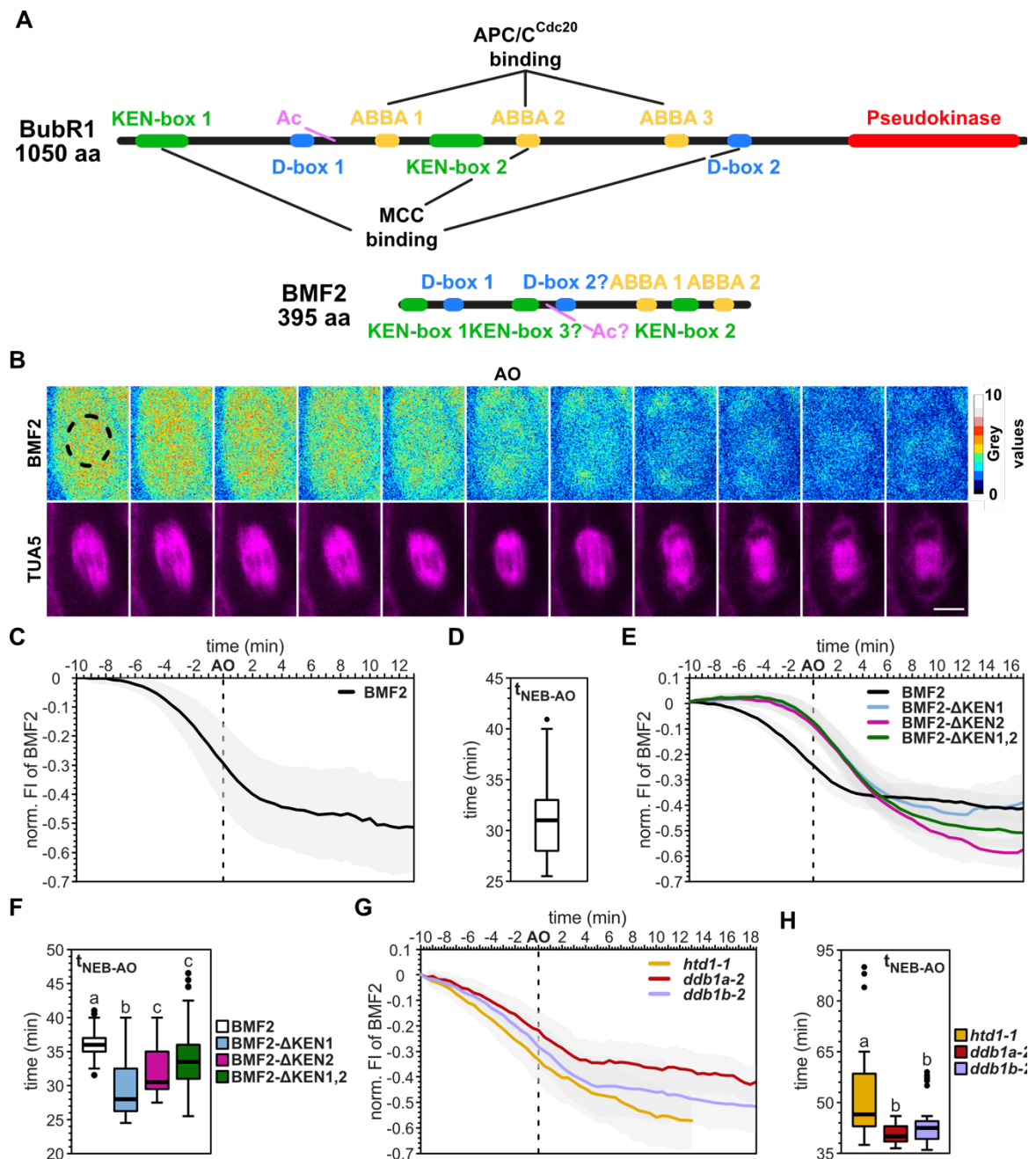
Figure 2 BMF2 is degraded prior to and immediately after AO. (A) Schematic representation of human BubR1 and Arabidopsis BMF2 drawn to scale. All the motifs necessary for binding the MCC and/or the APC/C^{Cdc20} are shown in BubR1. I also point out to the corresponding motifs in BMF2. **(B)** Representative cell highlighting the degradation of BMF2. BMF2 is fused to GFP and TUA5 to TagRFP (magenta). For the BMF2 channel, pixel intensity is represented by color. The dotted line in the first frame represents the ROI designed around the nucleus to measure BMF2 fluorescence intensity. Movies were recorded with a frame rate of 30 seconds. Scale bar: 5 μm. **(C, E, G)** Normalized BMF2 fluorescence intensity (FI) to the timepoint 10 minutes before AO: $FI_{t_n} - FI_{t_{(-10)}}) / FI_{t_{(-10)}}$. The colored line represents the average value and the grey area the standard deviation. **(D,**

F, H) Quantification of metaphase I duration. For **(C, D)**, I quantified 66 cells from 8 anthers. For **(E, F)**, I quantified 63-76 cells from 11-13 anthers. For **(G, H)**, I quantified 26-51 cells from 4-7 anthers. Different letters indicate significance (P < 0.01; pairwise comparison using Kruskal-Wallis test for independent samples with Bonferroni correction for multiple tests).

Considering the complex regulation of Mad3/BubR1 in yeast and human cells, we wondered whether the same would hold true in Arabidopsis. Thus, I took advantage of transgenic lines generated by Dr. Shinichiro Komaki where KEN-box 1 or KEN-box 2 or both KEN-boxes in BMF2 were mutated to alanine (KEN → AAA) in the *bmf2* background (Fig. 2A, E). However, in contrast to human cells (Choi et al., 2009), mutating one or both KEN-boxes was only sufficient to slow down but not stop the degradation of BMF2 (Fig. 2A, E). Metaphase I duration in ΔKEN-box 1 was significantly (P < 0.01) different to all other lines, while ΔKEN-box 2 as well as ΔKEN-box 1,2 were not significantly (P > 0.01) different from each other (Fig. 2E). However, none of the KEN-box mutants had timing as fast as the *bmf2* mutant (Chapter 1), suggesting that BMF2 had retained some of its activity as an APC/C inhibitor. Careful analysis of the BMF2 sequence revealed that it possesses a third KEN box (219-221 aa) as well as two potential D-boxes with the typical RxxL-motifs (59-62 aa and 242-245 aa) (Fig. 2A). Moreover, Di Fiore et al. (2016) identified bioinformatically two conserved ABBA-motifs spanning KEN-box 1 in the N-terminus of BMF2 (Fig. 2A). All this suggests, that in contrast to human cells, where mutating any of these motifs abrogates BubR1-mediated APC/C inhibition (Di Fiore et al., 2016), in Arabidopsis the situation might be more complicated. Hence it would be of particular interest to create a series of mutations of individual motifs and combinations thereof and measure metaphase I duration as well as BMF2 degradation kinetics in the *bmf2* background.

A TAP-tag performed by the Interactomics Facility at the VIB (University of Ghent) with a BMF2 vector generated by Dr. Shinichiro Komaki revealed that BMF2 is acetylated at K255 and K322 as well as phosphorylated at tyrosine 76 (Y76). Y76 is conserved between BMF2 and BubR1 (Y69), however no phosphorylation has been reported for this residue in BubR1 to the best of my knowledge. The acetylation of BMF2 K255 is of particular interest as it is very close to the human

BubR1 K250 that gets acetylated (Fig. 2A) (Choi et al., 2009). Actually, in the protein sequence alignment of BMF2 with human BubR1, BubR1 K250 corresponds to BMF2 K252 and BMF2 possesses also a K253. Hence, inspired by the work of Choi et al. (2009), it would be interesting to mutate K255 to arginine (R) to generate an acetylation-deficient mutant, while maintaining the positive charge of K, as well as to glutamine (Q) to generate an acetylation-mimic version of BMF2. Additionally, considering that K252 and K253 are so close to the acetylated K255 they might be able to substitute a mutated K255. Thus, it would be important to also generate double and triple substitution mutant combinations of BMF2.

Finally, in the BMF2 TAP-tag, one of the identified interactors was HEAT STRESS TOLERANT DWD1 (HTD1). HTD1 was previously reported as a negative regulator of thermotolerance in Arabidopsis and interacted with DAMAGED DNA BINDING 1a (DDB1a) and DDB1b, which are part of the Cullin4-RING ubiquitin ligase (CRL4) family of multi-subunit E3 ligases (S. H. Kim et al., 2014). DDB1 proteins mediate the connection between the CRL4 complex and the substrate receptor, i.e., a DDB1 BINDING WD40 (DWD)/WDxR protein (Angers et al., 2006; He et al., 2006; Higa et al., 2006). Considering that HTD1 acts presumably as a substrate receptor in a CRL4 complex (S. H. Kim et al., 2014) and it also interacted with BMF2, it prompted me to hypothesize that BMF2 might be additionally degraded by this pathway, independently of the hypothesized APC/C-mediated degradation based on data from human cells. Hence, I introgressed via genetic crossing the BMF2 and TUA5 reporters in the *htd1-1*, *ddb1a-2*, and *ddb1b-2* background (Bernhardt et al., 2010). Both *htd1-1* and *ddb1b-2* have strongly decreased transcript levels, while *ddb1a-2* is a null mutant (Bernhardt et al., 2010; S. H. Kim et al., 2014). My results suggest that the BMF2 degradation kinetics are different in *htd1-1* and *ddb1b-2* than the ones observed in *ddb1a-2* and *bmf2* (compare Fig. 2G with Fig. 2C and 2E). Both in *htd1-1* and *ddb1b-2* the BMF2 degradation started already at 10 minutes before AO and the curve appeared linear, i.e., the degradation was faster, compared to the more S-shaped degradation curve for BMF2 in *ddb1a-2* and *bmf2* (Fig. 2C, E, G). This is the opposite of what one would expect if HTD1

and/or DDB1b would be involved in the degradation of BMF2. Nonetheless, it should be noted, that no control with the BMF2 reporter in the *bmf2* background was included in this preliminary experiment making final conclusions rather difficult. Finally, metaphase I duration was significantly (P < 0.01) longer in *htd1-1* compared to *ddb1a-2* and *ddb1b-2*, the latter having metaphase I duration more similar to the BMF2 reporter in *bmf2* (Fig. 2D, 2F, 2H). Considering that the results from this preliminary experiment were not very clear, I propose that this is not the most promising line of inquiry for the future.

BUB3.3-KIN7O or KIN7O-BUB3.3 complex – Who is upstream of whom?

This work has highlighted a previously unidentified role for the Arabidopsis BUB3.3 in promoting chromosome congression to the metaphase plate. BUB3.3 binds to the kinetochore after NEB and disassociates from it after AO in a BMF1-and BMF3-independent manner (unpublished data from the Liu lab). Hence, it would be of great interest to identify upstream regulators of BUB3.3 that promote its recruitment to the kinetochore. Obviously, kinases such as MPS1 and AURORA, that have both cytosolic and kinetochore/centromeric fractions, or cyclin-dependent kinases (CDKs), that are the major regulators of cell-cycle progression, would be great candidates. Based on the lack of evidence for post-translational modifications (PTMs) of BUB3.3 on Arabidopsis proteomic screen databases and considering that BUB3.3 consists exclusively of 7 WD-40 domains, this regulation could be most probably achieved via phosphorylation of a BUB3.3 interactor residing at or recruited to the kinetochore through said PTM. However, protein-protein interactome screens have not identified potential candidates so far. A preliminary attempt from our side with the help of Zoltán Magyar and Aladár Pettkó-Szandtner from the Biological Research Centre Szeged in Hungary, who performed the immunoprecipitation experiment and proteomic analysis with 5-day old seedlings expressing *BUB3.3::gBUB3.3:GFP*, did not reveal any viable candidates either. It should be noted that the C-terminally tagged genomic *BUB3.3* reporter does not localize visibly to the kinetochore (Komaki & Schnittger, 2017; Chapter 1), in contrast to the N-terminally tagged reporter (unpublished data from the Liu lab). Hence, the C-terminally tagged reporter might not be fully functional or only weakly

associate with the kinetochore, enough to rescue the *bub3.3* sensitivity under oryzalin (Komaki & Schnittger, 2017), but not sufficiently to pull-down kinetochore interactors from whole seedlings. Alternatively, since we could not pull-down KIN7O either, an interaction that was confirmed by yeast-two-hybrid, I suggest that the proportion of diving cells in an entire seedling is potentially so low in comparison to non-dividing cells, that the background from the latter interferes with the interactions we were aiming to detect. Should this have been the only problem, though, then one would have expected Van Leene et al. (2010) to have identified potential kinetochore-bound interactors of BUB3.3, which was not the case. Hence, an alternative hypothesis must be sought regarding the BUB3.3 kinetochore localization.

One possible hypothesis is that BUB3.3 interacts with kinetochore-bound proteins, while KIN7O is attached to the kinetochore via BUB3.3. Alternatively, considering that (i) we and others could not identify kinetochore-bound interactors of BUB3.3, (ii) Dr. Shinichiro Komaki showed in a yeast-two-hybrid assay that BUB3.3 interacts with the last 84 amino acids in the C-terminus of KIN7O, where the MT-binding domain of human CENP-E is found (Liao et al., 1994), and (iii) BUB3.1 and BUB3.2 interact with MTs (Komaki & Schnittger, 2017; H. Zhang et al., 2018; Chapter 2), BUB3.3 might assist KIN7O in efficiently binding MTs, meaning that KIN7O is the kinetochore interacting part of the complex and BUB3.3 interacts with the kinetochore via KIN7O (Fig. 3).
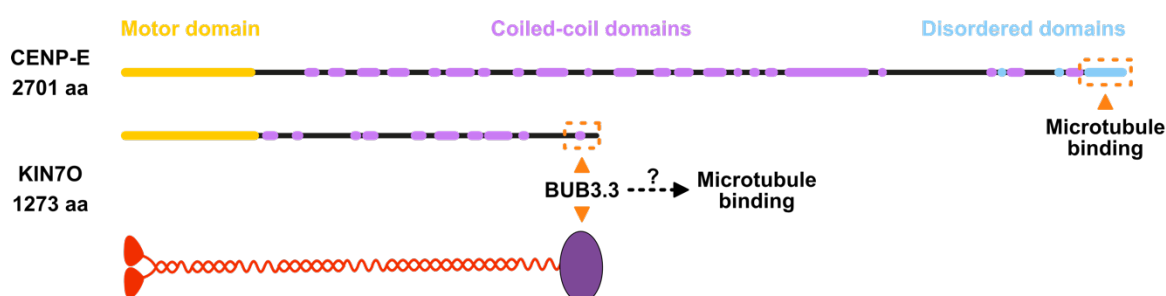
Figure 3 Schematic representation of human CENP-E and Arabidopsis KIN7O and its interaction with BUB3.3. The KIN7O dimer was drawn based on figure 1 from Craske & Welburn (2020). The CENP-E and KIN7O models are drawn to scale. All the known and/or predicted domains of the two proteins are highlighted. Please note the shorter C-terminus and lack of MT-binding disordered domain(s) in KIN7O. I propose that the MT-binding activity of the distal C-terminus of CENP-E is substituted by MT-binding mediated by BUB3.3 in Arabidopsis.

I am in favor of the second hypothesis and would like to present some arguments of why this might be the case. CENP-E undergoes major conformational rearrangements upon MT capture both *in vivo* (Taveras et al., 2019; Wan et al., 2009) and *in vitro* (Gudimchuk et al., 2018; Y. Kim et al., 2008). More specifically, the long coiled-coil domain separating the N-terminal motor from the C-terminal MT-binding domain can fold on itself, so that both terminally located domains interact with the MT (Fig. 4). The C-terminal domain actively maintains the association of CENP-E with the MT lattice during plus-end MT tracking (Gudimchuk et al., 2018; Musinipally et al., 2013). Interestingly, KIN7O is about half the size of CENP-E (KIN7O is 1273 aa long versus CENP-E that is 2701 aa long), and the half that is missing is specifically in the C-terminus, begging the question of whether KIN7O has lost the C-terminal MT-binding domain, which has been substituted by an interaction with BUB3.3. Indeed, motif search analysis does not reveal an intrinsically disordered domain in the C-terminus of KIN7O, which is the MT-binding domain in CENP-E. Although in Chapter 2 I argue that BUB3.3 has adopted a distinctive function from BUB3.1 and BUB3.2, their nearly identical predicted 3D structure does support a similar function in MT-binding. Nonetheless, I have shown that BUB3.3 does not work in the same pathway as BUB3.1 and BUB3.2, so they exert this potentially similar function in distinct pathways. Alternatively, if KIN7O has maintained its C-terminal MT-binding activity through an unidentified domain, BUB3.3 might play a regulatory role or further enhance this activity (Fig. 4). Finally, CENP-E recruitment to unattached kinetochores is a highly regulated process involving major kinases, such as Aurora A and B, Cdk1, and Mps1, as well as several kinetochore associated proteins, such as BubR1 and CENP-F (Craske & Welburn, 2020), making KIN7O a more attractive candidate for PTM-regulated kinetochore recruitment as well (see below).
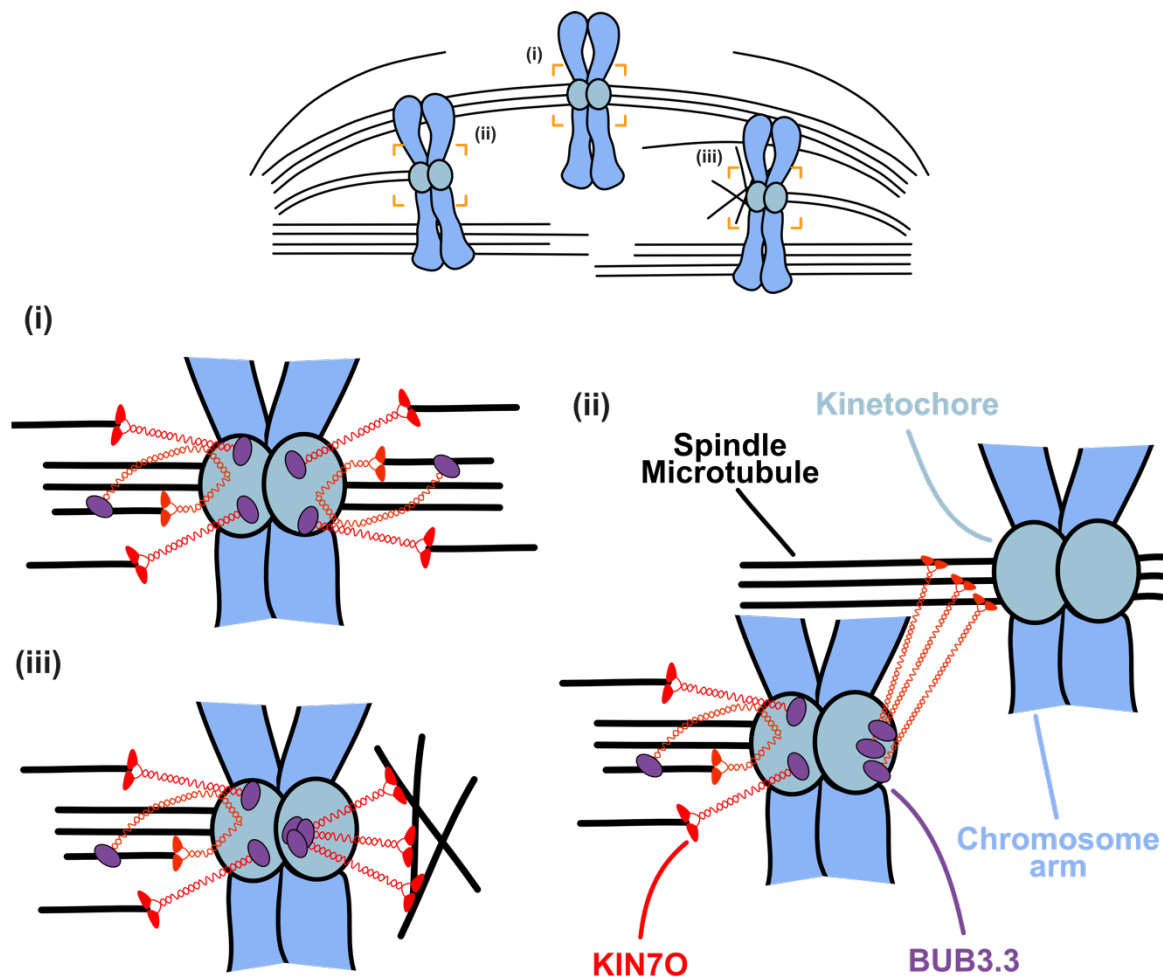
Figure 4 Proposed functions of the Arabidopsis KIN7O-BUB3.3 complex at the kinetochore based on known functions of the human CENP-E. This model was drawn after figures 2 and 3 from Craske & Welburn (2020). **(i)** KIN7O might track the plus-ends of kinetochore MTs, stabilizing these connections. KIN7O might adopt a folded conformation and BUB3.3 might interact with the lattice of kinetochore MTs, like the C-terminus of CENP-E that is missing in KIN7O. **(ii)** KIN7O might help polar chromosomes move along the MT lattice of adjacent kinetochore MTs bringing them towards the metaphase plate. **(iii)** KIN7O might interact with the lattice of adjacent MTs generating lateral K-MT attachments during the search and capture process in prometaphase.

To test the above-stated hypotheses, I would like to propose a couple of essential experiments. First, a localization study of a KIN7O functional reporter in *bub3.3* cells and vice versa, the BUB3.3 reporter generated in the Liu lab in the *kin7o* background would be the simplest test. Alternatively, due to the technical difficulties in obtaining a functional KIN7O reporter, one can take advantage of existing antibodies for CENP-E that appear to recognize plant KIN7s in field bean and barley (ten Hoopen et al., 2000, 2002). The *ki7o* null mutants identified in Chapter 2 can serve as negative controls. Depending on the outcome, one would

already know the order of binding of these two proteins as well as who recruits whom. Second, it would be of particular interest to see whether the C-terminus of KIN7O has maintained its MT-binding function and also, whether BUB3.3 can bind to MTs similar to its two other homologs. To test the MT-binding properties of BUB3.3 *in vivo*, I propose to transiently co-express a BUB3.3 and a tubulin reporter in tobacco as previously published in Lee et al. (2017), while for the C-terminus of KIN7O *in vitro* MT-binding assays might be more applicable (Musinipally et al., 2013). Finally, the regulation of KIN7O by kinases would be an interesting line of inquiry. Phosphoproteomic studies in Arabidopsis have identified several phosphorylation sites in KIN7O according to phosphorylation databases, making such a regulation very possible. For instance, human CENP-E T422 phosphorylation is mediated by Aurora A and B kinases and promotes CENP-E mediated chromosome congression, by reducing the affinity to MTs and thereby interrupting more frequently unproductive K-MT attachments and allowing productive attachments to be maintained (Y. Kim et al., 2010). On the contrary, binding of Protein Phosphatase 1 (PP1) promotes stable attachment to MTs, meaning that these two proteins finetune MT affinity of CENP-E (Y. Kim et al., 2010). CENP-E T422 corresponds to KIN7O T439 and the motif sequence around this threonine is highly conserved between the two proteins (KRKR*RVTW*CLGK in CENP-E versus KGKR*RDTW*CIGK in KIN7O). The italicized sequence is a typical PP1 binding motif, called the RVxF motif, and its phosphorylation prevents PP1 binding (Y. Kim et al., 2010). Conclusively, these experiments could enhance our mechanistic understanding of the KIN7O-BUB3.3 module described here.

Finally, additional motor proteins most probably regulate chromosome alignment in Arabidopsis, as chromosomes congressed in a more or less timely manner towards the metaphase plate both in *bub3.3* and *kin7o* null mutants (Chapters 1 and 2), in contrast to CENP-E knock-down in human cells, where at least some polar chromosomes persist eventually leading to missegregation (Bancroft et al., 2015; Barisic et al., 2014). Several other major kinesins have been shown to promote chromosome congression in human cells and their mechanism of action has been excellently reviewed in Maiato et al. (2017) and Risteski et al. (2021).

Indeed, transcripts of several homologs of these kinesins have been shown to be upregulated in Arabidopsis synchronized cell cultures (Vanstraelen et al., 2006), which solely suggests a potential function in chromosome congression and/or maintenance of chromosome metaphase plate alignment. As I've shown in Chapter 2 with KIN7N, whose transcript was strongly upregulated in Vanstraelen et al. (2006), it plays only a minor – if any – role in chromosome congression and the major functional equivalent of CENP-E is rather KIN7O, which was not reported to be upregulated on the trancript level in Vanstraelen et al. (2006). Besides, cells have multiple pathways to regulate protein level and activity and transcript level regulation is but one of these mechanisms. Hence, I can't preclude that kinesins, whose transcript was not upregulated in Vanstraelen et al. (2006), play a minor or major role in chromosome congression and/or maintenance of chromosome metaphase plate alignment. Additionally, in contrast to human cells that have only one or a couple kinesins in each family, Arabidopsis has several homologs in each family (Machens, 2018; Yamada & Goshima, 2017). Thus, it might be necessary to study higher order mutants as functional redundancy between members of the same family is quite likely.

Nevertheless, based on a plethora of studies in human cells and Vanstraelen et al. (2006) the most promising candidates are chromosome arm-localized Kinesin-4 and Kinesin-10 as well as kinetochore-localized Kinesin-7 and Kinesin-13 family members (Fig. 5). More specifically, the human chromokinesins Kif4a (kinesin-4) and Kid/Kif22 (kinesin-10) have been shown to have MT plus-end directed motility, with Kid/Kif22 or its homologs in other organisms having the major role in promoting chromosome congression even in acentrosomal model systems (Maiato et al., 2017; Risteski et al., 2021). Since Vanstraelen et al. (2006) reported that the transcripts of both *KINESIN-4B* (*KIN4B*; *AT3G50240*) and *KIN4C* (*AT5G60930*) as well as these of *KINESIN-10A* (*KIN10A*; *AT4G14330*), *KIN10B* (*AT5G02370*), and *KIN10C* (*AT5G23910*) were strongly upregulated in mitotic cells, I propose that some or all of these genes might be involved in this process in Arabidopsis (Fig. 5A). Next, in Chapter 2, I show a predominant role for KIN7O and a minor – if any – role for KIN7N in chromosome metaphase plate congression and propose that

KIN7O localizes to the kinetochore (Fig. 5A) similarly to its homolog and functional equivalent CENP-E in human cells (Craske & Welburn, 2020). Considering that Arabidopsis has 15 *KINESIN-7* family members (Richardson et al., 2006), it would be interesting to study further *KIN7* single as well as higher order mutants in the future. Finally, MCAK/Kif2c, one of the three human Kinesin-13 family members, is a non-motile, MT plus-end tracking, and binding motor protein that promotes MT depolymerization at the kinetochore, thus playing a key part in the correction of erroneous K-MT attachments with the help of CENP-E (Fig. 5B) (Maiato et al., 2017; Risteski et al., 2021; Shrestha & Draviam, 2013). Vanstraelen et al. (2006) reported a strong upregulation in the transcript of *KINESIN-13B* (*KIN13B*; *AT3G16060*), which I propose to be the most probable functional equivalent of MCAK in Arabidopsis, as the other member of the KIN13 family, namely KIN13A, is targeted to cortical MTs and regulates secondary cell wall pattern formation in xylem cells (Oda & Fukuda, 2013). Conclusively, there are several promising candidate kinesins in Arabidopsis that could explain the observed chromosome congression in the absence of KIN7O and/or BUB3.3, opening up the possibility for uncovering complementary and/or redundant pathways in the future.
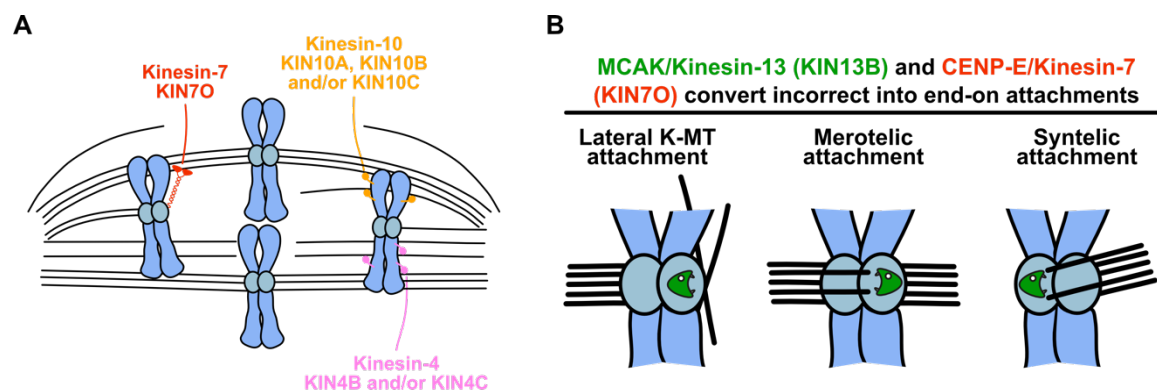
Figure 5 Proposed model for the motor-dependent chromosome metaphase plate alignment in Arabidopsis. This model was drawn after figures 2 and 3 from Craske & Welburn (2020). **(A)** Kinetochore-localized KIN7 family members transport unattached and/or monopolarly attached chromosomes along the lattice of adjacent kinetochore MTs. I propose that KIN7O is the major functional equivalent of human CENP-E (left). Human chromokinesins Kif4a (kinesin-4) and Kid/Kif22 (kinesin-10) localize to chromosome arms and generate forces propelling chromosomes along adjacent MTs and away from spindle poles. I propose that the Arabidopsis homologs KIN4B, KIN4C, KIN10A, KIN10B, and KIN10C might have similar function (right). **(B)** MCAK is a MT plus-end tracking and binding motor protein that promotes MT depolymerization at the kinetochore, thus converting erroneous into end-on attachments with the help of CENP-E. I propose that the Arabidopsis homolog KIN13B might play a similar role.

Concluding remarks

Overall, this work provides a framework for future studies of the SAC and chromosome congression in Arabidopsis. From a technical innovation perspective, the 2D and 3D live-cell imaging methods of metaphase in meiosis and mitosis as well as the detailed quantification approaches established here set the stage for further dissection of the inner workings of the plant SAC and chromosome metaphase plate alignment. From a biological perspective, the refined SAC model as well as the new function of the KIN7O-BUB3.3 complex should be expanded upon to enhance our mechanistic knowledge of the SAC and chromosome congression *in planta*, respectively. Finally, the unexpected results obtained in tetraploid meiosis and mitosis can serve as a stepping stone to elucidate the role of the SAC in maintaining genome integrity in neo-autotetraploids and its potential significance over evolutionary time.

References

Akiyoshi, B., & Gull, K. (2013). Evolutionary cell biology of chromosome segregation: Insights from trypanosomes. *Open Biology*, *3*(MAY). https://doi.org/10.1098/rsob.130023

Akiyoshi, B., Sarangapani, K. K., Powers, A. F., Nelson, C. R., Reichow, S. L., Arellano-Santoyo, H., Gonen, T., Ranish, J. A., Asbury, C. L., & Biggins, S. (2010). Tension directly stabilizes reconstituted kinetochore-microtubule attachments. *Nature*, *468*(7323), 576–579. https://doi.org/10.1038/nature09594

Alfieri, C., Chang, L., & Barford, D. (2018). Mechanism for remodelling of the cell cycle checkpoint protein MAD2 by the ATPase TRIP13. *Nature*, *559*(7713), 274–278. https://doi.org/10.1038/s41586-018-0281-1

Alfieri, C., Chang, L., Zhang, Z., Yang, J., Maslen, S., Skehel, M., & Barford, D. (2016). Molecular basis of APC/C regulation by the spindle assembly checkpoint. *Nature*, *536*(7617), 431–436. https://doi.org/10.1038/nature19083

Angers, S., Li, T., Yi, X., MacCoss, M. J., Moon, R. T., & Zheng, N. (2006). Molecular architecture and assembly of the DDB1-CUL4A ubiquitin ligase machinery. *Nature*, *443*(7111), 590–593. https://doi.org/10.1038/nature05175

Arnst, C. E. (2019). *TRIP13 AAA-ATPase Promotes Spindle Assembly Checkpoint Activation through Coordinating with MAD1 at Unattached Kinetochores* [University of Toledo]. http://rave.ohiolink.edu/etdc/view?acc_num=toledo1560867340515027

Bajer, A., & Molè-Bajer, J. (1955). Cine-micrographic studies on mitosis in endosperm - II. Chromosome, cytoplasmic and brownian movements. *Chromosoma*, *7*(1), 558–607. https://doi.org/10.1007/BF00329742

Balboni, M., Yang, C., Komaki, S., Brun, J., & Schnittger, A. (2020). COMET Functions as a PCH2 Cofactor in Regulating the HORMA Domain Protein ASY1. *Current Biology*, *30*(21), 4113-4127.e6. https://doi.org/10.1016/j.cub.2020.07.089

Bancroft, J., Auckland, P., Samora, C. P., & McAinsh, A. D. (2015). Chromosome congression is promoted by CENP-Q- and CENP-E-dependent pathways. *Journal of Cell Science*, *128*(1), 171–184. https://doi.org/10.1242/jcs.163659

Barisic, M., Aguiar, P., Geley, S., & Maiato, H. (2014). Kinetochore motors drive congression of peripheral polar chromosomes by overcoming random arm-ejection forces. *Nature Cell Biology*, *16*(12), 1249–1256. https://doi.org/10.1038/ncb3060

Bernhardt, A., Mooney, S., & Hellmann, H. (2010). Arabidopsis DDB1a and DDB1b are critical for embryo development. *Planta*, *232*(3), 555–566. https://doi.org/10.1007/s00425-010-1195-9

Bhatt, A. M., Lister, C., Page, T., Fransz, P., Findlay, K., Jones, G. H., Dickinson, H. G., & Dean, C. (1999). The DIF1 gene of Arabidopsis is required for meiotic chromosome segregation and belongs to the REC8/RAD21 cohesin gene family. *Plant Journal*, *19*(4), 463–472. https://doi.org/10.1046/j.1365-313X.1999.00548.x

Biggins, S., & Murray, A. W. (2001). The budding yeast protein kinase Ipl1/Aurora allows the absence of tension to activate the spindle checkpoint. *Genes and Development*, *15*(23), 3118–3129. https://doi.org/10.1101/gad.934801

Bloomfield, M., Chen, J., & Cimini, D. (2021). Spindle Architectural Features Must Be Considered Along With Cell Size to Explain the Timing of Mitotic Checkpoint Silencing. *Frontiers in Physiology*, *11*(January), 1–21. https://doi.org/10.3389/fphys.2020.596263

Bomblies, K. (2020). When everything changes at once: Finding a new normal after genome duplication: Evolutionary response to polyploidy. *Proceedings of the Royal Society B: Biological Sciences*, *287*(1939). https://doi.org/10.1098/rspb.2020.2154

Bomblies, K. (2023). Learning to tango with four (or more): the molecular basis of adaptation to polyploid meiosis. *Plant Reproduction*, *36*(1), 107–124. https://doi.org/10.1007/s00497-022-00448-1

Bomblies, K., Jones, G., Franklin, C., Zickler, D., & Kleckner, N. (2016). The challenge of evolving stable polyploidy: could an increase in "crossover interference distance" play a central role? *Chromosoma*, *125*(2), 287–300. https://doi.org/10.1007/s00412-015-0571-4

Brinkley, B. R., & Stubblefield, E. (1966). The fine structure of the kinetochore of a mammalian cell in vitro. *Chromosoma*, *19*(1), 28–43. https://doi.org/10.1007/BF00332792

Brito, D. A., & Rieder, C. L. (2006). Mitotic Checkpoint Slippage in Humans Occurs via Cyclin B Destruction in the Presence of an Active Checkpoint. *Current Biology*, *16*(12), 1194–1200. https://doi.org/10.1016/j.cub.2006.04.043

Broad, A. J., DeLuca, K. F., & DeLuca, J. G. (2020). Aurora B kinase is recruited to multiple discrete kinetochore and centromere regions in human cells. *Journal of Cell Biology*, *219*(3). https://doi.org/10.1083/jcb.201905144

Brulotte, M. L., Jeong, B. C., Li, F., Li, B., Yu, E. B., Wu, Q., Brautigam, C. A., Yu, H., & Luo, X. (2017). Mechanistic insight into TRIP13-catalyzed Mad2 structural transition and spindle checkpoint silencing. *Nature Communications*, *8*(1). https://doi.org/10.1038/s41467-017-02012-2

Burki, F., Roger, A. J., Brown, M. W., & Simpson, A. G. B. (2020). The New Tree of Eukaryotes. *Trends in Ecology & Evolution*, *35*(1), 43–55. https://doi.org/10.1016/j.tree.2019.08.008

Burroughs, N. J., Harry, E. F., & McAinsh, A. D. (2015). Super-resolution kinetochore tracking reveals the mechanisms of human sister kinetochore directional switching. *ELife*, *4*(6), 1035–1046. https://doi.org/10.7554/eLife.09500

Burton, J. L., & Solomon, M. J. (2007). Mad3p, a pseudosubstrate inhibitor of APCCdc20 in the spindle assembly checkpoint. *Genes & Development*, *21*(6), 655–667. https://doi.org/10.1101/gad.1511107

Cairo, G., Greiwe, C., Jung, G. I., Blengini, C., Schindler, K., & Lacefield, S. (2023). Distinct Aurora B pools at the inner centromere and kinetochore have different contributions to meiotic and mitotic chromosome segregation. *Molecular Biology of the Cell*, *34*(5), ar43. https://doi.org/10.1091/mbc.E23-01-0014

Cairo, G., MacKenzie, A. M., & Lacefield, S. (2020). Differential requirement for Bub1 and Bub3 in regulation of meiotic versus mitotic chromosome segregation. *Journal of Cell Biology*, *219*(4). https://doi.org/10.1083/jcb.201909136

Calvo-Baltanás, V., De Jaeger-Braet, J., Cher, W. Y., Schönbeck, N., Chae, E., Schnittger, A., & Wijnker, E. (2022). Knock-down of gene expression throughout meiosis and pollen formation by virus-induced gene silencing in Arabidopsis thaliana. *Plant Journal*, *111*(1), 19–37. https://doi.org/10.1111/tpj.15733

Cane, S., Ye, A. A., Luks-Morgan, S. J., & Maresca, T. J. (2013). Elevated polar ejection forces stabilize kinetochore-microtubule attachments. *The Journal of Cell Biology*, *200*(2), 203–218. https://doi.org/10.1083/jcb.201211119

Capitao, C., Tanasa, S., Fulnecek, J., Raxwal, V. K., Akimcheva, S., Bulankova, P., Mikulkova, P., Khaitova, L. C., Kalidass, M., Lermontova, I., Scheid, O. M., & Riha, K. (2021). A CENH3 mutation promotes meiotic exit and restores fertility in SMG7-deficient Arabidopsis. *PLoS Genetics*, *17*(9), 1–26. https://doi.org/10.1371/journal.pgen.1009779

Chan, G. K. T., Schaar, B. T., & Yen, T. J. (1998). Characterization of the kinetochore binding domain of CENP-E reveals interactions with the kinetochore proteins CENP-F and hBUBR1. *Journal of Cell Biology*, *143*(1), 49–63. https://doi.org/10.1083/jcb.143.1.49

Chelysheva, L., Diallo, S., Vezon, D., Gendrot, G., Vrielynck, N., Belcram, K., Rocques, N., Márquez-Lema, A., Bhatt, A. M., Horlow, C., Mercier, R., Mézard, C., & Grelon, M. (2005). AtREC8 and AtSCC3 are essential to the monopolar orientation of the kinetochores during meiosis. *Journal of Cell Science*, *118*(20), 4621–4632. https://doi.org/10.1242/jcs.02583

Chen, C., Whitney, I. P., Banerjee, A., Sacristan, C., Sekhri, P., Kern, D. M., Fontan, A., Kops, G. J. P. L., Tyson, J. J., Cheeseman, I. M., & Joglekar, A. P. (2019). Ectopic Activation of the Spindle Assembly Checkpoint Signaling Cascade Reveals Its Biochemical Design. *Current Biology*, *29*(1), 104-119.e10. https://doi.org/10.1016/j.cub.2018.11.054

Chen, G.-Y., Renda, F., Zhang, H., Gokden, A., Wu, D. Z., Chenoweth, D. M., Khodjakov, A., & Lampson, M. A. (2021). Tension promotes kinetochore-microtubule release by Aurora B kinase. *The Journal of Cell Biology, 220*(6). https://doi.org/10.1083/jcb.202007030

Chen, J., & Liu, J. (2016). Spindle Size Scaling Contributes to Robust Silencing of Mitotic Spindle Assembly Checkpoint. *Biophysical Journal, 111*(5), 1064–1077. https://doi.org/10.1016/j.bpj.2016.07.039

Choi, E., Choe, H., Min, J., Choi, J. Y., Kim, J., & Lee, H. (2009). BubR1 acetylation at prometaphase is required for modulating APC/C activity and timing of mitosis. *EMBO Journal, 28*(14), 2077–2089. https://doi.org/10.1038/emboj.2009.123

Ciossani, G., Overlack, K., Petrovic, A., Huis In 'T Veld, P. J., Koerner, C., Wohlgemuth, S., Maffini, S., & Musacchio, A. (2018). The kinetochore proteins CENP-E and CENP-F directly and specifically interact with distinct BUB mitotic checkpoint Ser/Thr kinases. *Journal of Biological Chemistry, 293*(26), 10084–10101. https://doi.org/10.1074/jbc.RA118.003154

Collin, P., Nashchekina, O., Walker, R., & Pines, J. (2013). The spindle assembly checkpoint works like a rheostat rather than a toggle switch. *Nature Cell Biology, 15*(11), 1378–1385. https://doi.org/10.1038/ncb2855

Comai, L. (2005). The advantages and disadvantages of being polyploid. *Nature Reviews Genetics, 6*(11), 836–846. https://doi.org/10.1038/nrg1711

Corno, A., Cordeiro, M. H., Allan, L. A., Wei, Q., Harrington, E., Smith, R. J., & Saurin, A. T. (2022). A bifunctional kinase-phosphatase module integrates mitotic checkpoint and error-correction signalling to ensure mitotic fidelity. *BioRxiv.* https://doi.org/10.1101/2022.05.22.492960

Craske, B., & Welburn, J. P. I. (2020). Leaving no-one behind: how CENP-E facilitates chromosome alignment. *Essays in Biochemistry, 64*(2), 313–324. https://doi.org/10.1042/EBC20190073

Crowder, M. E., Strzelecka, M., Wilbur, J. D., Good, M. C., Von Dassow, G., & Heald, R. (2015). A comparative analysis of spindle morphometrics across metazoans. *Current Biology, 25*(11), 1542–1550. https://doi.org/10.1016/j.cub.2015.04.036

D'Erfurth, I., Jolivet, S., Froger, N., Catrice, O., Novatchkova, M., & Mercier, R. (2009). Turning meiosis into mitosis. *PLoS Biology*, *7*(6). https://doi.org/10.1371/journal.pbio.1000124

De Jaeger-Braet, J., Krause, L., Buchholz, A., & Schnittger, A. (2021). Heat stress reveals a specialized variant of the pachytene checkpoint in meiosis of Arabidopsis thaliana. *The Plant Cell*, *2*(2), 91–98. https://doi.org/10.1093/plcell/koab257

de Oliveira, E. A. G., Romeiro, N. C., Ribeiro, E. da S., Santa-Catarina, C., Oliveira, A. E. A., Silveira, V., de Souza Filho, G. A., Venancio, T. M., & Cruz, M. A. L. (2012). Structural and functional characterization of the protein kinase Mps1 in Arabidopsis thaliana. *PloS One*, *7*(9), e45707. https://doi.org/10.1371/journal.pone.0045707

De Souza, C. P., Hashmi, S. B., Yang, X., & Osmani, S. A. (2011). Regulated inactivation of the spindle assembly checkpoint without functional mitotic spindles. *EMBO Journal*, *30*(13), 2648–2661. https://doi.org/10.1038/emboj.2011.176

DeLuca, K. F., Lens, S. M. A., & DeLuca, J. G. (2011). Temporal changes in Hec1 phosphorylation control kinetochore - Microtubule attachment stability during mitosis. *Journal of Cell Science*, *124*(4), 622–634. https://doi.org/10.1242/jcs.072629

Demidov, D., Hesse, S., Tewes, A., Rutten, T., Fuchs, J., Karimi Ashtiyani, R., Lein, S., Fischer, A., Reuter, G., & Houben, A. (2009). Aurora1 phosphorylation activity on histone H3 and its cross-talk with other post-translational histone modifications in Arabidopsis. *Plant Journal*, *59*(2), 221–230. https://doi.org/10.1111/j.1365-313X.2009.03861.x

Di Fiore, B., Davey, N. E., Hagting, A., Izawa, D., Mansfeld, J., Gibson, T. J., & Pines, J. (2015). The ABBA motif binds APC/C activators and is shared by APC/C substrates and regulators. *Developmental Cell*, *32*(3), 358–372. https://doi.org/10.1016/j.devcel.2015.01.003

Di Fiore, B., Wurzenberger, C., Davey, N. E., & Pines, J. (2016). The Mitotic Checkpoint Complex Requires an Evolutionary Conserved Cassette to Bind and Inhibit Active APC/C. *Molecular Cell*, *64*(6), 1144–1153. https://doi.org/10.1016/j.molcel.2016.11.006

Dick, A. E., & Gerlich, D. W. (2013). Kinetic framework of spindle assembly checkpoint signalling. *Nature Cell Biology*, *15*(11), 1370–1377. https://doi.org/10.1038/ncb2842

Dietz, R. (1957). Multiple Geschlechtschromosomen bei den cypriden Ostracoden, ihre Evolution und ihr Teilungsverhalten. *Chromosoma*, *9*(1), 359–440. https://doi.org/10.1007/BF02568086

Drinnenberg, I. A., & Akiyoshi, B. (2017). *Evolutionary Lessons from Species with Unique Kinetochores BT - Centromeres and Kinetochores: Discovering the Molecular Mechanisms Underlying Chromosome Inheritance* (B. E. Black (ed.); pp. 111–138). Springer International Publishing. https://doi.org/10.1007/978-3-319-58592-5_5

Drpic, D., Almeida, A. C., Aguiar, P., Renda, F., Damas, J., Lewin, H. A., Larkin, D. M., Khodjakov, A., & Maiato, H. (2018). Chromosome Segregation Is Biased by Kinetochore Size. *Current Biology*, *28*(9), 1344-1356.e5. https://doi.org/10.1016/j.cub.2018.03.023

Drpic, D., Pereira, A. J., Barisic, M., Maresca, T. J., & Maiato, H. (2015). Polar Ejection Forces Promote the Conversion from Lateral to End-on Kinetochore-Microtubule Attachments on Mono-oriented Chromosomes. *Cell Reports*, *13*(3), 460–468. https://doi.org/10.1016/j.celrep.2015.08.008

Dudka, D., Noatynska, A., Smith, C. A., Liaudet, N., McAinsh, A. D., & Meraldi, P. (2018). Complete microtubule–kinetochore occupancy favours the segregation of merotelic attachments. *Nature Communications*, *9*(1), 1–16. https://doi.org/10.1038/s41467-018-04427-x

Elowe, S., Dulla, K., Uldschmid, A., Li, X., Dou, Z., & Nigg, E. A. (2010). Uncoupling of the spindle-checkpoint and chromosome-congression functions of BubR1. *Journal of Cell Science*, *123*(1), 84–94. https://doi.org/10.1242/jcs.056507

Espert, A., Uluocak, P., Bastos, R. N., Mangat, D., Graab, P., & Gruneberg, U. (2014). PP2A-B56 opposes Mps1 phosphorylation of Knl1 and thereby promotes spindle assembly checkpoint silencing. *Journal of Cell Biology*, *206*(7), 833–842. https://doi.org/10.1083/jcb.201406109

Etemad, B., Kuijt, T. E. F., & Kops, G. J. P. L. (2015). Kinetochore–microtubule attachment is sufficient to satisfy the human spindle assembly checkpoint. *Nature Communications*, *6*(1), 8987. https://doi.org/10.1038/ncomms9987

Etemad, B., Vertesy, A., Kuijt, T. E. F., Sacristan, C., van Oudenaarden, A., & Kops, G. J. P. L. (2019). Spindle checkpoint silencing at kinetochores with submaximal microtubule occupancy. *Journal of Cell Science*, *132*(12), jcs231589. https://doi.org/10.1242/jcs.231589

Eytan, E., Wang, K., Miniowitz-Shemtov, S., Sitry-Shevah, D., Kaisari, S., Yen, T. J., Liu, S. T., & Hershko, A. (2014). Disassembly of mitotic checkpoint complexes by the joint action of the AAA-ATPase TRIP13 and p31comet. *Proceedings of the National Academy of Sciences of the United States of America*, *111*(33), 12019–12024. https://doi.org/10.1073/pnas.1412901111

Falconer, M. M., Donaldson, G., & Seagull, R. W. (1988). MTOCs in higher plant cells: an immunofluorescent study of microtubule assembly sites following depolymerization by APM. *Protoplasma*, *144*(1), 46–55. https://doi.org/10.1007/BF01320279

Fawcett, J. A., Maere, S., & Van De Peer, Y. (2009). Plants with double genomes might have had a better chance to survive the Cretaceous-Tertiary extinction event. *Proceedings of the National Academy of Sciences of the United States of America*, *106*(14), 5737–5742. https://doi.org/10.1073/pnas.0900906106

Foley, E. A., Maldonado, M., & Kapoor, T. M. (2011). Formation of stable attachments between kinetochores and microtubules depends on the B56-PP2A phosphatase. *Nature Cell Biology*, *13*(10), 1265–1271. https://doi.org/10.1038/ncb2327

Galli, M., & Morgan, D. O. (2016). Cell Size Determines the Strength of the Spindle Assembly Checkpoint during Embryonic Development. *Developmental Cell*, *36*(3), 344–352. https://doi.org/10.1016/j.devcel.2016.01.003

Gorbsky, G. J. (2015). The spindle checkpoint and chromosome segregation in meiosis. *FEBS Journal*, *282*(13), 2458–2474. https://doi.org/10.1111/febs.13166

Grelon, M., Vezon, D., Gendrot, G., & Pelletier, G. (2001). AtSPO11-1 is necessary for efficient meiotic recombination in plants. *EMBO Journal*, *20*(3), 589–600. https://doi.org/10.1093/emboj/20.3.589

Gudimchuk, N., Tarasovetc, E. V., Mustyatsa, V., Drobyshev, A. L., Vitre, B., Cleveland, D. W., Ataullakhanov, F. I., & Grishchuk, E. L. (2018). Probing Mitotic CENP-E Kinesin with the Tethered Cargo Motion Assay and Laser Tweezers. *Biophysical Journal*, *114*(11), 2640–2652. https://doi.org/10.1016/j.bpj.2018.04.017

Gudimchuk, N., Vitre, B., Kim, Y., Kiyatkin, A., Cleveland, D. W., Ataullakhanov, F. I., & Grishchuk, E. L. (2013). Kinetochore kinesin CENP-E is a processive bi-directional tracker of dynamic microtubule tips. *Nature Cell Biology*, *15*(9), 1079–1088. https://doi.org/10.1038/ncb2831

Guo, Y., Kim, C., Ahmad, S., Zhang, J., & Mao, Y. (2012). CENP-E-dependent bubr1 autophosphorylation enhances chromosome alignment and the mitotic checkpoint. *Journal of Cell Biology*, *198*(2), 205–217. https://doi.org/10.1083/jcb.201202152

Hadders, M. A., Hindriksen, S., Truong, M. A., Mhaskar, A. N., Pepijn Wopken, J., Vromans, M. J. M., & Lens, S. M. A. (2020). Untangling the contribution of Haspin and Bub1 to Aurora B function during mitosis. *Journal of Cell Biology*, *219*(3). https://doi.org/10.1083/jcb.201907087

Harashima, H., Dissmeyer, N., & Schnittger, A. (2013). Cell cycle control across the eukaryotic kingdom. *Trends in Cell Biology*, *23*(7), 345–356. https://doi.org/10.1016/j.tcb.2013.03.002

Hartwell, L. H., & Weinert, T. A. (1989). Checkpoints: Controls that ensure the order of cell cycle events. *Science*, *246*(4930), 629–634. https://doi.org/10.1126/science.2683079

Hauf, S., Cole, R. W., LaTerra, S., Zimmer, C., Schnapp, G., Walter, R., Heckel, A., Van Meel, J., Rieder, C. L., & Peters, J. M. (2003). The small molecule Hesperadin reveals a role for Aurora B in correcting kinetochore-microtubule attachment and in maintaining the spindle assembly checkpoint. *Journal of Cell Biology*, *161*(2), 281–294. https://doi.org/10.1083/jcb.200208092

He, Y. J., McCall, C. M., Hu, J., Zeng, Y., & Xiong, Y. (2006). DDB1 functions as a linker to recruit receptor WD40 proteins to CUL4-ROC1 ubiquitin ligases. *Genes and Development*, *20*(21), 2949–2954. https://doi.org/10.1101/gad.1483206

Heald, R., & Khodjakov, A. (2015). Thirty years of search and capture: The complex simplicity of mitotic spindle assembly. *Journal of Cell Biology*, *211*(6), 1103–1111. https://doi.org/10.1083/jcb.201510015

Herrmann, A., Livanos, P., Zimmermann, S., Berendzen, K., Rohr, L., Lipka, E., & Müller, S. (2021). KINESIN-12E regulates metaphase spindle flux and helps control spindle size in Arabidopsis. *Plant Cell*, *33*(1), 27–43. https://doi.org/10.1093/plcell/koaa003

Higa, L. A., Wu, M., Ye, T., Kobayashi, R., Sun, H., & Zhang, H. (2006). CUL4-DDB1 ubiquitin ligase interacts with multiple WD40-repeat proteins and regulates histone methylation. *Nature Cell Biology*, *8*(11), 1277–1283. https://doi.org/10.1038/ncb1490

Hiruma, Y., Sacristan, C., Pachis, S. T., Adamopoulos, A., Kuijt, T., Ubbink, M., von Castelmur, E., Perrakis, A., & Kops, G. J. P. L. (2015). CELL DIVISION CYCLE. Competition between MPS1 and microtubules at kinetochores regulates spindle checkpoint signaling. *Science (New York, N.Y.)*, *348*(6240), 1264–1267. https://doi.org/10.1126/science.aaa4055

Hollister, J. D. (2015). Polyploidy: adaptation to the genomic environment. *The New Phytologist*, *205*(3), 1034–1039. https://doi.org/10.1111/nph.12939

Hou, H., Kyriacou, E., Thadani, R., Klutstein, M., Chapman, J. H., & Cooper, J. P. (2021). Centromeres are dismantled by foundational meiotic proteins Spo11 and Rec8. *Nature*, *591*(7851), 671–676. https://doi.org/10.1038/s41586-021-03279-8

Howell, B. J., Moree, B., Farrar, E. M., Stewart, S., Fang, G., & Salmon, E. . (2004). Spindle Checkpoint Protein Dynamics at Kinetochores in Living Cells. *Current Biology*, *14*(11), 953–964. https://doi.org/10.1016/j.cub.2004.05.053

Hoyt, M. A., Totis, L., & Roberts, B. T. (1991). S. cerevisiae genes required for cell cycle arrest in response to loss of microtubule function. *Cell*, *66*(3), 507–517. https://doi.org/10.1016/0092-8674(81)90014-3

Huang, Y., Lin, L., Liu, X., Ye, S., Yao, P. Y., Wang, W., Yang, F., Gao, X., Li, J., Zhang, Y., Zhang, J., Yang, Z., Liu, X., Yang, Z., Zang, J., Teng, M., Wang, Z., Ruan, K., Ding, X., … Yao, X. (2019). BubR1 phosphorylates CENP-E as a switch enabling the transition from lateral association to end-on capture of spindle microtubules. *Cell Research*, *29*(7), 562–578. https://doi.org/10.1038/s41422-019-0178-z

Inoué, S., & Sato, H. (1967). Cell motility by labile association of molecules. The nature of mitotic spindle fibers and their role in chromosome movement. *The Journal of General Physiology*, *50*(6), Suppl:259-92. https://doi.org/10.1142/9789812790866_0025

Izawa, D., & Pines, J. (2015). The mitotic checkpoint complex binds a second CDC20 to inhibit active APC/C. *Nature*, *517*(7536), 631–634. https://doi.org/10.1038/nature13911

Jelluma, N., Brenkman, A. B., van den Broek, N. J. F., Cruijsen, C. W. A., van Osch, M. H. J., Lens, S. M. A., Medema, R. H., & Kops, G. J. P. L. (2008). Mps1 Phosphorylates Borealin to Control Aurora B Activity and Chromosome Alignment. *Cell*, *132*(2), 233–246. https://doi.org/10.1016/j.cell.2007.11.046

Jensen, C. G. (1982). Dynamics of spindle microtubule organization: Kinetochore fiber microtubules of plant endosperm. *Journal of Cell Biology*, *92*(2), 540–558. https://doi.org/10.1083/jcb.92.2.540

Ji, Z., Gao, H., Jia, L., Li, B., & Yu, H. (2017). A sequential multi-target Mps1 phosphorylation cascade promotes spindle checkpoint signaling. *ELife*, *6*, 1–23. https://doi.org/10.7554/eLife.22513

Ji, Z., Gao, H., & Yu, H. (2015). Kinetochore attachment sensed by competitive Mps1 and microtubule binding to Ndc80C. *Science*, *348*(6240), 1260–1264. https://doi.org/10.1126/science.aaa4029

Johnson, V. L., Scott, M. I. F., Holt, S. V., Hussein, D., & Taylor, S. S. (2004). Bub1 is required for kinetochore localization of BubR1, Cenp-E, Cenp-F and Mad2, and chromosome congression. *Journal of Cell Science*, *117*(8), 1577–1589. https://doi.org/10.1242/jcs.01006

Jumper, J., Evans, R., Pritzel, A., Green, T., Figurnov, M., Ronneberger, O., Tunyasuvunakool, K., Bates, R., Žídek, A., Potapenko, A., Bridgland, A., Meyer, C., Kohl, S. A. A., Ballard, A. J., Cowie, A., Romera-Paredes, B., Nikolov, S., Jain, R., Adler, J., … Hassabis, D. (2021). Highly accurate protein structure prediction with AlphaFold. *Nature*, *596*(7873), 583–589. https://doi.org/10.1038/s41586-021-03819-2

Kalinina, I., Nandi, A., Delivani, P., Chacón, M. R., Klemm, A. H., Ramunno-Johnson, D., Krull, A., Lindner, B., Pavin, N., & Tolić-Nørrelykke, I. M. (2013). Pivoting of microtubules around the spindle pole accelerates kinetochore capture. *Nature Cell Biology*, *15*(1), 82–87. https://doi.org/10.1038/ncb2640

Kapoor, T. M., Lampson, M. A., Hergert, P., Cameron, L., Cimini, D., Salmon, E. D., McEwen, B. F., & Khodjakov, A. (2006). Chromosomes Can Congress to the Metaphase Plate Before Biorientation. *Science*, *311*(5759), 388–391. https://doi.org/10.1126/science.1122142

Kim, D. H., Han, J. S., Ly, P., Ye, Q., McMahon, M. A., Myung, K., Corbett, K. D., & Cleveland, D. W. (2018). TRIP13 and APC15 drive mitotic exit by turnover of interphase- and unattached kinetochore-produced MCC. *Nature Communications*, *9*(1). https://doi.org/10.1038/s41467-018-06774-1

Kim, S. H., Lee, J. H., Seo, K. I., Ryu, B., Sung, Y., Chung, T., Deng, X. W., & Lee, J. H. (2014). Characterization of a novel DWD protein that participates in heat stress response in Arabidopsis. *Molecules and Cells*, *37*(11), 833–840. https://doi.org/10.14348/molcells.2014.0224

Kim, Y., Heuser, J. E., Waterman, C. M., & Cleveland, D. W. (2008). CENP-E combines a slow, processive motor and a flexible coiled coil to produce an essential motile kinetochore tether. *Journal of Cell Biology*, *181*(3), 411–419. https://doi.org/10.1083/jcb.200802189

Kim, Y., Holland, A. J., Lan, W., & Cleveland, D. W. (2010). Aurora kinases and protein phosphatase 1 mediate chromosome congression through regulation of CENP-E. *Cell*, *142*(3), 444–455. https://doi.org/10.1016/j.cell.2010.06.039

King, E. M. J., van der Sar, S. J. A., & Hardwick, K. G. (2007). Mad3 KEN Boxes Mediate both Cdc20 and Mad3 Turnover, and Are Critical for the Spindle Checkpoint. *PLoS ONE*, *2*(4), e342. https://doi.org/10.1371/journal.pone.0000342

King, J. M., & Nicklas, R. B. (2000). Tension on chromosomes increases the number of kinetochore microtubules but only within limits. *Journal of Cell Science*, *113*(21), 3815–3823. https://doi.org/10.1242/jcs.113.21.3815

Kirschner, M., & Mitchison, T. (1986). Beyond self-assembly: From microtubules to morphogenesis. *Cell*, *45*(3), 329–342. https://doi.org/10.1016/0092-8674(86)90318-1

Komaki, S., & Schnittger, A. (2016). The spindle checkpoint in plants — a green variation over a conserved theme? *Current Opinion in Plant Biology*, *34*, 84–91. https://doi.org/10.1016/j.pbi.2016.10.008

Komaki, S., & Schnittger, A. (2017). The Spindle Assembly Checkpoint in Arabidopsis Is Rapidly Shut Off during Severe Stress. *Developmental Cell*, *43*(2), 172-185.e5. https://doi.org/10.1016/j.devcel.2017.09.017

Komaki, S., Takeuchi, H., Hamamura, Y., Heese, M., Hashimoto, T., & Schnittger, A. (2020). Functional Analysis of the Plant Chromosomal Passenger Complex. *Plant Physiology*, *183*(4), 1586–1599. https://doi.org/10.1104/pp.20.00344

Kops, G. J. P. L., Snel, B., & Tromer, E. C. (2020). Evolutionary Dynamics of the Spindle Assembly Checkpoint in Eukaryotes. *Current Biology*, *30*(10), R589–R602. https://doi.org/10.1016/j.cub.2020.02.021

Kozgunova, E., Nishina, M., & Goshima, G. (2019). Kinetochore protein depletion underlies cytokinesis failure and somatic polyploidization in the moss Physcomitrella patens. *ELife*, *8*, 1–16. https://doi.org/10.7554/eLife.43652

Krüger, F. (2017). *Vacuole biogenesis in Arabidopsis thaliana.* [Ruperto-Carola University of Heidelberg]. https://doi.org/10.11588/heidok.00023502

Kuhn, J., & Dumont, S. (2017). Spindle assembly checkpoint satisfaction occurs via end-on but not lateral attachments under tension. *The Journal of Cell Biology*, *216*(6), 1533–1542. https://doi.org/10.1083/jcb.201611104

Kuhn, J., & Dumont, S. (2019). Mammalian kinetochores count attached microtubules in a sensitive and switch-like manner. *The Journal of Cell Biology*, 1–14. https://doi.org/10.1083/jcb.201902105

Kumar, S., Suleski, M., Craig, J. M., Kasprowicz, A. E., Sanderford, M., Li, M., Stecher, G., & Hedges, S. B. (2022). TimeTree 5 : An Expanded Resource for Species Divergence Times. *Molecular Biology and Evolution*, *39*(8), 1–6. https://doi.org/10.1093/molbev/msac174

Kurihara, D., Matsunaga, S., Kawabe, A., Fujimoto, S., Noda, M., Uchiyama, S., & Fukui, K. (2006). Aurora kinase is required for chromosome segregation in tobacco BY-2 cells. *Plant Journal*, *48*(4), 572–580. https://doi.org/10.1111/j.1365-313X.2006.02893.x

Kuznetsova, A. Y., Seget, K., Moeller, G. K., de Pagter, M. S., de Roos, J. A. D. M., Dürrbaum, M., Kuffer, C., Müller, S., Zaman, G. J. R., Kloosterman, W. P., & Storchová, Z. (2015). Chromosomal instability, tolerance of mitotic errors and multidrug resistance are promoted by tetraploidization in human cells. *Cell Cycle*, *14*(17), 2810–2820. https://doi.org/10.1080/15384101.2015.1068482

Kyogoku, H., & Kitajima, T. S. (2017). Large Cytoplasm Is Linked to the Error-Prone Nature of Oocytes. *Developmental Cell*, *41*(3), 287-298.e4. https://doi.org/10.1016/j.devcel.2017.04.009

Lampson, M. A., & Kapoor, T. M. (2005). The human mitotic checkpoint protein BubR1 regulates chromosome-spindle attachments. *Nature Cell Biology*, *7*(1), 93–98. https://doi.org/10.1038/ncb1208

Lane, S. I. R., & Jones, K. T. (2017). Chromosome biorientation and APC activity remain uncoupled in oocytes with reduced volume. *Journal of Cell Biology*, *216*(12), 3949–3957. https://doi.org/10.1083/jcb.201606134

Lara-Gonzalez, P., Pines, J., & Desai, A. (2021). Spindle assembly checkpoint activation and silencing at kinetochores. *Seminars in Cell and Developmental Biology*, *117*, 86–98. https://doi.org/10.1016/j.semcdb.2021.06.009

Lara-Gonzalez, P., Scott, M. I. F., Diez, M., Sen, O., & Taylor, S. S. (2011). BubR1 blocks substrate recruitment to the APC/C in a KEN-box-dependent manner. *Journal of Cell Science*, *124*(24), 4332–4345. https://doi.org/10.1242/jcs.094763

Larsen, N. A., Al-Bassam, J., Wei, R. R., & Harrison, S. C. (2007). Structural analysis of Bub3 interactions in the mitotic spindle checkpoint. *Proceedings of the National Academy of Sciences*, *104*(4), 1201–1206. https://doi.org/10.1073/pnas.0610358104

Ledbetter, M. C., & Porter, K. R. (1963). A "MICROTUBULE" IN PLANT CELL FINE STRUCTURE. *Journal of Cell Biology*, *19*(1), 239–250. https://doi.org/10.1083/jcb.19.1.239

Lee, Y. R. J., Hiwatashi, Y., Hotta, T., Xie, T., Doonan, J. H., & Liu, B. (2017). The Mitotic Function of Augmin Is Dependent on Its Microtubule-Associated Protein Subunit EDE1 in Arabidopsis thaliana. *Current Biology*, *27*(24), 3891-3897.e4. https://doi.org/10.1016/j.cub.2017.11.030

Lee, Y. R. J., & Liu, B. (2019). Microtubule nucleation for the assembly of acentrosomal microtubule arrays in plant cells. *New Phytologist*, *222*(4), 1705–1718. https://doi.org/10.1111/nph.15705

Legal, T., Hayward, D., Gluszek-Kustusz, A., Blackburn, E. A., Spanos, C., Rappsilber, J., Gruneberg, U., & Welburn, J. P. I. (2020). The C-terminal helix of BubR1 is essential for CENP-E-dependent chromosome alignment. *Journal of Cell Science*, *133*(16). https://doi.org/10.1242/jcs.246025

Lermontova, I., Fuchs, J., & Schubert, I. (2008). The Arabidopsis checkpoint protein Bub3.1 is essential for gametophyte development. *Frontiers in Bioscience*, *13*, 5202–5211. https://doi.org/10.2741/3076

Li, R., & Murray, A. W. (1991). Feedback control of mitosis in budding yeast. *Cell*, *66*(3), 519–531. https://doi.org/10.1016/0092-8674(81)90015-5

Liang, C., Zhang, Z., Chen, Q., Yan, H., Zhang, M., Zhou, L., Xu, J., Lu, W., & Wang, F. (2020). Centromere-localized Aurora B kinase is required for the fidelity of chromosome segregation. *Journal of Cell Biology*, *219*(2). https://doi.org/10.1083/jcb.201907092

Liao, H., Li, G., & Yen, T. J. (1994). Mitotic Regulation of Microtubule Cross-Linking Activity of CENP-E Kinetochore Protein. *Science*, *265*(5170), 394–398. https://doi.org/10.1126/science.8023161

Lischetti, T., Zhang, G., Sedgwick, G. G., Bolanos-Garcia, V. M., & Nilsson, J. (2014). The internal Cdc20 binding site in BubR1 facilitates both spindle assembly checkpoint signalling and silencing. *Nature Communications*, *5*. https://doi.org/10.1038/ncomms6563

Logarinho, E., Resende, T., Torres, C., & Bousbaa, H. (2008). The human spindle assembly checkpoint protein Bub3 is required for the establishment of efficient kinetochore-microtubule attachments. *Molecular Biology of the Cell*, *19*(4), 1798–1813. https://doi.org/10.1091/mbc.e07-07-0633

London, N., & Biggins, S. (2014). Signalling dynamics in the spindle checkpoint response. *Nature Reviews Molecular Cell Biology*, *15*(11), 735–747. https://doi.org/10.1038/nrm3888

London, N., Ceto, S., Ranish, J. A., & Biggins, S. (2012). Phosphoregulation of Spc105 by Mps1 and PP1 regulates Bub1 localization to kinetochores. *Current Biology*, *22*(10), 900–906. https://doi.org/10.1016/j.cub.2012.03.052

Luo, X., Tang, Z., Rizo, J., & Yu, H. (2002). The Mad2 spindle checkpoint protein undergoes similar major conformational changes upon binding to either Mad1 or Cdc20. *Molecular Cell*, *9*(1), 59–71. https://doi.org/10.1016/S1097-2765(01)00435-X

Luo, X., Tang, Z., Xia, G., Wassmann, K., Matsumoto, T., Rizo, J., & Yu, H. (2004). The Mad2 spindle checkpoint protein has two distinct natively folded states. *Nature Structural and Molecular Biology*, *11*(4), 338–345. https://doi.org/10.1038/nsmb748

Ma, H. T., & Poon, R. Y. C. (2016). TRIP13 Regulates Both the Activation and Inactivation of the Spindle-Assembly Checkpoint. *Cell Reports*, *14*(5), 1086–1099. https://doi.org/10.1016/j.celrep.2016.01.001

Ma, H. T., & Poon, R. Y. C. (2018). TRIP13 Functions in the Establishment of the Spindle Assembly Checkpoint by Replenishing O-MAD2. *Cell Reports*, *22*(6), 1439–1450. https://doi.org/10.1016/j.celrep.2018.01.027

Machens, I. (2018). *Characterization of two novel kinesin-14 subfamilies from Arabidopsis thaliana* [University of Hamburg]. https://ediss.sub.uni-hamburg.de/handle/ediss/7752

Magidson, V., He, J., Ault, J. G., O'Connell, C. B., Yang, N., Tikhonenko, I., McEwen, B. F., Sui, H., & Khodjakov, A. (2016). Unattached kinetochores rather than intrakinetochore tension arrest mitosis in taxol-treated cells. *Journal of Cell Biology*, *212*(3), 307–319. https://doi.org/10.1083/jcb.201412139

Magidson, V., O'Connell, C. B., Lončarek, J., Paul, R., Mogilner, A., & Khodjakov, A. (2011). The spatial arrangement of chromosomes during prometaphase facilitates spindle assembly. *Cell*, *146*(4), 555–567. https://doi.org/10.1016/j.cell.2011.07.012

Maiato, H., Gomes, A. M., Sousa, F., & Barisic, M. (2017). Mechanisms of chromosome congression during mitosis. *Biology*, *6*(1), 1–56. https://doi.org/10.3390/biology6010013

Malureanu, L. A., Jeganathan, K. B., Hamada, M., Wasilewski, L., Davenport, J., & van Deursen, J. M. (2009). BubR1 N Terminus Acts as a Soluble Inhibitor of Cyclin B Degradation by APC/CCdc20 in Interphase. *Developmental Cell*, *16*(1), 118–131. https://doi.org/10.1016/j.devcel.2008.11.004

Mao, Y., Abrieu, A., & Cleveland, D. W. (2003). Activating and silencing the mitotic checkpoint through CENP-E-dependent activation/inactivation of BubR1. *Cell*, *114*(1), 87–98. https://doi.org/10.1016/S0092-8674(03)00475-6

Maresca, T. J., & Salmon, E. D. (2009). Intrakinetochore stretch is associated with changes in kinetochore phosphorylation and spindle assembly checkpoint activity. *Journal of Cell Biology*, *184*(3), 373–381. https://doi.org/10.1083/jcb.200808130

McAinsh, A. D., & Kops, G. J. P. L. (2023). Principles and dynamics of spindle assembly checkpoint signalling. *Nature Reviews Molecular Cell Biology*. https://doi.org/10.1038/s41580-023-00593-z

McEwen, B. F., Chan, G. K. T., Zubrowski, B., Savoian, M. S., Sauer, M. T., & Yen, T. J. (2001). CENP-E Is Essential for Reliable Bioriented Spindle Attachment, but Chromosome Alignment Can Be Achieved via Redundant Mechanisms in Mammalian Cells. *Molecular Biology of the Cell*, *12*(9), 2776–2789. https://doi.org/10.1091/mbc.12.9.2776

McEwen, B. F., & Dong, Y. (2010). Contrasting models for kinetochore microtubule attachment in mammalian cells. *Cellular and Molecular Life Sciences*, *67*(13), 2163–2172. https://doi.org/10.1007/s00018-010-0322-x

McIntosh, J. R., & Hays, T. (2016). A brief history of research on mitotic mechanisms. *Biology*, *5*(4), 1–38. https://doi.org/10.3390/biology5040055

McVey, S. L., Cosby, J. K., & Nannas, N. J. (2021). Aurora b tension sensing mechanisms in the kinetochore ensure accurate chromosome segregation. *International Journal of Molecular Sciences*, *22*(16). https://doi.org/10.3390/ijms22168818

Meraldi, P., Draviam, V. M., & Sorger, P. K. (2004). Timing and checkpoints in the regulation of mitotic progression. *Developmental Cell*, *7*(1), 45–60. https://doi.org/10.1016/j.devcel.2004.06.006

Meraldi, P., & Sorger, P. K. (2005). A dual role for Bub1 in the spindle checkpoint and chromosome congression. *EMBO Journal*, *24*(8), 1621–1633. https://doi.org/10.1038/sj.emboj.7600641

Molè-Bajer, J. (1958). Cine-micrographic analysis of c-mitosis in endosperm. *Chromosoma*, *9*(1), 332–358. https://doi.org/10.1007/BF02568085

Mukherjee, S., Sandri, B. J., Tank, D., McClellan, M., Harasymiw, L. A., Yang, Q., Parker, L. L., & Gardner, M. K. (2019). A Gradient in Metaphase Tension Leads to a Scaled Cellular Response in Mitosis. *Developmental Cell*, *49*(1), 63-76.e10. https://doi.org/10.1016/j.devcel.2019.01.018

Murray, A. W., & Kirschner, M. W. (1989). Dominoes and Clocks: the Union of Two Views of the Cell Cycle. *Science*, *246*(4930), 614–621. https://doi.org/10.1126/science.2683077

Musacchio, A. (2011). Spindle assembly checkpoint: The third decade. *Philosophical Transactions of the Royal Society B: Biological Sciences*, *366*(1584), 3595–3604. https://doi.org/10.1098/rstb.2011.0072

Musacchio, A. (2015). The Molecular Biology of Spindle Assembly Checkpoint Signaling Dynamics. *Current Biology*, *25*(20), R1002–R1018. https://doi.org/10.1016/j.cub.2015.08.051

Musinipally, V., Howes, S., Alushin, G. M., & Nogales, E. (2013). The microtubule binding properties of CENP-E's C-terminus and CENP-F. *Journal of Molecular Biology*, *425*(22), 4427–4441. https://doi.org/10.1016/j.jmb.2013.07.027

Nebel, B. R., & Ruttle, M. L. (1938). The cytological and genetical significance of colchicine. *Journal of Heredity*, *29*(1), 3–10. https://doi.org/10.1093/oxfordjournals.jhered.a104406

Nelson, C. R., Hwang, T., Chen, P. H., & Bhalla, N. (2015). TRIP13PCH-2 promotes Mad2 localization to unattached kinetochores in the spindle checkpoint response. *Journal of Cell Biology*, *211*(3), 503–516. https://doi.org/10.1083/jcb.201505114

Nicklas, R. B., & Koch, C. A. (1969). Chromosome micromanipulation. 3. Spindle fiber tension and the reorientation of mal-oriented chromosomes. *The Journal of Cell Biology*, *43*(1), 40–50. https://doi.org/10.1083/jcb.43.1.40

O'Connell, C. B., Lončarek, J., Hergert, P., Kourtidis, A., Conklin, D. S., & Khodjakov, A. (2008). The spindle assembly checkpoint is satisfied in the absence of interkinetochore tension during mitosis with unreplicated genomes. *Journal of Cell Biology*, *183*(1), 29–36. https://doi.org/10.1083/jcb.200801038

O'Toole, E. T., Winey, M., & McIntosh, J. R. (1999). High-voltage electron tomography of spindle pole bodies and early mitotic spindles in the yeast Saccharomyces cerevisiae. *Molecular Biology of the Cell*, *10*(6), 2017–2031. https://doi.org/10.1091/mbc.10.6.2017

Oda, Y., & Fukuda, H. (2013). Rho of plant GTPase signaling regulates the behavior of Arabidopsis kinesin-13A to establish secondary cell wall patterns. *The Plant Cell*, *25*(11), 4439–4450. https://doi.org/10.1105/tpc.113.117853

Overlack, K., Primorac, I., Vleugel, M., Krenn, V., Maffini, S., Hoffmann, I., Kops, G. J. P. L., & Musacchio, A. (2015). A molecular basis for the differential roles of Bub1 and BubR1 in the spindle assembly checkpoint. *ELife*, *4*(4), 1–24. https://doi.org/10.7554/eLife.05269

Paim, L. M. G., & FitzHarris, G. (2019). Tetraploidy causes chromosomal instability in acentriolar mouse embryos. *Nature Communications, 10*(1), 4834. https://doi.org/10.1038/s41467-019-12772-8

Panchy, N., Lehti-Shiu, M., & Shiu, S. H. (2016). Evolution of gene duplication in plants. *Plant Physiology, 171*(4), 2294–2316. https://doi.org/10.1104/pp.16.00523

Peterson, R., Slovin, J. P., & Chen, C. (2010). A simplified method for differential staining of aborted and non-aborted pollen grains. *International Journal of Plant Biology, 1*(2), 66–69. https://doi.org/10.4081/pb.2010.e13

Primorac, I., Weir, J. R., Chiroli, E., Gross, F., Hoffmann, I., van Gerwen, S., Ciliberto, A., & Musacchio, A. (2013). Bub3 reads phosphorylated MELT repeats to promote spindle assembly checkpoint signaling. *ELife, 2013*(2), 1–20. https://doi.org/10.7554/eLife.01030

Prosser, S. L., & Pelletier, L. (2017). Mitotic spindle assembly in animal cells: A fine balancing act. *Nature Reviews Molecular Cell Biology, 18*(3), 187–201. https://doi.org/10.1038/nrm.2016.162

Prusicki, M. A., Keizer, E. M., van Rosmalen, R. P., Komaki, S., Seifert, F., Müller, K., Wijnker, E., Fleck, C., & Schnittger, A. (2019). Live cell imaging of meiosis in Arabidopsis thaliana. *ELife, 8*, 1–31. https://doi.org/10.7554/elife.42834

Quinton, R. J., DiDomizio, A., Vittoria, M. A., Kotýnková, K., Ticas, C. J., Patel, S., Koga, Y., Vakhshoorzadeh, J., Hermance, N., Kuroda, T. S., Parulekar, N., Taylor, A. M., Manning, A. L., Campbell, J. D., & Ganem, N. J. (2021). Whole-genome doubling confers unique genetic vulnerabilities on tumour cells. *Nature, 590*(7846), 492–497. https://doi.org/10.1038/s41586-020-03133-3

Rahmani, Z., Gagou, M. E., Lefebvre, C., Emre, D., & Karess, R. E. (2009). Separating the spindle, checkpoint, and timer functions of BubR1. *Journal of Cell Biology, 187*(5), 597–605. https://doi.org/10.1083/jcb.200905026

Ramsey, J., & Schemske, D. W. (1998). Pathways, mechanisms, and rates of polyploid formation in flowering plants. *Annual Review of Ecology and Systematics, 29*, 467–501. https://doi.org/10.1146/annurev.ecolsys.29.1.467

Ravi, M., Marimuthu, M. P. A., & Siddiqi, I. (2008). Gamete formation without meiosis in Arabidopsis. *Nature, 451*(7182), 1121–1124. https://doi.org/10.1038/nature06557

Richardson, D. N., Simmons, M. P., & Reddy, A. S. N. (2006). Comprehensive comparative analysis of kinesins in photosynthetic eukaryotes. In *BMC Genomics* (Vol. 7). https://doi.org/10.1186/1471-2164-7-18

Rieder, C. L., & Alexander, S. P. (1990). Kinetochores are transported poleward along a single astral microtubule during chromosome attachment to the spindle in newt lung cells. *The Journal of Cell Biology, 110*(1), 81–95. https://doi.org/10.1083/jcb.110.1.81

Rieder, C. L., Cole, R. W., Khodjakov, A., & Sluder, G. (1995). The checkpoint delaying anaphase in response to chromosome monoorientation is mediated by an inhibitory signal produced by unattached kinetochores. *Journal of Cell Biology, 130*(4), 941–948. https://doi.org/10.1083/jcb.130.4.941

Rieder, C. L., & Maiato, H. (2004). Stuck in Division or Passing through. *Developmental Cell, 7*(5), 637–651. https://doi.org/10.1016/j.devcel.2004.09.002

Rieder, C. L., Schultz, A., Cole, R., & Sluder, G. (1994). Anaphase onset in vertebrate somatic cells is controlled by a checkpoint that monitors sister kinetochore attachment to the spindle. *Journal of Cell Biology, 127*(5), 1301–1310. https://doi.org/10.1083/jcb.127.5.1301

Risteski, P., Jagrić, M., Pavin, N., & Tolić, I. M. (2021). Biomechanics of chromosome alignment at the spindle midplane. *Current Biology, 31*(10), R574–R585. https://doi.org/10.1016/j.cub.2021.03.082

Romeiro Motta, M., Zhao, X., Pastuglia, M., Belcram, K., Roodbarkelari, F., Komaki, M., Harashima, H., Komaki, S., Kumar, M., Bulankova, P., Heese, M., Riha, K., Bouchez, D., & Schnittger, A. (2022). B1-type cyclins control microtubule organization during cell division in Arabidopsis. *EMBO Reports, 23*(1), e53995. https://doi.org/10.15252/embr.202153995

Roos, U. P. (1976). Light and electron microscopy of rat kangaroo cells in mitosis - III. Patterns of chromosome behavior during prometaphase. *Chromosoma, 54*(4), 363–385. https://doi.org/10.1007/BF00292816

Roscioli, E., Germanova, T. E., Smith, C. A., Embacher, P. A., Erent, M., Thompson, A. I., Burroughs, N. J., & McAinsh, A. D. (2020). Ensemble-Level Organization of Human Kinetochores and Evidence for Distinct Tension and Attachment Sensors. *Cell Reports*, *31*(4), 107535. https://doi.org/10.1016/j.celrep.2020.107535

Ross, K. J., Fransz, P., & Jones, G. H. (1996). A light microscopic atlas of meiosis in Arabidopsis thaliana. *Chromosome Research : An International Journal on the Molecular, Supramolecular and Evolutionary Aspects of Chromosome Biology*, *4*(7), 507–516. https://doi.org/10.1007/BF02261778

Roy, B., Han, S. J. Y., Fontan, A. N., Jema, S., & Joglekar, A. P. (2022). Aurora B phosphorylates Bub1 to promote spindle assembly checkpoint signaling. *Current Biology : CB*, *32*(1), 237-247.e6. https://doi.org/10.1016/j.cub.2021.10.049

Santaguida, S., Vernieri, C., Villa, F., Ciliberto, A., & Musacchio, A. (2011). Evidence that Aurora B is implicated in spindle checkpoint signalling independently of error correction. *EMBO Journal*, *30*(8), 1508–1519. https://doi.org/10.1038/emboj.2011.70

Saurin, A. T., Van Der Waal, M. S., Medema, R. H., Lens, S. M. A., & Kops, G. J. P. L. (2011). Aurora B potentiates Mps1 activation to ensure rapid checkpoint establishment at the onset of mitosis. *Nature Communications*, *2*(1). https://doi.org/10.1038/ncomms1319

Schaar, B. T., Chan, G. K. T., Maddox, P., Salmon, E. D., & Yen, T. J. (1997). CENP-E function at kinetochores is essential for chromosome alignment. *Journal of Cell Biology*, *139*(6), 1373–1382. https://doi.org/10.1083/jcb.139.6.1373

Schindelin, J., Arganda-Carreras, I., Frise, E., Kaynig, V., Longair, M., Pietzsch, T., Preibisch, S., Rueden, C., Saalfeld, S., Schmid, B., Tinevez, J. Y., White, D. J., Hartenstein, V., Eliceiri, K., Tomancak, P., & Cardona, A. (2012). Fiji: An open-source platform for biological-image analysis. *Nature Methods*, *9*(7), 676–682. https://doi.org/10.1038/nmeth.2019

Sczaniecka, M., Feoktistova, A., May, K. M., Chen, J. S., Blyth, J., Gould, K. L., & Hardwick, K. G. (2008). The spindle checkpoint functions of Mad3 and Mad2 depend on a Mad3 KEN box-mediated interaction with Cdc20-anaphase-promoting complex (APC/C). *Journal of Biological Chemistry*, *283*(34), 23039–23047. https://doi.org/10.1074/jbc.M803594200

Sewart, K., & Hauf, S. (2017). Different Functionality of Cdc20 Binding Sites within the Mitotic Checkpoint Complex. *Current Biology*, *27*(8), 1213–1220. https://doi.org/10.1016/j.cub.2017.03.007

Shah, J. V, Botvinick, E., Bonday, Z., Furnari, F., Berns, M., & Cleveland, D. W. (2004). Dynamics of Centromere and Kinetochore Proteins. *Current Biology*, *14*(11), 942–952. https://doi.org/10.1016/j.cub.2004.05.046

Shepperd, L. A., Meadows, J. C., Sochaj, A. M., Lancaster, T. C., Zou, J., Buttrick, G. J., Rappsilber, J., Hardwick, K. G., & Millar, J. B. A. A. (2012). Phosphodependent recruitment of Bub1 and Bub3 to Spc7/KNL1 by Mph1 kinase maintains the spindle checkpoint. *Current Biology*, *22*(10), 891–899. https://doi.org/10.1016/j.cub.2012.03.051

Shrestha, R. L., & Draviam, V. M. (2013). Lateral to end-on conversion of chromosome-microtubule attachment requires kinesins cenp-e and MCAK. *Current Biology*, *23*(16), 1514–1526. https://doi.org/10.1016/j.cub.2013.06.040

Sikirzhytski, V., Renda, F., Tikhonenko, I., Magidson, V., McEwen, B. F., & Khodjakov, A. (2018). Microtubules assemble near most kinetochores during early prometaphase in human cells. *Journal of Cell Biology*, *217*(8), 2647–2659. https://doi.org/10.1083/jcb.201710094

Sironi, L., Mapelli, M., Knapp, S., De Antoni, A., Jeang, K. T., & Musacchio, A. (2002). Crystal structure of the tetrameric Mad1-Mad2 core complex: Implications of a "safety belt" binding mechanism for the spindle checkpoint. *EMBO Journal*, *21*(10), 2496–2506. https://doi.org/10.1093/emboj/21.10.2496

Sofroni, K., Takatsuka, H., Yang, C., Dissmeyer, N., Komaki, S., Hamamura, Y., Böttger, L., Umeda, M., & Schnittger, A. (2020). CDKD-dependent activation of CDKA;1 controls microtubule dynamics and cytokinesis during meiosis. *The Journal of Cell Biology*, *219*(8). https://doi.org/10.1083/jcb.201907016

Soltis, D. E., Visger, C. J., & Soltis, P. S. (2014). The polyploidy revolution then...and now: Stebbins revisited. *American Journal of Botany*, *101*(7), 1057–1078. https://doi.org/10.3732/ajb.1400178

Soltis, P. S., & Soltis, D. E. (2009). The role of hybridization in plant speciation. *Annual Review of Plant Biology*, *60*, 561–588. https://doi.org/10.1146/annurev.arplant.043008.092039

Storchová, Z., Breneman, A., Cande, J., Dunn, J., Burbank, K., O'Toole, E., & Pellman, D. (2006). Genome-wide genetic analysis of polyploidy in yeast. *Nature*, *443*(7111), 541–547. https://doi.org/10.1038/nature05178

Storlazzi, A., Gargano, S., Ruprich-Robert, G., Falque, M., David, M., Kleckner, N., & Zickler, D. (2010). Recombination Proteins Mediate Meiotic Spatial Chromosome Organization and Pairing. *Cell*, *141*(1), 94–106. https://doi.org/10.1016/j.cell.2010.02.041

Stucke, V. M., Silljé, H. H. W., Arnaud, L., & Nigg, E. A. (2002). Human Mps1 kinase is required for the spindle assembly checkpoint but not for centrosome duplication. *EMBO Journal*, *21*(7), 1723–1732. https://doi.org/10.1093/emboj/21.7.1723

Su, H., Liu, Y., Dong, Q., Feng, C., Zhang, J., Liu, Y., Birchler, J. A., & Han, F. (2017). Dynamic location changes of Bub1-phosphorylated-H2AThr133 with CENH3 nucleosome in maize centromeric regions. *New Phytologist*, *214*(2), 682–694. https://doi.org/10.1111/nph.14415

Su, H., Liu, Y., Wang, C., Liu, Y., Feng, C., Sun, Y., Yuan, J., Birchler, J. A., & Han, F. (2021). Knl1 participates in spindle assembly checkpoint signaling in maize. *Proceedings of the National Academy of Sciences of the United States of America*, *118*(20), 1–11. https://doi.org/10.1073/pnas.2022357118

Sudakin, V., Chan, G. K. T., & Yen, T. J. (2001). Checkpoint inhibition of the APC/C in HeLa cells is mediated by a complex of BUBR1, BUB3, CDC20, and MAD2. *Journal of Cell Biology*, *154*(5), 925–936. https://doi.org/10.1083/jcb.200102093

Tanaka, K., Mukae, N., Dewar, H., van Breugel, M., James, E. K., Prescott, A. R., Antony, C., & Tanaka, T. U. (2005). Molecular mechanisms of kinetochore capture by spindle microtubules. *Nature*, *434*(7036), 987–994. https://doi.org/10.1038/nature03483

Tauchman, E. C., Boehm, F. J., & DeLuca, J. G. (2015). Stable kinetochore-microtubule attachment is sufficient to silence the spindle assembly checkpoint in human cells. *Nature Communications*, *6*. https://doi.org/10.1038/ncomms10036

Taveras, C., Liu, C., & Mao, Y. (2019). A tension-independent mechanism reduces Aurora B-mediated phosphorylation upon microtubule capture by CENP-E at the kinetochore. *Cell Cycle*, *18*(12), 1349–1363. https://doi.org/10.1080/15384101.2019.1617615

Taylor, S. S., Ha, E., & McKeon, F. (1998). The Human Homologue of Bub3 Is Required for Kinetochore Localization of Bub1 and a Mad3/Bub1-related Protein Kinase. *Journal of Cell Biology*, *142*(1), 1–11. https://doi.org/10.1083/jcb.142.1.1

Te Beest, M., Le Roux, J. J., Richardson, D. M., Brysting, A. K., Suda, J., Kubešová, M., & Pyšek, P. (2012). The more the better? The role of polyploidy in facilitating plant invasions. *Annals of Botany*, *109*(1), 19–45. https://doi.org/10.1093/aob/mcr277

ten Hoopen, R., Manteuffel, R., Dolezel, J., Malysheva, L., & Schubert, I. (2000). Evolutionary conservation of kinetochore protein sequences in plants. *Chromosoma*, *109*(7), 482–489. https://doi.org/10.1007/s004120000109

ten Hoopen, R., Schleker, T., Manteuffel, R., & Schubert, I. (2002). Transient CENP-E-like kinetochore proteins in plants. *Chromosome Research : An International Journal on the Molecular, Supramolecular and Evolutionary Aspects of Chromosome Biology*, *10*(7), 561–570. https://doi.org/10.1023/a:1020962618696

Tromer, E., Bade, D., Snel, B., & Kops, G. J. P. L. (2016). Phylogenomics-guided discovery of a novel conserved cassette of short linear motifs in BubR1 essential for the spindle checkpoint. *Open Biology*, *6*(12), 160315. https://doi.org/10.1098/rsob.160315

Tulin, F., & Cross, F. R. (2014). A microbial avenue to cell cycle control in the plant superkingdom. *Plant Cell*, *26*(10), 4019–4038. https://doi.org/10.1105/tpc.114.129312

Uchida, K. S. K., Jo, M., Nagasaka, K., Takahashi, M., Shindo, N., Shibata, K., Tanaka, K., Masumoto, H., Fukagawa, T., & Hirota, T. (2021). Kinetochore stretching-mediated rapid silencing of the spindle-assembly checkpoint required for failsafe chromosome segregation. *Current Biology*, 1–11. https://doi.org/10.1016/j.cub.2021.01.062

Uchida, K. S. K., Takagaki, K., Kumada, K., Hirayama, Y., Noda, T., & Hirota, T. (2009). Kinetochore stretching inactivates the spindle assembly checkpoint. *Journal of Cell Biology*, *184*(3), 383–390. https://doi.org/10.1083/jcb.200811028

Van De Peer, Y., Mizrachi, E., & Marchal, K. (2017). The evolutionary significance of polyploidy. *Nature Reviews Genetics*, *18*(7), 411–424. https://doi.org/10.1038/nrg.2017.26

Van Der Waal, M. S., Saurin, A. T., Vromans, M. J. M., Vleugel, M., Wurzenberger, C., Gerlich, D. W., Medema, R. H., Kops, G. J. P. L., & Lens, S. M. A. (2012). Mps1 promotes rapid centromere accumulation of Aurora B. *EMBO Reports*, *13*(9), 847–854. https://doi.org/10.1038/embor.2012.93

Van Leene, J., Hollunder, J., Eeckhout, D., Persiau, G., Van De Slijke, E., Stals, H., Van Isterdael, G., Verkest, A., Neirynck, S., Buffel, Y., De Bodt, S., Maere, S., Laukens, K., Pharazyn, A., Ferreira, P. C. G., Eloy, N., Renne, C., Meyer, C., Faure, J. D., … De Jaeger, G. (2010). Targeted interactomics reveals a complex core cell cycle machinery in Arabidopsis thaliana. *Molecular Systems Biology*, *6*(397). https://doi.org/10.1038/msb.2010.53

Vanneste, K., Baele, G., Maere, S., & Van De Peer, Y. (2014). Analysis of 41 plant genomes supports a wave of successful genome duplications in association with the Cretaceous-Paleogene boundary. *Genome Research*, *24*(8), 1334–1347. https://doi.org/10.1101/gr.168997.113

Vanoosthuyse, V., Meadows, J. C., van der Sar, S. J. A., Millar, J. B. A., & Hardwick, K. G. (2009). Bub3p Facilitates Spindle Checkpoint Silencing in Fission Yeast. *Molecular Biology of the Cell*, *20*(24), 5096–5105. https://doi.org/10.1091/mbc.e09-09-0762

Vanstraelen, M., Inzé, D., & Geelen, D. (2006). Mitosis-specific kinesins in Arabidopsis. *Trends in Plant Science*, *11*(4), 167–175. https://doi.org/10.1016/j.tplants.2006.02.004

Vázquez-Diez, C., Paim, L. M. G., & FitzHarris, G. (2019). Cell-Size-Independent Spindle Checkpoint Failure Underlies Chromosome Segregation Error in Mouse Embryos. *Current Biology*, *29*(5), 865-873.e3. https://doi.org/10.1016/j.cub.2018.12.042

Vleugel, M., Hoogendoorn, E., Snel, B., & Kops, G. J. P. L. (2012). Evolution and Function of the Mitotic Checkpoint. *Developmental Cell*, *23*(2), 239–250. https://doi.org/10.1016/j.devcel.2012.06.013

Vleugel, M., Omerzu, M., Groenewold, V., Hadders, M. A., Lens, S. M. A., & Kops, G. J. P. L. (2015). Sequential Multisite Phospho-Regulation of KNL1-BUB3 Interfaces at Mitotic Kinetochores. *Molecular Cell*, *57*(5), 824–835. https://doi.org/10.1016/j.molcel.2014.12.036

Vleugel, M., Tromer, E., Omerzu, M., Groenewold, V., Nijenhuis, W., Snel, B., & Kops, G. J. P. L. (2013). Arrayed BUB recruitment modules in the kinetochore scaffold KNL1 promote accurate chromosome segregation. *Journal of Cell Biology*, *203*(6), 943–955. https://doi.org/10.1083/jcb.201307016

Wan, X., Cimini, D., Cameron, L. A., & Salmon, E. D. (2012). The coupling between sister kinetochore directional instability and oscillations in centromere stretch in metaphase PtK1 cells. *Molecular Biology of the Cell*, *23*(6), 1035–1046. https://doi.org/10.1091/mbc.E11-09-0767

Wan, X., O'Quinn, R. P., Pierce, H. L., Joglekar, A. P., Gall, W. E., DeLuca, J. G., Carroll, C. W., Liu, S. T., Yen, T. J., McEwen, B. F., Stukenberg, P. T., Desai, A., & Salmon, E. D. (2009). Protein Architecture of the Human Kinetochore Microtubule Attachment Site. *Cell*, *137*(4), 672–684. https://doi.org/10.1016/j.cell.2009.03.035

Wang, X., Babu, J. R., Harden, J. M., Jablonski, S. A., Gazi, M. H., Lingle, W. L., de Groen, P. C., Yen, T. J., & van Deursen, J. M. A. (2001). The Mitotic Checkpoint Protein hBUB3 and the mRNA Export Factor hRAE1 Interact with GLE2p-binding Sequence (GLEBS)-containing Proteins. *Journal of Biological Chemistry*, *276*(28), 26559–26567. https://doi.org/10.1074/jbc.M101083200

Weiss, E., & Winey, M. (1996). The Saccharomyces cerevisiae spindle pole body duplication gene MPS1 is part of a mitotic checkpoint. *The Journal of Cell Biology*, *132*(1), 111–123. https://doi.org/10.1083/jcb.132.1.111

Welburn, J. P. I., Vleugel, M., Liu, D., Yates, J. R., Lampson, M. A., Fukagawa, T., & Cheeseman, I. M. (2010). Aurora B Phosphorylates Spatially Distinct Targets to Differentially Regulate the Kinetochore-Microtubule Interface. *Molecular Cell*, *38*(3), 383–392. https://doi.org/10.1016/j.molcel.2010.02.034

Westhorpe, F. G., Tighe, A., Lara-Gonzalez, P., & Taylor, S. S. (2011). p31 comet-mediated extraction of Mad2 from the MCC promotes efficient mitotic exit. *Journal of Cell Science*, *124*(22), 3905–3916. https://doi.org/10.1242/jcs.093286

Wu, S., Han, B., & Jiao, Y. (2020). Genetic Contribution of Paleopolyploidy to Adaptive Evolution in Angiosperms. *Molecular Plant*, *13*(1), 59–71. https://doi.org/10.1016/j.molp.2019.10.012

Yamada, M., & Goshima, G. (2017). Mitotic spindle assembly in land plants: Molecules and mechanisms. *Biology*, *6*(1). https://doi.org/10.3390/biology6010006

Yang, Y., Tsuchiya, D., & Lacefield, S. (2015). Bub3 promotes Cdc20-dependent activation of the APC/C in S. cerevisiae. *Journal of Cell Biology*, *209*(4), 519–527. https://doi.org/10.1083/jcb.201412036

Ye, Q., Rosenberg, S. C., Moeller, A., Speir, J. A., Su, T. Y., & Corbett, K. D. (2015). TRIP13 is a protein-remodeling AAA+ ATPase that catalyzes MAD2 conformation switching. *ELife*, *2015*(4), 1–44. https://doi.org/10.7554/eLife.07367

Yoo, T. Y., Choi, J. M., Conway, W., Yu, C. H., Pappu, R. V., & Needleman, D. J. (2018). Measuring NDC80 binding reveals the molecular basis of tension-dependent kinetochore-microtubule attachments. *ELife*, *7*, 1–34. https://doi.org/10.7554/eLife.36392

Younis, A., Hwang, Y.-J., & Lim, K.-B. (2014). Exploitation of induced 2n-gametes for plant breeding. *Plant Cell Reports*, *33*(2), 215–223. https://doi.org/10.1007/s00299-013-1534-y

Yu, H G, Muszynski, M. G., & Kelly Dawe, R. (1999). The maize homologue of the cell cycle checkpoint protein MAD2 reveals kinetochore substructure and contrasting mitotic and meiotic localization patterns. *The Journal of Cell Biology*, *145*(3), 425–435. https://doi.org/10.1083/jcb.145.3.425

Yu, Hong Guo, Hiatt, E. N., Chan, A., Sweeney, M., & Dawe, R. K. (1997). Neocentromere-mediated chromosome movement in maize. *The Journal of Cell Biology*, *139*(4), 831–840. https://doi.org/10.1083/jcb.139.4.831

Yu, Z., Haage, K., Streit, V. E., Gierl, A., & Torres Ruiz, R. A. (2009). A large number of tetraploid Arabidopsis thaliana lines, generated by a rapid strategy, reveal high stability of neo-tetraploids during consecutive generations. *Theoretical and Applied Genetics*, *118*(6), 1107–1119. https://doi.org/10.1007/s00122-009-0966-9

Zaytsev, A. V., Sundin, L. J. R., DeLuca, K. F., Grishchuk, E. L., & DeLuca, J. G. (2014). Accurate phosphoregulation of kinetochore-microtubule affinity requires unconstrained molecular interactions. *Journal of Cell Biology*, *206*(1), 45–59. https://doi.org/10.1083/jcb.201312107

Zhang, G., Kruse, T., López-Méndez, B., Sylvestersen, K. B., Garvanska, D. H., Schopper, S., Nielsen, M. L., & Nilsson, J. (2017). Bub1 positions Mad1 close to KNL1 MELT repeats to promote checkpoint signalling. *Nature Communications*, *8*(June). https://doi.org/10.1038/ncomms15822

Zhang, H., Deng, X., Sun, B., Lee Van, S., Kang, Z., Lin, H., Lee, Y. R. J., & Liu, B. (2018). Role of the BUB3 protein in phragmoplast microtubule reorganization during cytokinesis. *Nature Plants*, *4*(7), 485–494. https://doi.org/10.1038/s41477-018-0192-z

Zich, J., May, K., Paraskevopoulos, K., Sen, O., Syred, H. M., van der Sar, S., Patel, H., Moresco, J. J., Sarkeshik, A., Yates, J. R., Rappsilber, J., & Hardwick, K. G. (2016). Mps1Mph1 Kinase Phosphorylates Mad3 to Inhibit Cdc20Slp1-APC/C and Maintain Spindle Checkpoint Arrests. *PLoS Genetics*, *12*(2), 1–25. https://doi.org/10.1371/journal.pgen.1005834

Publications and Presentations

Publications

A cytological and functional framework of the meiotic spindle assembly checkpoint in *Arabidopsis thaliana*

Konstantinos Lampou[1], Franziska Böwer[1], Shinichiro Komaki[2], Maren Köhler[1], and Arp Schnittger[1,*]

Presentations

Oral presentations

The 31st International Conference on Arabidopsis Research, 21st-25th of June 2022, Virtual
Presentation title: "Shedding light on the meiotic spindle assembly checkpoint"

Gordon Research Seminar on Plant and Microbial Cytoskeleton titled "An Evolving Cytoskeleton: Diverging Mechanisms and Converging Patterns", 13th-14th of August 2022, Andover, New Hampshire, USA
Presentation title: "O' chromosomes, where art thou? An unexpected role for BUB3.3 in *Arabidopsis thaliana*"
Awarded as 1 of 3 best talks

Motors in Quarantine, 15th of February 2023, Virtual
Presentation title: "O' chromosomes, where art thou? An unexpected role for BUB3.3 in *Arabidopsis thaliana*"

Poster presentations

EMBO workshop "Dynamic kinetochore", 28th of June-1st of July 2022, Oslo, Norway

Poster title: "O' chromosomes, where art thou? A novel role for BUB3.3 in *Arabidopsis thaliana*"

Gordon Research Conference on Plant and Microbial Cytoskeleton titled "Cytoskeletal Diversification Across the Domains of Life", 14th-19th of August 2022, Andover, New Hampshire, USA

Poster title: "O' chromosomes, where art thou?"

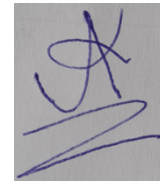## Eidesstaatliche Versicherung / Declaration on oath

Hiermit erkläre ich an Eides statt, dass ich die vorliegende Dissertationsschrift selbst und keine anderen als die angegebenen Quellen und Hilfsmittel benutzt habe.

I hereby declare, on oath, that I have written the present dissertation by my own and have not used other than the acknowledged resources and aids.

Hamburg, den 02. Juni 2023   Unterschrift

Acknowledgements

I have been dreaming of doing a PhD since my first day at the University of Heidelberg back in 2012. Oh well, here I am, handing in my thesis, after challenging four years. Where to start…

First of all, I'd like to thank my supervisor Prof. Dr. Arp Schnittger for giving me the opportunity to work on this wonderful project. From our first meeting back in November 2018, he was very understanding to my capricious wishes of wanting to do exclusively live-cell imaging and nothing else. Well, I guess this thesis is kind of a proof that this ended up being the case. However, this could not have been possible without the help of several collaborators, that I will mention below. Arp supported me throughout this work, provided crucial ideas to explore, critical comments on my work as well as the necessary support/soft kick in the butt whenever needed. It was a pleasure to work on this project and it's an experience I've never forget. Thanks, Arp! Oh, and sorry that you had to read my ridiculously long e-mails/rants. I guess this thesis is arguably short compared to them…

I'd also like to thank Dr. Magdalena Weingartner, not only for agreeing to be the second referee, but also for helpful discussions at the SP8 for mitosis imaging.

This work could not have been done without the crucial contribution of Dr. Shinichiro Komaki, an absolutely fantastic collaborator! Not only did Shini leave behind a treasure chest full of wonderful reporters and mutant lines, but he has also performed several crucial experiments and has been always there answering my questions and my very, very, very long e-mails. Without his help and work this thesis would have never been what it is today, so I am truly deeply indebted to you, Shini!

I am also very grateful to have had the support of Maren Köhler, an excellent, patient, always friendly and careful coworker, who has significantly contributed to my main project and has performed several essential experiments, that would have

been haunting me in my worst nightmares. Similarly, Dr. Yuki Hamamura and Franziska Böwer have helped me majorly in this work. Yuki with her critical input about live-cell imaging and Franzi for many many things from the simplest lab techniques to performing experiments that I hated to having a long collaboration on a very cool project that you'll find in her thesis. Also, I'd like to thank Maren Röper for incredible support on the administrative level and having always an answer to my many random questions about anything as well as getting everything done asap and keeping our lab running smoothly. Dr. Maren Heese has been a great discussion partner, a fantastic sounding board for exploring new hypotheses and a great help with bioinformatics work as well as in-depth database search. Finally, I'd like to thank the rest of team Asia (Yuki, Bingyan Hu, Dr. Seijiro Ono and Misato Ono), Lucas Lang, Dr. Oscar Sanz Mora, Max van der Heide, Dr. Joke de Jaeger-Braet, and the rest of the Schnittger lab for helping survive this difficult journey.

Last but not least, I'd like to thank my friends and family for supporting me throughout this long journey. My parents, Zoi and Giorgos, as well as my closest family members, Christina, Maro, Theodoros, Ntinos, Gianna, Antonis, and Elsa, have been always there through thick and thin and have made life wonderful in many different ways. My great Hamburgian friends, Marco, Hasibe, Andrii, and of course the iconic Hamburg Players (Jo, Lexi, David Duke, Birte, Forrest and many many more absolutely fantastic poeple) have made life in Hamburg truly joyful. How could I forget my friends in Berlin, Athens, and wherever they are in the world now who have kept me (somewhat) sane throughout these years? I think they know how important they have been in my life, so it'll suffice for now just to mention them by name: Aris, Odysseas, Gouz, Katina, Smaroli, Ntina Gkouma, Dimitra, Irmena, Anastasia, Antoniana, Safak, Tomasito muchachito, Burce and Julia. Finally, an absolutely ginormous thank you to Ecem who has supported me unbelievably much and has helped me be who I am today.